

Intertidal beach morphodynamics of a macro-tidal sandy coast (Belgium)

Evelien Brand

Intertidal beach morphodynamics of a macro-tidal sandy coast (Belgium)

Thesis submitted in fulfilment of the requirements for the award of the
degree of Doctor in Engineering Sciences
(Doctor in de Ingenieurswetenschappen)

Evelien Brand

Department of Hydrology and Hydraulic Engineering
Vrije Universiteit Brussel

Alle Rechten voorbehouden. Niets van deze uitgave mag worden vermenigvuldigd en/of openbaar gemaakt worden door middel van druk, fotokopie, microfilm, elektronisch of op welke andere wijze ook, zonder voorafgaande schriftelijke toestemming van de auteur.

All rights reserved. No part of this publication may be produced in any form by print, photoprint, microfilm, electronic or any other means without permission from the author.

Printed by
Crazy Copy Center Productions
VUB Pleinlaan 2, 1050 Brussel
Tel / fax : +32 2 629 33 44
crazycopy@vub.ac.be
www.crazycopy.be

ISBN :
NUR CODE : 935

Composition of the doctoral jury:

Promotor

Prof. dr. ir. Margaret Chen Vrije Universiteit Brussel

Chairman

Prof. dr. ir. Gerd Vandersteen Vrije Universiteit Brussel

Vice-chairman

Prof. dr. ir. Rik Pintelon Vrije Universiteit Brussel

Secretary

Dr. Anne-Lise Montreuil Vrije Universiteit Brussel

External examiners

Prof. dr. Arnaud Héquette Université du Littoral Côte d'Opale
Dr. Sebastian Dan Flanders Hydraulics Research

Abstract

The intertidal zone plays an important role in the protection of the coast. It is a very dynamic area subject to waves, tide, and wind and topographic changes can be large over a short period of time. For macro-tidal coasts (tidal range > 4 m) like the Belgian one, tide is an important factor in the intertidal beach morphodynamics but it remains unclear what specific hydrodynamic conditions lead to topographic changes. This is mainly due to a scarcity of reliable field data of sediment transport and beach topography. This study investigates the intertidal beach morphodynamics based on extensive measurements of hydrodynamics, sediment transport, and beach topography resulting in a conceptual model of hydrodynamic forcing and topographic response. Two study sites along the Belgian coast are examined: a natural, multi-barred beach (Groenendijk) and a managed beach with a featureless intertidal zone (Mariakerke).

The monthly to seasonal dynamics in beach topography is investigated based on multiannual monthly cross-shore beach profiles. It is found that topographic changes on this scale are mainly event-driven with, in general, erosion during energetic events and beach recovery in between. The ridges and runnels at Groenendijk move onshore and become more pronounced during energetic conditions, while the intertidal beach topography is smoothed during calm conditions. Monthly variations in intertidal beach volume are on average 2% of the total beach volume and they can be up to 7% for energetic (non-storm) events. There is a large alongshore variability in topographic response to hydrodynamic forcing and this response can even be opposite over a distance of tens of meters.

In comparison to the nearshore hydrodynamics and sediment dynamics it is found that the intertidal beach grows when waves are small (wave steepness < 0.010), whereas it erodes when waves are large (> 0.025). For medium wave steepness (0.010-0.025) this is opposite, which is attributed to a sudden rise in sediment supply. This rise is likely related to waves breaking over the sandbanks in front of the coast and at beaches southwest of the study sites.

On a daily scale, the relationship between wave steepness and intertidal beach volume is heavily distorted by spring-neap variations in tidal current direction. Strong alongshore currents transport sediment away from the beach during spring tide which enhances erosion. In contrast, currents are cross-shore and wave-dominated during neap tide. The impact of variations in tidal current direction on the intertidal beach topography is in the same order of magnitude as wave impact. The effect of variations in sediment supply is subordinate to the impact of waves and tide.

The main mode of sediment transport in the intertidal zone is in suspension. Currents peak at approximately 1.5 m above the bed, resulting in a peak in sediment transport at 1/3 of the high tide level. The mean sediment transport is onshore by tidal currents during calm conditions, while it is offshore by undertow during energetic wave conditions (wave height > 0.6 m or wave steepness > 0.025). Oscillatory transport is always onshore because of wave asymmetry but is subordinate to the mean transport. A good qualitative and quantitative relationship is found between measured sediment transport rates and observed topographic changes. This is ascribed to the use of acoustic backscatter intensity from a high resolution current sensor, allowing the estimation of suspended sediment concentrations over the full water column. Furthermore, this good relationship is attributed to the use of a static laser scanner to obtain accurate beach volume changes.

In general, it can be concluded that waves are not necessarily the dominant forcing factor on macro-tidal beaches. Tidal currents can be equally important and they can contribute significantly to the transport of sediment. Besides waves and tidal currents, variations in sediment supply influence the changes in the intertidal beach topography. A conceptual model is provided to illustrate the relationship between hydrodynamic forcing and topographic response.

Samenvatting

Het intergetijdengebied speelt een belangrijke rol in de bescherming van de kust omdat er een groot deel van de golfenergie geabsorbeerd wordt. Naast golven is het intergetijdengebied ook onderhevig aan getij en wind. Het is dus een erg dynamisch gebied en topografische veranderingen kunnen er groot zijn over korte periodes. Over het algemeen groeit het strand als golven klein zijn en vindt erosie plaats als golven groot zijn. Voor kusten met macro-getij (getijdenverschil > 4 m), zoals ook de Belgische kust, is het getij ook een belangrijke onderdeel van de morfodynamiek van het strand, maar het is nog onduidelijk welke rol het getij precies speelt. Dit komt vooral door een gebrek aan betrouwbare metingen van sedimenttransport en topografie in het intergetijdengebied. Het doel van deze studie is om een conceptueel model op te stellen van hydrodynamische oorzaak vs. topografisch gevolg aan de hand van uitgebreide veldmetingen in het intergetijdengebied van twee verschillende stranden met macro-getij: een natuurlijk strand met zandbanken (Groenendijk) en een beheerd strand met een vlak intergetijdengebied (Mariakerke).

De seizoensgebonden dynamiek in topografie is onderzocht aan de hand van meerdere jaren aan maandelijkse strandprofielen. Er lijkt geen seizoenscyclus te zijn in topografie, maar erosie tijdens maanden waarin de golfhoogte de 3.75 m overschrijdt en herstel in de perioden daartussen. De zandbanken bij Groenendijk worden hoger en verplaatsen zich meer landwaarts tijdens die energieke maanden, terwijl de topografie wordt afgevlakt tijdens de kalme periodes. Maandelijkse veranderingen in het strandvolume bedragen gemiddeld 2 % van het totale volume maar kunnen oplopen tot 7 % tijdens energieke omstandigheden. Er is een grote kustlange variatie in topografische veranderingen en dwarsprofielen die enkele tientallen meters uit elkaar liggen kunnen zich zelfs tegenovergesteld gedragen.

Het maandelijks strandvolume laat een groei zien als golven klein zijn (golfsteilheid < 0.010) en een afname als golven groot zijn (golfsteilheid > 0.025). Dit is omgekeerd wanneer de golven een gemiddelde steilheid hebben (0.010-0.025). Dit wordt verklaard door een toename in sedimentaanvoer die

waarschijnlijk gerelateerd is aan het breken van golven over de getijdebanken voor de kust.

Op een dagelijkse schaal wordt de relatie tussen golfsteilheid en strandvolume sterk beïnvloed door het getij. Sterke kustlangse stromingen transporteren sediment weg van de kust tijdens springtij, terwijl de stroming vooral golf-gedomineerd en kustdwars is tijdens doottij. De impact van springtij-doottij variaties op het strandvolume is in dezelfde orde van grootte als de impact van golven. Het effect van variaties in sedimentaanvoer is kleiner dan de impact van golven en getij.

In het intergetijdengebied wordt sediment voornamelijk getransporteerd in suspensie. De stroming is het sterkst op ongeveer 1.5 m boven de zeebodem wat resulteert in een piek in sedimenttransport op ongeveer 1/3 van de maximale waterkolom (3-5.5 m). Sedimenttransport is landwaarts door getijdenstroming tijdens kalme dagen en zeewaarts door de onderstroom van de golven tijdens energieke dagen (golfhoogte > 0.6 m, golfsteilheid > 0.025). Het oscillerende transport is altijd landwaarts door de golfasymmetrie maar is ondergeschikt aan het gemiddelde transport. Een goede kwalitatieve en kwantitatieve relatie is gevonden tussen sedimenttransport en topografische veranderingen. Dit komt door het gebruik van akoestische apparatuur waarmee sedimentconcentraties over de hele waterkolom kunnen worden gekwantificeerd en het gebruik van een statische laser scanner waarmee de topografie kan worden gemeten met een hoge resolutie.

Er kan worden geconcludeerd dat op stranden met een macro-getij golven niet noodzakelijk de belangrijkste drijfveer voor topografische veranderingen zijn. De invloed van getijdenstroming kan net zo belangrijk zijn als die van golven en deze stroming kan significant bijdragen aan het transport van sediment. Naast getij en golven zijn ook variaties in de aanvoer van sediment bepalend voor topografische veranderingen, hoewel in mindere mate.



Contents

Abstract	vii
Samenvatting	ix
Contents	xiii
List of figures	xv
List of tables	xix
List of abbreviations	xx
List of symbols	xxi
Chapter 1 - General introduction	2
1.1. Introduction	2
1.2. Study area	4
1.3. Objectives and study approach	8
1.4. Outline of the thesis	10
Chapter 2 - Literature review: optimizing measurements of sediment transport in the intertidal zone	12
2.1. Introduction	12
2.2. Measuring techniques to quantify sediment transport	14
2.3. Cross-checking suspended load measurements	23
2.4. Cross-checking bed load and total load measurements	25
2.5. Matching the scale of different measurements	27
2.6. Conclusion	30
Chapter 3 - Seasonal variations in intertidal beach topography	32
3.1. Introduction	32
3.2. Methods	33
3.3. Results	35
3.4. Discussion	40
3.5. Conclusion	43

Chapter 4 - Intertidal beach dynamics in relation to nearshore hydrodynamics on a monthly scale -----	46
4.1. Introduction -----	46
4.2. Methods -----	47
4.3. Results -----	51
4.4. Discussion -----	58
4.5. Conclusion -----	62
Chapter 5 - Intertidal beach morphodynamics on a daily scale -----	63
5.1. Introduction -----	63
5.2. Methods -----	64
5.3. Results -----	68
5.4. Discussion -----	78
5.5. Conclusion -----	82
Chapter 6 - Sediment transport in the intertidal zone -----	85
6.1. Introduction -----	85
6.2. Methods -----	86
6.3. Results -----	91
6.4. Discussion -----	98
6.5. Conclusion -----	103
Chapter 7 - General conclusions and recommendations -----	105
7.1. Conclusions -----	105
7.2. Recommendations -----	109
Bibliography -----	115
Appendix A: wave buoy and tide gauge measuring locations -----	131
Appendix B: nearshore flow velocity -----	133
Appendix C: OBS calibration -----	135
Appendix D: background of TLS -----	137
Appendix E: human interference -----	138
Research output -----	141
Acknowledgements -----	145

List of figures

Figure 1. Beach morphodynamics system.	2
Figure 2. Overview map of the Belgian coast with the study sites (Groenendijk and Mariakerke) indicated.....	4
Figure 3. Different zones on a beach (modified from Vito and Afdeling Kust, 2009).	5
Figure 4. Offshore wave rose based on wave measurements from the Westhinder wave buoy (Appendix A) from 2000-2017.....	6
Figure 5. Ground pictures of the beach at Mariakerke.	7
Figure 6. Ground pictures of the beach at Groenendijk.	7
Figure 7. Temporal and spatial scales of hydrodynamics (<i>italic</i>) and morphology (<i>normal</i>) (Ruessink 1998). The grey box represents scales covered in this study	8
Figure 8. Summary of the investigated topographic and hydrodynamic data at Mariakerke and Groenendijk.	9
Figure 9. Outline of the thesis.....	10
Figure 10. Schematized wave propagation across the different beach zones.....	13
Figure 11. Timeline of measuring techniques for sediment transport from the 1960s until now. Dashed lines indicate limited use.....	14
Figure 12. SSC derived from acoustic backscatter compared SSC derived from OBS. These measurements were carried out in a tidal inlet, the Marsdiep inlet (The Netherlands). Black (grey) points represent data for which the depth-averaged velocity < 0.5 m/s (> 0.5 m/s). Drawn is the linear fit through the black data points (Nauw et al., 2014).....	16
Figure 13. Contour plots showing the spatial distribution of sand tracers from a central injection point (dot) at different locations across a barred beach in Northern France. The tracer migration is represented by the pink scale (Sedrati and Anthony, 2007).	18
Figure 14. Timeline of measuring techniques for intertidal beach topography from the 1960s until now. Dashed lines indicate limited use.	20
Figure 15. The effect of particle size (colours) on acoustic backscatter intensity based on measurements around the low water line on a sandy beach at Groenendijk, Belgium (Brand et al., 2019).....	25
Figure 16. Temporal and spatial scale of different measuring techniques. Methods to measure sediment transport are in bold and to measure topography in <i>italic</i>	28
Figure 17. Example of bed level sensor measurements. The blue bars represent raw data from the bed level sensor and the thick line represents the one-minute averaged bed level relative to the mean sea level (NM). Measurements were carried out in the intertidal zone of a beach in southwestern France (from: Masselink et al., 2009)....	29
Figure 18. Location of the cross-shore profiles at Groenendijk and Mariakerke.....	33
Figure 19. Calculating the beach volume using trapezoidal rules.....	34

Figure 20. Mean (thick black line), envelope (black lines), and standard deviation over time (dashed grey line) of the topography of a representative cross-shore beach profile for Mariakerke and Groenendijk.	35
Figure 21. Intertidal beach volume compared to the volume in February 2017 (t_0), which signifies the start of the measurements at Groenendijk. Beach volume changes are averaged for all profiles at Mariakerke and Groenendijk. Months that were characterized by energetic events are displayed in bold.	36
Figure 22. Time series of monthly maximum, average of highest 10%, and median significant wave height from September 2015 to March 2019. Note: data gaps are due to malfunctioning of the wave buoy.	37
Figure 23. Cross-shore position and elevation of the peak of the bars for all profiles at Groenendijk and all surveys combined.	39
Figure 24. Top: Absolute height of the bars in the intertidal zone (i.e. the elevation of the ridge compared to the elevation of the landward runnel). Bottom: Relative position of the bars compared to the average position. Data is averaged over time. No surveys were carried out in July and August.	40
Figure 25. Total intertidal (IT) beach volume for Mariakerke and Groenendijk with the linear trend indicated by a dashed line.	43
Figure 26. Map of the study area with the location of the cross-shore profiles and hydrodynamic measurements indicated.	48
Figure 27. One of the measuring frames with the AWAC at the top and the three OBS at the bottom.	49
Figure 28. Wave steepness from the wave buoy compared to wave steepness from the nearest frame (section 104, -8 m TAW). The wave steepness is 2-hour averaged. ..	50
Figure 29. Time series of significant wave height, significant wave period, wave steepness, maximum water level, and SSC for the three measuring campaigns (for the frame at -8 m TAW at section 104, averaged over a 6-hour period). SSC data is not considered when biofouling occurred on the OBS.	52
Figure 30. Beach topography and topographic changes. Top/middle: envelopes and average profiles for profiles a, b, and c. Bottom: monthly intertidal beach volume changes for both sections. Top and bottom left correspond to section 100, middle and bottom right to section 104.	53
Figure 31. Comparison between monthly-averaged wave steepness and intertidal beach volume change (top left); SSC and intertidal beach volume change (top right); wave steepness and SSC (bottom left); and between three-day-averaged wave steepness and SSC (bottom right).	55
Figure 32. Volume change of the intertidal zone over wave steepness based on wave buoy and tide gauge data, for sections 100 and 104 separately (left, top and bottom respectively) and both sections combined (right).	56
Figure 33. Volume change of the intertidal beach over beach slope (top left), volume change of the dry beach (top right), wave direction (bottom left), and wave energy (bottom right). All points are monthly averages.	57
Figure 34. Time series of $2H_0/h$ and SSC from the three frames (averaged over the three OBS) for all nearshore measuring campaigns.	60
Figure 35. SSC versus $2H_0/h$ for the three nearshore measuring frames averaged over a three-day period.	60

Figure 36. Conceptual model of suspended sediment transport and intertidal beach morphological response over wave steepness. Dark grey arrows represent net sediment transport by waves, striped arrows represent net sediment transport by currents.....	61
Figure 37. Maps of the study sites with the intertidal frame and cross-shore topographic profiles indicated.	65
Figure 38. Left: The intertidal measuring frame (1 m high, 2.2 m wide) with (from left to right) the down-looking ADCP, the OBS, the ECM, and the up-looking ADCP. Right: The RTK-GNSS mounted on a beach cart.	66
Figure 39. 30-minute-averaged hydrodynamics: significant wave height, wave steepness, water level, and SSC for all the campaigns. The measured water level is supplemented with tide gauge data from Oostende Harbor for low tide.	69
Figure 40. Typical current roses for spring vs. neap tide (left vs right) and calm vs energetic conditions (top vs. bottom). Currents were measured at 35 cm above the bed at Mariakerke and currents are not included for water levels <2.39 m TAW. The shoreline orientation is indicated by the black line. Each current rose represents one tidal cycle.	71
Figure 41. Cross-shore (top) and alongshore (bottom) flow velocity at 35 cm above the bed over one tidal cycle during spring tide & calm wave conditions (left) vs. neap tide & energetic wave conditions (right), with the measured flow velocity in grey and the 10-minute averaged flow velocity in black.	72
Figure 42. Top: Comparison between SSC and wave steepness when both are averaged over a tidal cycle. Data that was affected by the nearby sediment disposal during the Spring-flat campaign was removed. Bottom: Time series of SSC (grey line) and wave steepness (black, dotted line) for all campaigns. Wave steepness was supplemented with data from the wave buoy at Raversijde to illustrate the wave conditions before the campaign.	74
Figure 43. Beach topography. Bottom: cross-shore topographic profiles at the start of each campaign in m TAW with the NHW and NLW line indicated. Middle: the standard deviation of the representative central profile (b). Top: daily volumetric changes alongshore-averaged.....	75
Figure 44. A PCA biplot between volume change and hydrodynamic forcing factors: wave steepness, maximum tidal water level, and SSC.	76
Figure 45. Daily intertidal beach volume change compared to daily-averaged wave steepness.....	78
Figure 46. Conceptual summary of the combined effects of waves through wave steepness, tide, and sediment supply on the intertidal beach volume, with checkered, white, and spotted indicating accretion, stability, and erosion respectively.....	81
Figure 47. DEM of the study site with the position of the intertidal measuring frame, cross-shore topographic profiles, the permanent TLS, and the berm, NHW, 2.5 m, and NLW line.....	87
Figure 48. Left: The intertidal measuring frame (1 m high, 2.2 m wide) with the down-looking ADCP, up-looking ADCP (not on the frame), three OBS, ECM, and up-looking ADCP. Right: the LISST.....	88
Figure 49. Tidally-averaged SSC at 30 cm above the bed based on ADCP vs OBS measurements.	89
Figure 50. Set-up of the permanent TLS at the study site.....	90

Figure 51. 30-minute-averaged significant wave height (H_{sig}) and wave steepness, cross-shore (positive velocities indicate onshore flow, negative offshore) and alongshore flow velocity (positive velocities indicate NE flow, negative SW) and SSC over depth (in m TAW) for November (left) and April (right).....	92
Figure 52. 5-minute-averaged grain size of the suspended sediment over one tidal cycle (LT = Low Tide, HT = High Tide, 18 April 2018). Grain size of the smallest 10% (D_{10}), the largest 10% (D_{90}), and the median grain size (D_{50}).....	93
Figure 53. Mean and oscillatory cross-shore suspended sediment transport at 10 cm above the bed over the first week of the November campaign (bottom) with the water level for reference (top).....	94
Figure 54. Left: Velocity skewness (30 cm above the bed) vs. wave steepness. Middle: cross-shore sediment transport vs. velocity skewness. Right: cross-shore sediment transport vs. wave steepness. Each point represents one tidal cycle. Cross-shore sediment transport was calculated over the lowest meter of the water column and is averaged for the 3 OBS.	94
Figure 55. Total cross-shore suspended load over a tidal cycle. Top: Distribution of the transport over the water column for offshore (left) and onshore (right) transport events. Bottom: Examples of the cross-shore suspended sediment load over depth for one tidal cycle when transport was maximum offshore (left) and onshore (right). Note that the x-axis are uneven.....	95
Figure 56. DoD of the first and last survey for the November (left) and April (right). ..	97
Figure 57. Daily intertidal beach volume changes (NLW – toe of the berm) for the November (left) and April (right) campaign. Measurements are lacking for 7, 11, 13-15 November and 17 April.....	97
Figure 58. Beach slope (left = November, right = April) with zones of maximum erosion/accretion indicated for days when considerable offshore (left) or onshore (right) suspended sediment transport was measured by the frame.	98
Figure 59. Schematized cross-shore beach profile with sediment transport and resulting topographic change during energetic (red, dotted) and calm (green, dashed) days. .	99
Figure 60. Cross-shore sediment transport per m beach width compared to the observed intertidal beach volume change. Points represent one day each. Lines represent a 1:1 relationship between cross-shore sediment transport and beach volume change (black) and 2x (dark grey) and 10x (light grey) over- and underestimation of the volume change.	100
Figure 61. Ground photograph of the berm following the high water of 12 November.	102
Figure 62. Hourly elevation of the toe of the berm (average of the five cross-shore profiles) compared to the wind speed and the water level on 12/13 November.....	101
Figure 63. Conceptual model of the combined effects of waves through wave steepness, tide, and sediment supply on the intertidal beach volume.	107
Figure 64. The Groenendijk study site.....	108
Figure 65. Wind-driven sediment transport at Groenendijk	111

List of tables

Table 1. Advantages and drawbacks of the most common techniques.....	22
Table 2. Hydrodynamic conditions during the events identified as energetic, with the conditions exceeding the Haerens et al. (2012) storm thresholds in bold.....	37
Table 3. Months with and without an energetic event showing beach erosion, stability, or accretion. Numbers indicate percentages.	38
Table 4. Pearson correlation matrix of the monthly volume changes at Mariakerke, profiles numbered 1-6 from west to east (top), and at Groenendijk, profiles numbered 1-5 from west to east (bottom). Correlations > 0.5 are indicated in bold.	38
Table 5. Timetable of topographic profiles with the hydrodynamic measurements for the three campaigns.....	48
Table 6. Average and maximum significant wave height, average significant wave period, average wave steepness, and average SSC for the three campaigns.....	51
Table 7. Overview of the intertidal measuring campaigns. (Note that ‘flat’ here corresponds to the developed site Mariakerke and ‘barred’ corresponds to the natural site Groenendijk).....	65
Table 8. Overview of the average (avg) and maximum (max)hydrodynamic conditions and SSC for all campaigns	70
Table 9. Occurrence of hydrodynamic conditions.	71
Table 10. Correlations between daily dominant current direction, daily-averaged wave steepness, maximum tidal water level, and the first principal component for both study sites combined. High correlations are bold (>0.5) and underlined (0.3-0.5)..	73
Table 11. Correlations between daily intertidal beach volume change, daily-averaged wave steepness, maximum water level, daily-averaged SSC, and the first two principal components for Mariakerke and Groenendijk. High correlations are bold (>0.5) and underlined (0.3-0.5).	77

List of abbreviations

ADCP	Acoustic Doppler Current Profiler
ADV	Acoustic Doppler Velocimeter
ASM	Argus Surface Meter
AWAC	Acoustic Wave And Current profiler
CCM	Conductivity Concentration Meter
DEM	Digital Elevation Model
DoD	DEM of Difference
ECM	Electromagnetic Current Meter
EDM	Electromagnetic Distance Measuring
HT	High Tide
IDW	Inverse Distance Weighting
LiDAR	Light Detection And Ranging
LISST	Laser In-Situ Scattering and Transmissometry
LT	Low Tide
NHW	Neap High Water
NLW	Neap Low Water
OBS	Optical Backscatter point Sensor
PCA	Principal Component Analysis
RTK-GNSS	Real-Time Kinematic Global Navigation Satellite System
RTK-GPS	Real-Time Kinematic GPS
SSC	Suspended sediment concentration
TAW	Tweede Algemene Waterpassing: Belgian reference level, <i>i.e.</i> relative to the lowest astronomical tide at Ostend
TLS	Terrestrial Laser Scanner
UAV	Unmanned Aerial Vehicle

List of symbols

AMP	Acoustic backscatter
a_w	Water absorption
c	Suspended sediment concentration
C_d	Drag coefficient
D_{10}	Grain size of the smallest 10% of the grains
D_{50}	Median grain size
D_{90}	Grain size of the largest 10% of the grains
EI	Echo Intensity
g	Gravitational acceleration
h	Water level
H	Wave height
H_b	Breaking wave height
H_{sig}	Significant wave height
L	Wavelength
R	Range along the acoustic beam
ρ	Water density
SSC	Suspended sediment concentration
T	Wave period
T_{sig}	Significant wave period
τ_c	Current-induced bed shear stress
TR	Tidal range
τ_w	Wave-induced bed shear stress
u	Flow velocity
u_{cross}	Cross-shore flow velocity
U_b	Near bed orbital velocity
U_{sk}	Velocity skewness
ω_f	Fall velocity



Chapter 1

General introduction

1.1. Introduction

Beaches are among the most dynamic environments and they constantly grow and erode in response to waves, currents, and wind. The intertidal zone, the zone between the low and high tide line, is particularly dynamic because it is subject to most of the wave breaking and swash action as well as to tidal and residual currents. These hydrodynamic processes lead to the transport of sediment. If gradients in sediment transport exist, this will result in erosion or deposition of sediment and thus in topographic changes. This in turn affects the hydrodynamics and sediment transport. This cycle of interactions is called beach morphodynamics (Wright and Thom, 1977, Figure 1).

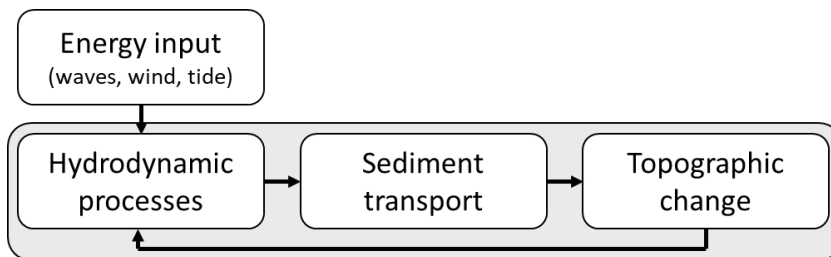


Figure 1. Beach morphodynamics system.

The intertidal beach morphodynamics has been studied extensively in the past, but it remains difficult to relate (hydrodynamic) forcing to sediment

transport and topographic response. It is not straightforward to distinguish between the multiple processes that act simultaneously on the beach, interactions between forcing and topographic response are often non-linear, time lags can occur, and sometimes critical thresholds need to be exceeded before any changes occur (Philips and Van Dyke, 2016).

Accurate field measurements are necessary to understand the intertidal beach morphodynamics, but it is especially challenging to measure sediment transport and beach topography in the intertidal zone (*e.g.* Cohn *et al.*, 2014). Several studies attempted to relate topographic changes in the intertidal zone to hydrodynamics and sediment transport (*e.g.* Sedrati and Anthony, 2007, Masselink *et al.*, 2008, Masselink *et al.*, 2009) but measured sediment transport rates are often in a different order of magnitude or even in a different direction than what topographic changes suggest. Consequently, there are still important gaps in our knowledge of the intertidal beach morphodynamics.

A profound knowledge of the intertidal beach dynamics is necessary because the intertidal zone is a key area for coastal protection at many beaches worldwide (Simm, 1996, Doody, 2012, Hanley, 2014). During storms the wave energy is reduced across the intertidal zone and the sediment in this zone serves as a buffer for erosion of the dry beach and dunes. Sediment that is eroded during storms is generally transported back to the beach during calm conditions. A good understanding of the resilience of the intertidal zone is crucial to optimize coastal protection. This becomes increasingly important as sea levels are rising and the frequency and magnitude of extreme weather events are increasing due to climate change (MacDonald and O'Connor, 1995, de Winter *et al.*, 2013).

Resilience is defined here as the ability to adapt to changing conditions and to withstand, or rapidly recover from, disruptions due to disasters. The determination of the resilience capacity is complex. Recovery often takes place over several months or even years (*e.g.* Coco *et al.*, 2013), but there are only a few datasets that cover such a long period with frequent topography measurements. Furthermore, beach erosion is not always the result of single, isolated disruptions (*i.e.* storms) but often stems from several smaller events that follow each other (Klein *et al.*, 1998). In general, what is lacking are holistic studies to coastal resilience on a medium (seasonal to monthly) to small (daily) scale on real cases. Especially the forcing factors behind beach recovery are still poorly understood. Storm impact has been studied on several occasions (*e.g.* Haerens *et al.*, 2012, Lanckriet *et al.*, 2015, Kolokythas *et al.*, 2016 for the Belgian coast) but small to medium scale studies to beach accretion are very much lacking (Maspataud *et al.*, 2009). In this thesis the hydrodynamic conditions resulting in erosion and accretion of the intertidal zone will be investigated for the macro-tidal, sandy coast of Belgium.

1.2. Study area

The Belgian coast is situated at the southern edge of the North Sea basin (Figure 2). It has a total length of 65 km and a southwest-northeast orientation ($235\text{-}55^\circ$). The current Belgian coastal barrier was shaped after the last ice age when the global sea level was rapidly rising and the Flemish plain was flooded (10,000-5,000 years ago). The sandy beaches that can be found nowadays have been built up over thousands of years by wave action, tides, and wind (Houthuys *et al.*, 1993).

Offshore numerous sandbanks called “The Flemish Banks” can be found (Figure 2). These can be subdivided into tidal banks and shoreface-connected ridges. The tidal banks are found further from the coast and they are formed by strong tidal currents. The shoreface-connected ridges are located closer to the coast and have an angle of $20\text{-}50^\circ$ with respect to the dominant wind-driven flow during storms. Both are tens of kilometers long and up to a few kilometers wide (van Oyen *et al.*, 2013). The bank closest to the shore, The Stroombank, has a maximum elevation of -3 m TAW (Belgian reference level, *i.e.* relative to the lowest astronomical tide).

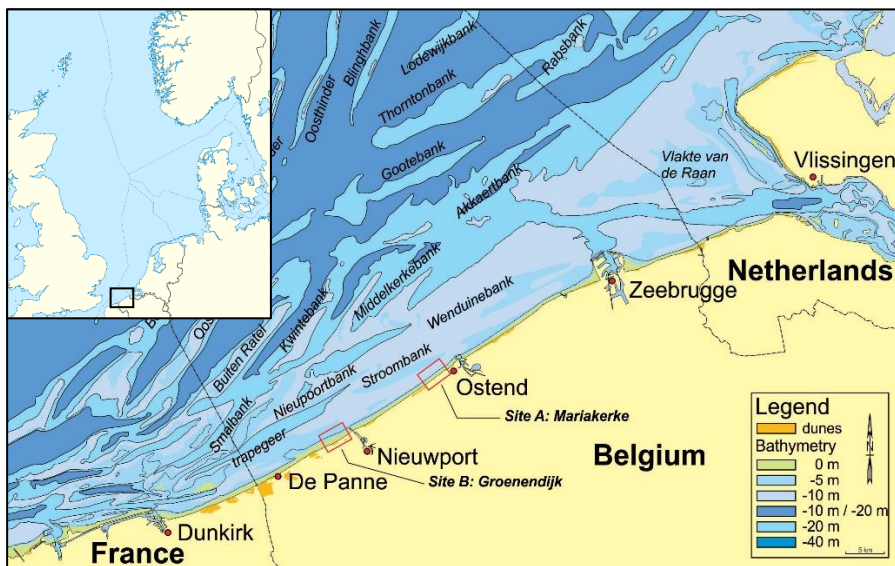


Figure 2. Overview map of the Belgian coast with the study sites (Groenendijk and Mariakerke) indicated.

The focus of this study is on the intertidal zone, which is defined as the area between the Neap High Water (NHW; +4.39 m TAW) and Neap Low Water (NLW; +1.39 m TAW) line (Figure 3). The intertidal zone is up to 600 m wide in the southwest and up to 200 m in the northeast of the Belgian coast. It is gently-sloping along the entire coast, but the slope increases from 1 % to 2 % towards the northeast. Hard coastal protection measures are present along approximately 60% of the Belgian coast (Lebbe *et al.*, 2008). The beaches in the southwest are more natural than the beaches in the northeast. Since a few decades the focus for coastal protection has shifted more towards soft measurements and nowadays small-scale beach scrapings and large-scale beach and underwater nourishments are carried out regularly. The beaches are composed of sand with a median grain size (D_{50}) of 250 μm under natural conditions, but the sand gradually becomes coarser, up to 400 μm , towards the northeast due to a natural gradient and an increase in nourishment activities (Deronde *et al.*, 2008).

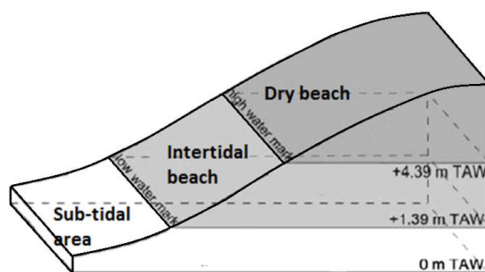


Figure 3. Different zones on a beach (modified from Vito and Afdeling Kust, 2009).

The tidal range along the Belgian coast varies between 3 m at neap and 5 m at spring tide, and the beaches are therefore on the boundary between meso-tidal (2-4 m) and macro-tidal (> 4 m). Taking the limited wave height into account, the Belgian coast is considered macro-tidal in this thesis, following the reasoning of Masselink and Short (1993). The large tidal range results in strong tidal currents of over 1 m/s in the nearshore area (Haerens *et al.*, 2012). Wave energy is medium with an average wave height of 0.5-1 m and an average wave period of 4 s. Offshore waves are mainly driven by westerly (WSW-NW) winds and the dominant offshore wave directions are WSW and N (Figure 4). In combination with the orientation of the shoreline this results in a longshore drift towards the northeast. During storms SW, W, or NW waves prevail. Waves are typically short-crested due to the shallow water depth and relatively short fetch. Storm surges of over +5.5 m TAW can occur during north and northwestern storms (Haerens *et al.*, 2012).

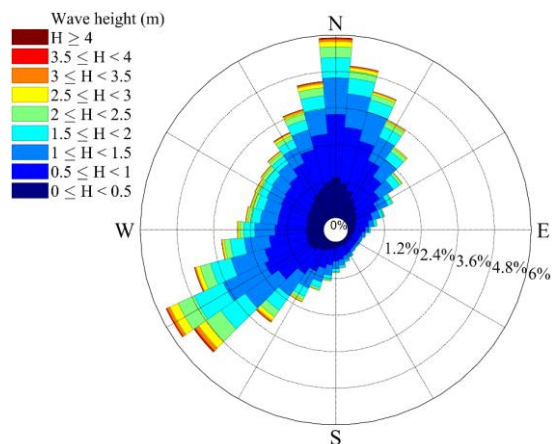


Figure 4. Offshore wave rose based on wave measurements from the Westhinder wave buoy (Appendix A) from 2000-2017.

Two study sites were investigated. The first is Mariakerke, a managed beach with a featureless intertidal zone, near Ostend. The second is Groenendijk, a more natural beach characterized by ridges and runnels, near Nieuwport (Figure 2).

At Mariakerke a seawall and groins have been present for several centuries. Additionally, small-scale beach nourishments and beach scrapings have been carried out since some decades and large beach and underwater nourishments are regularly carried out since 2006 (Houthuys, 2012). The last nourishments took place in 2014 when 900.000 m³ was added to the beach and 300.000 m³ to the shoreface along a coastal stretch of 2-4 km. The intertidal beach is featureless (Figure 5), but the transition to the dry beach is characterized by a steep slope of approximately 2 m high (37 %). The intertidal beach is 160 m wide, and gently-sloping (2 %). It consists of well-sorted, medium sand with a D_{50} of 325 μm . This is coarser than the natural grain size (150-250 μm) as a result of the nourishments. The natural trend of the beach at Mariakerke is erosive (-8 m³/m/yr), but thanks to the nourishments the beach has been growing over the past decades (+4 m³/m/yr; Houthuys 2012).

Groenendijk is a natural beach where no protective measures have been taken. It is characterized by four intertidal bars (ridges and runnels) of 5 to 60 cm high and is connected to a dune area (Figure 6). The intertidal beach is 290 m wide and gently-sloping (1 %). The sediment on the beach is medium fine sand with a D_{50} of 200 μm . The beach at Groenendijk has been growing steadily over the past decades (+18 m³/m/yr, Houthuys, 2012).



Figure 5. Ground pictures of the beach at Mariakerke.



Figure 6. Ground pictures of the beach at Groenendijk.

1.3. Objectives and study approach

To determine the resilience of the intertidal zone it is necessary to unravel the hydrodynamic forcing factors behind beach growth and erosion. Reliable field data covering both calm and energetic conditions is necessary for this, but accurate field measurements in the intertidal zone are scarce. The general aim of this study is to investigate the intertidal beach morphodynamics based on extensive measurements of hydrodynamics, sediment transport, and beach topography and to obtain a conceptual model of hydrodynamic forcing and topographic response.

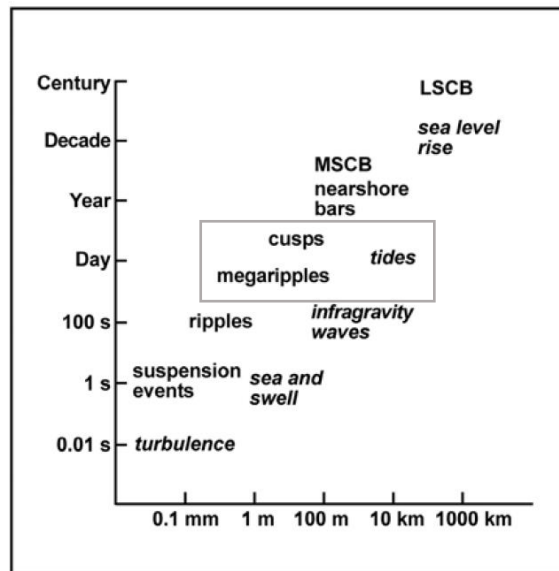


Figure 7. Temporal and spatial scales of hydrodynamics (*italic*) and morphology (*normal*). The grey box represents temporal and spatial scales covered in this study (adapted from Ruessink, 1998).

The components that influence the beach morphodynamics cover many spatial and temporal scales, from turbulent vortices to sea level rise and from individual ripples to the shoreline position (Figure 7). To achieve the general aim, specific research objectives are defined to understand the beach morphodynamics from a medium scale (seasonal to weekly) to a small (daily) scale:

1. Investigate and quantify the spatial and temporal variability of the intertidal beach topography on a medium scale (*i.e.* seasonal to monthly);
2. Relate nearshore hydrodynamics and sediment dynamics to changes in intertidal beach topography on a medium scale (*i.e.* monthly);
3. Relate hydrodynamics and sediment dynamics in the intertidal zone to changes in intertidal beach topography on a small scale (*i.e.* daily);
4. Quantify the net sediment transport from or to the intertidal zone on a daily scale and compare it to the hydrodynamic conditions and to topographic changes in the intertidal zone.

An overview of the topographic, hydrodynamic, and sediment transport data that was analyzed is given in Figure 8. Monthly topographic surveys, wave buoy and tide gauge data, and three two-month nearshore measuring campaigns were analyzed to investigate the medium scale morphodynamics. Three fortnight measuring campaigns were carried out at both sites during which hydrodynamics, sediment transport, and beach topography were measured to investigate the daily morphodynamics. Additionally, the beach topography was monitored semi-hourly with a terrestrial laser scanner during more than a year at Mariakerke.

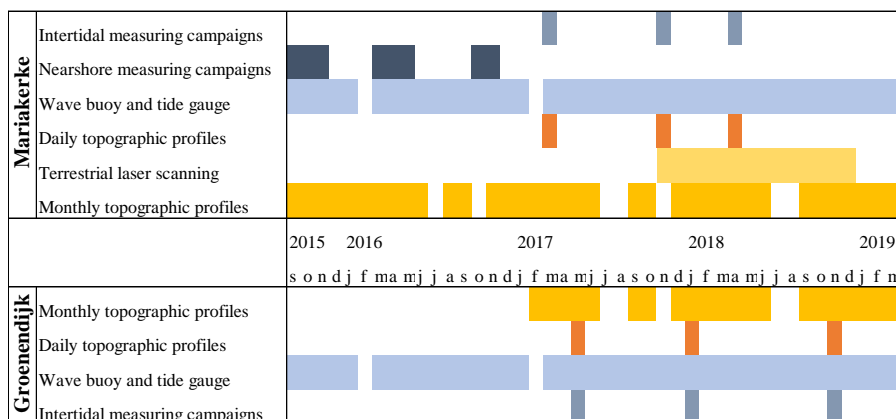


Figure 8. Summary of the investigated topographic and hydrodynamic data at Mariakerke and Groenendijk.

1.4. Outline of the thesis

This thesis presents a thorough investigation and quantification of the hydrodynamic processes, sediment transport, and the resulting topographic changes in the intertidal zone at Groenendijk and Mariakerke. Chapter 1 is a general introduction on intertidal beach morphology, followed by the objectives of this study, a presentation of the study area, and the outline of this thesis. Chapter 2 provides an extensive literature review of methodologies to measure sediment transport and beach topography in the intertidal zone. Chapter 3 to chapter 6 unravels the intertidal beach morphodynamics from a medium (*i.e.* seasonal to monthly) to small (*i.e.* daily) scale (Figure 9), based on measurements along the Belgian coast.

Chapters 3 and 4 focus on the medium scale beach morphodynamics and are based on monthly beach topography measurements. In chapter 3 spatial and temporal trends in beach topography are investigated based on more than three years of monthly topographic profiles. Seasonality in the hydrodynamic conditions and beach topography and the impact of energetic events on the beach topography are studied. Chapter 4 focuses on the effect of nearshore hydrodynamics and sediment dynamics on the intertidal beach topography based on six months of nearshore measurements and monthly cross-shore topographic profiles.

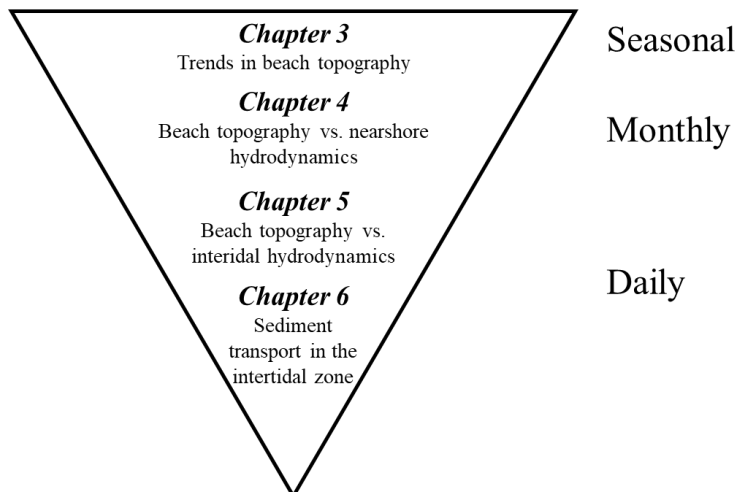


Figure 9. Outline of the thesis.

Chapters 5 and 6 present the investigation of the morphodynamics of the intertidal zone on a daily scale. Chapter 5 discusses daily topographic changes in relation to hydrodynamic forcing based on six fortnight measuring campaigns in the intertidal zone. Chapter 6 describes sediment transport in the intertidal zone and the relation between hydrodynamics, sediment transport, and beach topography at Mariakerke. Furthermore, chapter 6 gives a more detailed explanation of topographic changes in the intertidal zone of Mariakerke based on the terrestrial laser scanning surveys.

Finally, Chapter 7 synthesizes the main findings of this work, highlighting the role of tide in the intertidal beach morphodynamics of macro-tidal beaches with medium wave energy. Recommendations for coastal management, future intertidal measuring campaigns, and future research topics are given. The main findings of this study are presented in a conceptual model.

Chapter 2

Literature review: optimizing measurements of sediment transport in the intertidal zone*

2.1. Introduction

The intertidal beach, the zone between low and high tide (Figure 10), is very dynamic. It is subject to most of the wave breaking and swash action, resulting in high sediment transport rates. Besides the effect of waves, sediment is also transported by tidal currents, residual currents, and wind. If gradients in sediment transport exist, this will result in either erosion or deposition of sediment, which in turn will influence the hydrodynamics and sediment transport. This cycle of marine (and aeolian) forcing, sediment transport, and beach morphology is referred to as the beach morphodynamics (Masselink *et al.*, 2011).

Sediment transport in the intertidal zone has been a topic of scientific interest since the middle of the 20th century (*e.g.* Bagnold, 1947). Most of the research was directed to theoretical studies and laboratory wave tank investigations (Hails, 1974), but there were also a few pioneering field studies in the 20th century (*e.g.* Inman, 1949, Terry, 1951, Watts, 1953, Caldwell, 1956, Thornton, 1968, Komar and Inman 1970, Jaffe *et al.*, 1984, Kraus, 1987). It was soon acknowledged that restrictive physical factors, such as large waves and heavy turbulence, limited in-situ measurements and that this was most likely the cause of the poor correlations that were found between field data and laboratory results and theoretical predictions (Hails, 1974).

* Submitted as: Brand, E., Chen, M., Montreuil, A-L., 2019. Optimizing measurements of sediment transport in the intertidal zone. *Earth-Science Reviews*, submitted

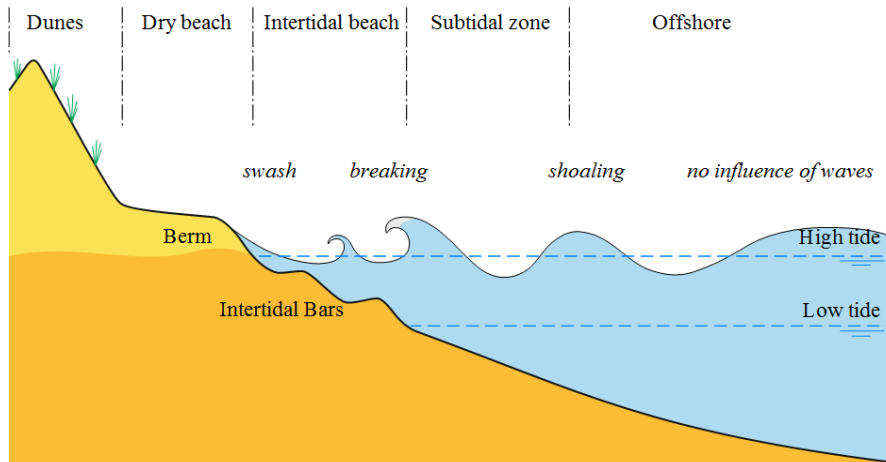


Figure 10. Schematized wave propagation across the different beach zones.

Techniques to measure sediment transport evolved continuously and advanced sensors have been developed (*e.g.* Mikkelsen and Pejrup, 2001, Turner *et al.*, 2008). As a result, our qualitative understanding of sediment transport in the intertidal zone has greatly improved (*e.g.* Aagaard *et al.*, 2004, Aagaard *et al.*, 2005, Houser *et al.*, 2006). The two main modes of sediment transport are bed load transport and suspended load transport. Bed load transport is defined as gliding, rolling, and saltating particles in close contact with the bed, while suspended load transport is defined as the transport of particles in the water column by turbulence-induced drag forces (Van Rijn, 1993). Sediment transport rates are generally highest close to the bed (Kraus, 1987, Tonk and Masselink, 2005, Cartier and Héquette, 2015), but energetic waves or strong tidal currents may mix the sediment through the entire water column. In general, it is acknowledged that cross-shore sediment transport is controlled by the balance between onshore transport due to wave skewness and offshore transport by undertow, but the ratio of onshore/offshore transport is determined by the wave energy (*e.g.* Voulgaris, 1996, Masselink *et al.*, 2008). This difference between onshore and offshore transport over individual waves builds up over a tidal cycle and may result in large topographic changes.

Quantifying net sediment transport remains difficult, while reliable and accurate measurements of sediment transport rates are essential to better understand intertidal beach morphodynamics, to manage the beach, and to calibrate and validate sediment transport models. Field measurements are

often labour intensive, time consuming, and costly. Thus, it is necessary to optimize field measurements to obtain accurate results with limited resources. To our knowledge, no literature exists that reports the advantages and disadvantages of techniques to measure sediment transport in the intertidal zone of sandy beaches. Therefore, this paper provides an in-depth review of measuring techniques, in terms of their advantages, disadvantages, and performance in the field, which leads to some recommendations for future measuring campaigns in the intertidal zone. The accuracy of measured transport rates cannot be determined or validated without cross-checking of sediment transport rates from different methods or approaches. Therefore, this paper mainly addresses studies that compared measured sediment transport rates to transport rates derived from topographic change and/or predictive formulas.

2.2. Measuring techniques to quantify sediment transport

2.2.1. Suspended load

The first measurements of sediment transport date back to the middle of last century. The first techniques that were used are extensively described by Hails (1974). Figure 11 illustrates the evolution of the most common or promising techniques since then, based on the references used in this section. Solid lines represent periods of time when techniques were used in intertidal measuring campaigns. Dashed lines indicate that techniques were upcoming or that the use decreased. The main shift in sediment transport measurements has been from manual sampling to the use of sensors. In this section the techniques to measure suspended sediment transport will be described, in the next section techniques to measured bed load or total load are presented.

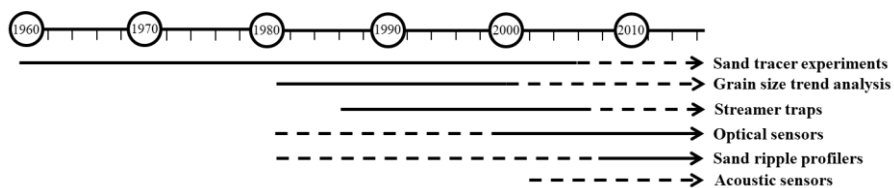


Figure 11. Timeline of measuring techniques for sediment transport from the 1960s until now. Dashed lines indicate limited use.

Suspended sediment transport can be quantified by combining measurements of flow velocity and suspended sediment concentration (SSC), assuming that sediment particles have the same velocity as the water that carries them. Flow velocity measurements are most often carried out with **acoustic** (*e.g.* Acoustic Doppler Current Profilers, ADCP, and Acoustic Doppler Velocimeters, ADV) or **electromagnetic current meters** (ECM). Techniques to measure SSC are discussed below.

Taking water samples and filtering them is a classic technique to determine SSC. Many samplers, such as simple bottles, trap samples, or more advanced samplers like pump samplers exist. However, taking water samples is very time-consuming and it is difficult to take water samples in the intertidal zone, especially under breaking waves (Hails, 1974).

Since the eighties, **optical backscatter sensors** (OBS) are most often used to determine SSC (*e.g.* Jaffe *et al.*, 1984, Aagaard *et al.*, 2004, Aagaard *et al.*, 2005, Houser *et al.*, 2006, Masselink *et al.*, 2009). These sensors were developed by Downing *et al.* (1981). They emit an infra-red light and record its backscatter, which is a measure for turbidity. They measure with a frequency up to 10 Hz, so they are suitable to study very fast variations in SSC. They can be deployed in the field for a long time (weeks to months). However, they are subject to biofouling and thus need to be cleaned regularly or they need to be equipped with a mechanical wiper. A limitation of OBS is that they only perform point measurements, so multiple OBS are needed to measure a profile of SSC over the water column.

Recently attempts have also been made to measure the SSC in the intertidal zone based on **acoustic backscatter** (Aagaard *et al.*, 2012). Before, this method was only used in river, estuary, and bay environments (*e.g.* Gartner, 2004, Merckelbach and Ridderinkhof, 2006, Weiss *et al.*, 2015). The major benefit of acoustic sensors is that they provide a vertical profile of SSC. A limitation is that acoustic sensors are not capable of detecting particles that are smaller than the wavelength of the acoustic pulse, which depends on the type of acoustic sensor.

The response of optical and acoustic sensors strongly depends on particle characteristics, such as size, shape, and colour. The sensors thus need to be calibrated with samples from the study site to convert backscatter to SSC. A major problem regarding this calibration is that it is specific for the particle size of the sample. Both optical and acoustic sensors are not able to differentiate between changes in concentration and changes in particle size distribution. Optical sensors are more sensitive to clay and their response to particles of 2 μm is 50 times greater than to particles of 100 μm for the same concentration (Battisto *et al.*, 1999). Acoustic sensors, on the other hand, are more sensitive to sand (Thorne *et al.*, 1991).

Furthermore, acoustic sensors are sensitive to turbulence (Nauw *et al.*, 2014). Under strong turbulent conditions scatterers may no longer be randomly distributed and the Kolmogorov wavelength can become smaller than the wavelength of the acoustic pulse. In that case, small scale turbulent eddies of Kolmogorov scale disturb the measurements of SSC. Therefore, an additional calibration of acoustic sensors is needed under turbulent conditions, as described in Merckelbach and Ridderinkhof (2006). Only a few studies have used acoustic sensors to measure SSC in turbulent conditions (Nauw *et al.*, 2014). An example of the effect of turbulence on measurements of SSC is given in Figure 12, for which it is assumed that the OBS results are reliable, which was validated with water samples. It indicates that acoustic sensors may significantly overestimate SSC under turbulent conditions. It is uncertain to what extent acoustic sensors can be used in the highly dynamic intertidal zone.

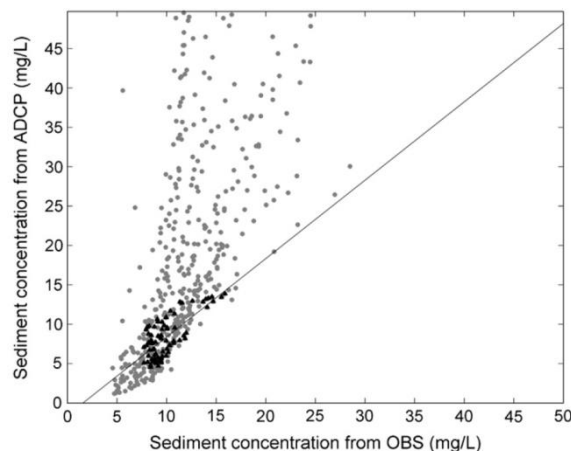


Figure 12. SSC derived from acoustic backscatter compared SSC derived from OBS. These measurements were carried out in a tidal inlet, the Marsdiep inlet (The Netherlands). Black (grey) points represent data for which the depth-averaged velocity < 0.5 m/s (> 0.5 m/s). Drawn is the linear fit through the black data points (Nauw *et al.*, 2014).

2.2.2. Bed load and total load

From field measurements it is known that bed load transport can make up more than half of the total load transport (Tonk and Masselink, 2005, Masselink *et al.*, 2008). Measurements of bed load transport are thus key when studying the intertidal beach morphodynamics. However, it is difficult

to measure bed load transport in-situ. Instead, predictive formulas are often used to estimate bed load transport (*e.g.* Sedrati and Anthony, 2007, Masselink *et al.*, 2009). Both field techniques and predictions to quantify bed load transport are discussed here.

Firstly, measuring techniques exist to get insight in the spatial pattern of the total load transport. **Grain size trend analysis** is a relatively easy tool, suitable for marine environments in which there is no a priori information on sediment transport (*e.g.* Masselink, 1992, Pedreros *et al.*, 1996, Delgado *et al.*, 2002, Poizot *et al.*, 2006). For this analysis, invented by McLaren (1981), grain size, sorting, and skewness in grain size are determined from sediment samples. It is assumed that spatial variations in grain size parameters are the result of sediment transport processes such as abrasion, selective transport and mixing of sediment (McLaren, 1981, McLaren and Bowles, 1985, Gao and Collins, 1991, Le Roux, 1994). McLaren (1981) stated that the sediment will become better sorted and either finer and more negatively skewed or coarser and more positively skewed in the direction of transport. This theory was later modified by Gao and Collins (1991, 1992, 1994) for multi-directional sediment transport. This resulted in not two, but eight possible cases of grain size trends (Gao and Collins, 1994). Le Roux (1994) modified the grain size trend analysis for when sampling locations are not in a perfect grid. A limitation of this method is that it is not quantitative. Furthermore, the period of time that is represented by the calculated transport directions is uncertain (Gao and Collins, 1992).

Sand tracer experiments can be used to monitor patterns of sand transport on a shorter timescale. Beach sand is tagged with a fluorescent paint and after a certain amount of time beach sediment samples are taken for which the fraction of tagged grains is determined (Medvedev and Aibulatov, 1956, Wright, 1962). Tracer experiments are usually carried out over a few hours up to one tidal cycle, because the sand will be spread too far afterwards. Although in some cases they can be used to quantify sediment transport (Komar and Inman, 1970, Fernández-Fernández *et al.*, 2016), these experiments are often qualitative due to low overall tracer recovery (Levoy *et al.*, 1997, Voulgaris *et al.*, 1998, Stépanian *et al.*, 2001, Tonk and Masselink, 2005, Sedrati and Anthony, 2007). Nevertheless, they provide valuable insights in the transport direction and they can be used to support suspended sediment transport and topographic measurements (Tonk and Masselink, 2005, Fernández-Fernández, 2016). An example of this is Figure 13, which illustrates how a sand tracer experiment revealed changes in sediment transport direction across a beach. An added value of both grain size trend analysis and tracer experiments is that they reveal total load transport, including the bed load transport which remains difficult to measure (Tonk and

Masselink, 2005). Furthermore, they can be used in both calm and energetic conditions. A downside is that sand tracer experiments are time-consuming.

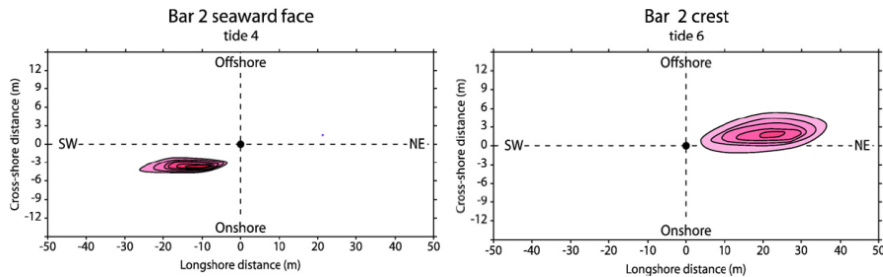


Figure 13. Contour plots showing the spatial distribution of sand tracers from a central injection point (dot) at different locations across a barred beach in Northern France. The tracer migration is represented by the pink scale (Sedрати and Anthony, 2007).

Secondly, techniques exist to quantify bed or total load transport. One of the oldest techniques to measure suspended and bed load transport are **streamer traps**, or total load traps, developed by Kraus (1987). These traps are made of a long, rectangular, sieve cloth bag that can be mounted on a steel rack. In the past they were often used to measure the vertical and lateral distribution of the sand transport rate in the intertidal zone (*e.g.* Levoy *et al.*, 1994, Hughes *et al.*, 1997, Masselink and Hughes, 1998). Nowadays their use is limited due to some drawbacks associated with this method. For instance, the traps need to be emptied manually every few minutes, which makes this method labour intensive and unsuitable for long-term measurements (Kraus, 1987, Tonk and Masselink, 2005). Also, the use of streamer traps is restricted to the intertidal and lower swash zone and to calm wave conditions because they need to be deployed manually (Kraus, 1987, Tonk and Masselink, 2005). Furthermore, streamer traps are prone to oversampling due to initial stirring and undersampling due to gaps between the bed and the sampler mouth and obstruction of bed load transport (Masselink *et al.*, 2009).

Conductivity sensors (Conductivity Concentration Meter: CCM) were developed to measure high concentrations of sand (< 2 kg/l, Ribberink and Al-Salem, 1992) to quantify sediment concentrations in the direct vicinity of the bed. These sensors have mainly been deployed to study sediment transport under sheet flow in laboratory studies (McLean *et al.*, 2001, Lanckriet *et al.*, 2013). Although these sensors have been used in the field (Dohmen-Janssen and Hanes, 2002), they are more suitable for laboratory experiments as their elevation above the bed should be constant.

Another method to measure bed load transport is the **bed-form tracking of sand ripples**, where acoustic profilers (side scan sonar) measure bed profiles at successive time intervals. From these scanned profiles the ripple migration is known from which bed load transport rate can be computed. This is thus an indirect way to estimate bed load transport based on the migration of bed forms and as a result the obtained transport rates may not always be accurate. This method has been tested in flumes (Simons *et al.*, 1965, Thorne *et al.*, 2009) and river or estuary environments (Havinga, 1982, Bell *et al.*, 1998) and has more recently also been used in a beach environment (Masselink *et al.*, 2008).

Besides measuring techniques, several **predictive formulas** for both suspended and bed load exist (*e.g.* Inman and Bagnold, 1963, CERC, 1984, Bailard, 1984, Kamphuis, 1991, Van Rijn, 2014). Some of them are based on wave characteristics (CERC, 1984), sometimes in combination with beach characteristics (Kamphuis, 1991). An advantage of these formulas is that they can be used across the entire intertidal zone. The main drawback of these formulas is that they should be calibrated with empirical coefficients, so the quality of the results depends amongst others on the quality of field data. In ideal conditions the CERC (1984) formula has an accuracy of $\pm 30\text{-}50\%$ (Wang *et al.*, 2002) and the Kamphuis (1991) formula 40% (Schoonees and Theron, 1996). Other simpler formulas assume that the sediment flux is related to the velocity to a power, usually 3 or 5. The Bailard (1984) equation, based on Bagnold's (1963) energetic approach to sediment transport is one of the most widely applied formulas of this type. It can reach an accuracy of 70% (Schoonees and Theron, 1995) and it works best for energetic conditions (Thornton *et al.*, 1996, Gallagher *et al.*, 1998), although it can also work for calm conditions (Hoefel and Elgar, 2003). Formulas based on flow velocity are less applicable to the higher intertidal and swash zone (Butt *et al.*, 2005, Masselink and Russell, 2006). The use of predictive formulas is thus often limited to specific conditions and even in ideal conditions they can be highly inaccurate.

2.2.3. Net transport reflected on topographic changes

Net sediment transport rates can also be derived from topographic changes, hence the most common and most promising techniques to measure beach volume changes are described in this section. Beach topography has been measured for centuries, but the first measurements with an accuracy in the order of centimeters date back to the 1960s. Figure 14 presents a timeline of the measuring techniques that have been used since then based on the references mentioned in this section. Surveying profiles has been popular

since the beginning. In the 1960s rods were used to measure profiles of beach topography. Although still functional, rods have largely been replaced by the more accurate and time efficient Real-Time Kinematic GPS (RTK-GPS) and total station since the 2000s. Recently, techniques to measure the topography with a higher spatial or temporal resolution, such as the terrestrial laser scanner (TLS), have been developed.

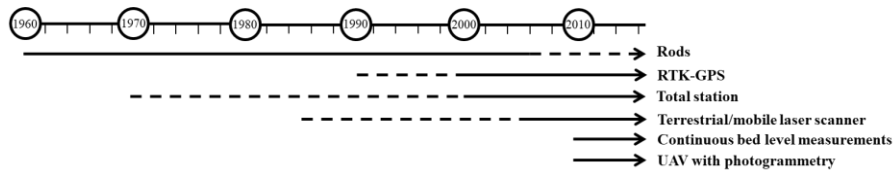


Figure 14. Timeline of measuring techniques for intertidal beach topography from the 1960s until now. Dashed lines indicate limited use.

A broad range of methods exist to measure topography, but not all are suitable for the intertidal beach. Emery (1961) proposed a simple method to measure beach topography using two graduated **rods**. Their alignment and intersection with the horizon allows determining differences in bed level. The principle has stayed the same over time, although some improvements have been made (Andrade and Ferreira, 2006). The measurement errors associated with rods are not well documented, but they are less accurate than modern techniques. However, thanks to the simplicity and the low cost, rods have long been used to survey cross-shore beach profiles (e.g. Houser *et al.*, 2006). Nowadays, profiles are more often measured with a **total station** (Masselink *et al.*, 2008, Aagaard *et al.*, 2012) or an **RTK-GPS** (Aagaard *et al.*, 2005). A total station has a vertical accuracy in the order of millimeters. The accuracy of the RTK-GPS is 2-3 cm for the x, y and z coordinates combined, but is more practical to use than the total station. A GPS can also be mounted on a vehicle for faster surveys (e.g. Parisot *et al.*, 2009). Typically, these methods are used to survey cross-shore profiles, resulting in 2D data.

It is popular to measure cross-shore profiles because it is relatively easy and equipment is low-cost. Generally, one central profile with additional profiles on each side is surveyed from the low water line to the foot of the dune every day during low tide. However, large differences in topographic response to the incoming hydrodynamics may exist alongshore (Eamer and Walker, 2013, Fernández-Fernández *et al.*, 2016, Cohn *et al.*, 2017). Therefore, profiles may be insufficient to represent the beach morphology, especially when the profile spacing is more than 100 m (Swales, 2002, Bernstein *et al.*, 2003, Pietro *et al.*, 2008). Theuerkauf and Rodriguez (2012)

studied the impact of transect location on the calculated volumes. They found that the profile-based volumetric change becomes inaccurate with the increase of along-beach morphologic variability, such as the presence of beach cusps, beach nourishments, or pockets of anomalous erosion/accretion.

The development of **terrestrial laser scanning** technology has enabled to collect high resolution, instantaneous, and accurate topographic data of large areas in 3D. The system composed of a transmitter that generates a laser beam which is reflected back to a receiver after hitting the bed surface. It can be mounted on a static or mobile platform, like a vehicle (Incoul *et al.*, 2014). When the laser is used statically an additional rotation axis can also make the sampling three-dimensional (Jaud *et al.*, 2011, Vousdoukas *et al.*, 2014, Vos *et al.*, 2017, Vos *et al.*, 2019). TLS have been used to measure beach topography profiles since the late 1980s (Huising and Pereira, 1998). Major advantages of laser scanning are that the accuracy is a few millimeters and that high-density topographic measurements are obtained. The main limitation is that data processing is time consuming, because large datasets are generated. With LiDAR (LIght Detection And Ranging, airborne laser scanning) and satellite imagery it is also possible to survey beach topography with a high point density, but the high costs make these options less suitable for local scales and rapid or frequently repeated surveys.

Recently, improvements have also been made in determining the beach topography with **photogrammetry**, based on measurements with a photo camera on an Unmanned Aerial Vehicle (UAV; J.A.J. Berni *et al.*, 2009, Delacourt *et al.*, 2009, Jaud *et al.*, 2011, Westoby *et al.*, 2012). With UAV local scale, rapid, and frequent surveys are economically feasible for the coastal zone, but a drawback is that drones typically cannot be used in energetic wind conditions.

2.2.4. Advantages and drawbacks of the most common techniques

The most common measuring techniques to quantify sediment transport in the intertidal zone were introduced in this section. Other techniques exist for laboratory experiments or to measure beach topography on a larger scale (e.g. LiDAR and Argus), but only techniques that were previously used to quantitatively compare measured sediment transport and beach volume changes were included here. The advantages and drawbacks of the techniques mentioned that are most common or promising for measuring sediment transport in the intertidal zone are summarized in Table 1.

Table 1. Advantages and drawbacks of the most common techniques.

		Advantages	Drawbacks
Suspend load	Water samples	<ul style="list-style-type: none"> • Low cost • Simple 	<ul style="list-style-type: none"> • Time-consuming • Inaccurate under breaking waves
	Optical backscatter	<ul style="list-style-type: none"> • Accurate 	<ul style="list-style-type: none"> • Only point measurements • Sensitive to grain size
	Acoustic backscatter	<ul style="list-style-type: none"> • Full water column 	<ul style="list-style-type: none"> • Sensitive to grain size • Sensitive to turbulence
Bed load or total load	Grain size trend analysis	<ul style="list-style-type: none"> • Relatively easy • Gives general idea about the sediment transport pattern 	<ul style="list-style-type: none"> • Not quantitative
	Sand tracer experiments	<ul style="list-style-type: none"> • Gives insight in transport patterns • Total load • Can be applied under all conditions 	<ul style="list-style-type: none"> • Time-consuming • Often not quantitative • Result depends on the used material
	Streamer traps	<ul style="list-style-type: none"> • Gives insight in the vertical and lateral distribution of sediment transport 	<ul style="list-style-type: none"> • Time-consuming • Restricted to low water levels • Restricted to calm conditions • Rarely quantitative
	Conductivity sensors	<ul style="list-style-type: none"> • Can measure high concentrations close to the bed 	<ul style="list-style-type: none"> • Needs to be at a constant elevation above the bed
	Bed-form tracking of ripples	<ul style="list-style-type: none"> • Measures (part of) the bed load transport 	<ul style="list-style-type: none"> • Has not often been used in the intertidal zone yet, needs to be validated
	Rods	<ul style="list-style-type: none"> • Simple • Low cost 	<ul style="list-style-type: none"> • Only profiles • Not very accurate • Limited to low tide
Beach topography	Total station	<ul style="list-style-type: none"> • Accurate 	<ul style="list-style-type: none"> • Only profiles • Limited to low tide
	RTK-GPS	<ul style="list-style-type: none"> • Accurate • Easy to use 	<ul style="list-style-type: none"> • Only profiles • Limited to low tide
	Laser scanning	<ul style="list-style-type: none"> • Accurate • Full beach topography 	<ul style="list-style-type: none"> • Time-consuming • Expensive • Limited to low tide
	Photogrammetry	<ul style="list-style-type: none"> • Fast acquisition 	<ul style="list-style-type: none"> • Can only be applied in calm weather • Limited to low tide

2.3. Cross-checking suspended load measurements

Suspended sediment transport is generally measured with flow velocity sensors and an array of OBS at the low water line. Many variations to this measuring set-up exist. To cross-check the measured transport quantitatively it is usually averaged over a tidal cycle and compared to volume changes observed in the intertidal zone. Most studies that compared sediment transport and beach volume changes found similar trends between the two, but they were often only related in a qualitative way (Aagaard *et al.*, 2004, Aagaard *et al.*, 2005, Houser *et al.*, 2006, Sedrati and Anthony, 2007). Here, quantitative comparisons will be reviewed in order to determine the best set-up to quantify suspended sediment transport.

Jaffe *et al.* (1984), a pioneer in this type of research, quantitatively compared hourly bed level changes across a profile with changes predicted from convergences and divergences in cross-shore suspended sediment transport. This was done based on observations with five OBS at different elevations (0.1-0.6 m above the bed) during a high tide in storm conditions. Their number of observations was limited to six and only three of these observations were in the intertidal zone, the others were located in the subtidal. The measured suspended sediment fluxes were sometimes in a different direction and often of a different magnitude than what the topographic changes suggest. Nevertheless, profile changes and suspended sediment fluxes generally exhibited a similar trend, which made Jaffe *et al.* (1984) among the first to prove the value of OBS in intertidal beach research. This was later reaffirmed by many other studies, for example based on comparisons between OBS and streamer traps (*e.g.* Tonk and Masselink, 2005).

Years later, Masselink *et al.* (2008) also quantitatively compared measured sediment transport rates and beach volume changes. They measured suspended sediment transport with OBS at five locations across the intertidal zone and bed load transport with two sand ripple profilers. Volume changes were derived from three cross-shore topographic profiles. Topographic changes were found to be 1.5 to 3 times larger than the net sediment transport. Although this is not a perfect agreement, it is in the same direction and order of magnitude. These good results were attributed to the inclusion of the sand ripple profilers and the use of 13 OBS over 20 cm at one of the frames. This high coverage allowed to accurately estimate SSC over this distance. Such a small array of OBS is easily realised and may be sufficient when suspended sediment transport is concentrated near the bed. Recently, the **Argus Surface Meter** (ASM) was developed which is even more convenient to measure SSC

over a small water column. It has an array of optical sensors embedded and is especially designed to measure several decimeters of the water column with a centimeter interval. This equipment has been used in rivers (Furgerot *et al.*, 2016), lakes (Vijverberg *et al.*, 2011), estuaries (Albers and von Lieberman, 2010), and laboratory experiments (Zhang *et al.*, 2018), but has yet to be applied in the intertidal zone.

For macro-tidal beaches, where several meters of water can inundate the beach, the top part of the water column is more difficult to survey. It is essential to survey the entire water column though when the suspended sediment is mixed but vertically stratified. For these beaches it is desired to further investigate the use of acoustic sensors, that are often already deployed to survey the flow velocity, to determine SSC. Aagaard *et al.* (2012) were among the first to also use acoustic sensors to measure suspended sediment transport in the intertidal zone and relate it to topographic changes. They obtained a reasonably good correlation between SSC from acoustic and optical backscatter. The difference in the means was only 5%, but the variance was significantly larger. Similar trends in measured sediment transport and observed topographic changes were found, but they were not related in a quantitative way. Nevertheless, this study suggests that acoustic sensors are able to quantify suspended sediment transport rates in the highly dynamic zone. However, there is still a need for the validation of the accuracy of acoustic sensors and the effect of variations in grain size and turbulence on these sensors remains unclear.

Results from previous research thus suggest that net transport rates based on optical or acoustic backscatter are reasonable, but not perfect. One of the causes for errors in measured suspended sediment transport rates is that transport is rarely measured very close to the bed. The deployment of instruments in shallow water often results in either burial of the instruments or them being too far from the bed (Hughes *et al.*, 1997, Masselink *et al.*, 2009) due to high turbulence and suspension levels as well as rapidly changing bed levels. As a result, swash transport is rarely included in field measurements, resulting in large errors (*e.g.* Emmanuel *et al.*, 2009). Furthermore, measured sediment transport rates may be inaccurate, because of variations in particle size for example. Therefore, it is strongly encouraged to measure particle size simultaneously and to correct the measurements for variations in it. Particle size distributions can be measured with water samples, but this is very labour intensive. It can also be done with a sensor like the **Laser In-Situ Scattering and Transmissometry (LISST)**, that measures turbidity and in-situ particle size distribution (*e.g.* Mikkelsen and Pejrup, 2001). As an example, acoustic backscatter is compared to optical backscatter and particle size based on LISST measurements in Figure 15. The

effect of particle size (colours) on acoustic backscatter intensity based on measurements around the low water line on a sandy beach at Groenendijk, Belgium (Brand *et al.*, 2019). Figure 15 (Brand *et al.*, 2019). All were measured at 35 cm above the bed around the low water line of a macro-tidal, sandy beach (Groenendijk, Belgium). Acoustic backscatter was corrected for transmission loss due to spreading and absorption. Optical backscatter was converted to sediment concentration based on a calibration with water samples. In this example, the acoustic sensor clearly overestimated the SSC when the particle size was large ($> 63 \mu\text{m}$). It was found that the acoustic backscatter measurements were barely affected by turbulence. Hence, this example shows that measurements of particle size are important when acoustic backscatter is used to determine SSC.

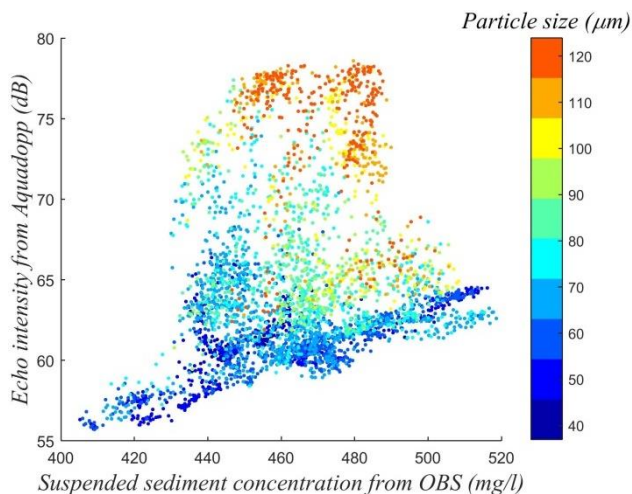


Figure 15. The effect of particle size (colours) on acoustic backscatter intensity based on measurements around the low water line on a sandy beach at Groenendijk, Belgium (Brand *et al.*, 2019).

2.4. Cross-checking bed load and total load measurements

Bed load transport can make up more than half of the total load transport (Tonk and Masselink, 2005, Masselink *et al.*, 2008), but measuring techniques for bed load transport are limited. Bed load transport can be studied with streamer traps or sand tracer experiments, but these methods are labour intensive and not very successful in quantifying transport. For

example, Hughes et al. (1997) tested the streamer traps over one tidal cycle in relation to beach topography measurements with rods. They found that the transport rates were 2-3 orders of magnitude larger than the observed topographic changes. Masselink et al. (2009) measured sediment transport with streamer traps in combination with topography measurements with ultrasonic bed level sensors that continuously measure the bed elevation. In this study, the transport fluxes derived from the bed level sensors were larger than those from the traps. This was attributed to undersampling of the bed load transport due to gaps between the bed and the trap and obstruction of the bed load transport by the trap.

Recently, sand ripple profilers have been used to measure bed load transport in the intertidal zone. Masselink et al. (2008) used one in combination with measurements of suspended sediment transport and topographic change. Thanks to the use of the sand ripple profiler a reasonably good correlation between measured sediment transport and topographic change was obtained, because the bed load transport made up more than half of the total load. This technique is thus very promising, but more studies with this equipment are needed to reaffirm these results under different conditions.

Since it remains difficult to quantify bed load transport, it is often predicted instead. Predictions of sediment transport have been tested by comparing them to sand tracer experiments on many occasions. On low-energy beaches the measured sediment transport rates can be three to ten times larger than the predicted rates (e.g. Ciavola et al., 1997, Nordstrom et al., 2003, Tonk and Masselink, 2005, Silva et al., 2007). On high-energy beaches the measured sediment transport is a few times lower than the predicted rates (Bertin et al., 2008). In general, measured sediment transport seems more often significantly over- or underestimated than predicted correctly with any of the existing predictive formulas (Fernández-Fernández et al., 2016).

Sediment transport predictions have also been compared to measurements of suspended sediment transport and topography measurements (Tonk and Masselink, 2005, Masselink et al., 2008, Emmanuel et al., 2009). Large differences were found when comparing them quantitatively. Bagnold-type formulas predict considerably smaller rates than the actual rates under calm wave conditions (Gallagher et al., 1998, Masselink et al., 2008, Emmanuel et al., 2009). These type of predictions work better under energetic wave conditions. This is mainly due to the exclusion of the swash zone in these predictions (Masselink et al., 2009, Emmanuel et al., 2009). Predictive formulas based on wave characteristics (e.g. CERC, 1984, Kamphuis, 1991) can predict currents rather accurately, but they perform less in predicting the cross-shore variation in sediment concentration (Van Maanen et al., 2009).

As a result, their main application is for longshore sediment transport (Tonk and Masselink, 2005, Rogers and Ravens, 2008, Esteves et al., 2009). They are often far off when used to predict cross-shore sediment transport, especially for storm, but also for calm conditions (Bayram et al., 2001, Van Maanen et al., 2009).

In conclusion, predictive formulas are reasonably good in estimating the direction of long- and cross-shore sediment transport. However, at the moment they should be used with care when calculating sediment concentrations and thus transport rates, because of them often significantly over- or underestimating the transport. Under energetic conditions sediment transport is often overpredicted. Under calm conditions sediment transport is often underpredicted. The improvement of predictive formulas is ongoing, which will allow to verify measured transport rates or to calculate bed load transport in the future.

2.5. Matching the scale of different measurements

It has become clear that it is very difficult to accurately quantify suspended sediment and bed load transport. However, differences in net sediment transport and beach volume changes may also be due to mismatches between sediment transport and topography measurements. When comparing them, it is often assumed that sediment only enters or leaves the intertidal beach by underwater transport across the low water line, while wind-driven transport or gradients in alongshore sediment transport may also result in topographic changes in the intertidal zone. In addition, sediment transport and topographic change are rarely measured on the same temporal and/or spatial scale (Figure 16, *e.g.* Sénéchal *et al.*, 2011). Sediment transport is usually measured at one or a few cross-shore locations in the intertidal zone, whereas topography is often measured across, and sometimes along, the entire intertidal zone. To get insight in the spatial pattern of sediment transport some researchers install multiple measuring frames in cross- or alongshore direction (*e.g.* Masselink *et al.*, 2009). However, equipment is costly, limiting the number of locations where sediment transport can be measured. Grain size trend analysis and sand tracer experiments can also be used to get some insight in spatial patterns in sediment transport, but they are usually not quantitative.

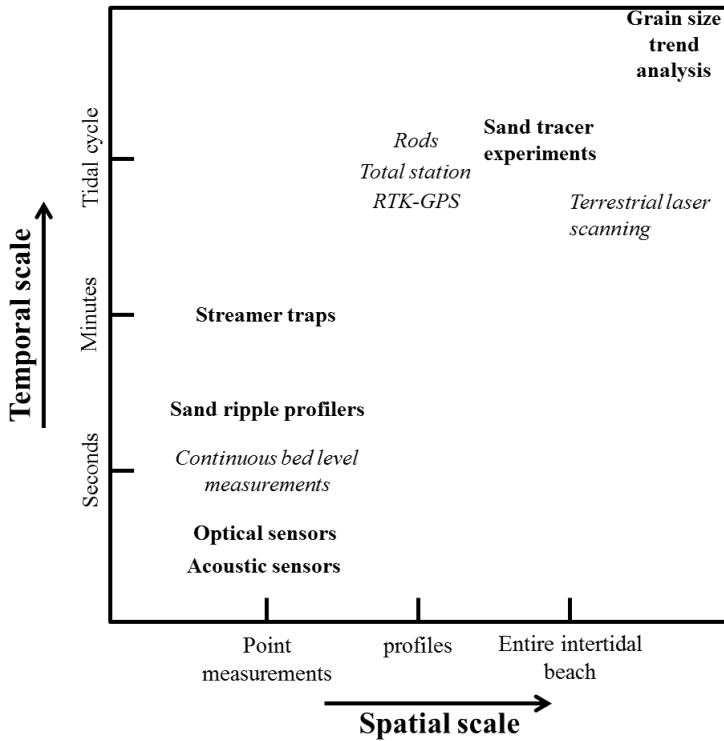


Figure 16. Temporal and spatial scale of different measuring techniques. Methods to measure sediment transport are in bold and to measure topography in italic.

Most studies in which sediment transport observations were compared to beach volume changes used cross-shore topographic profiles to quantify beach volumes. However, it was proven that a strong alongshore variability in topographic response to hydrodynamic forcing may exist (Theuerkauf and Rodriguez, 2012). This may explain why studies in which the topography was measured with a high spatial resolution (Masselink *et al.*, 2009) perform better than studies with a low spatial resolution (*e.g.* Hughes *et al.*, 1997, Masselink *et al.*, 2008) when comparing measured sediment transport and topographic changes. However, studies based on full beach surveys show even better correlations between measured transport rates and beach volume changes. Based on previous studies it is thus highly recommended to survey the full beach topography with a TLS or with photogrammetry. If this is not possible because of restrictions in time and resources, it is recommended to survey many closely spaced profiles.

Apart from differences in spatial scale, there is usually also a mismatch in the frequency of sediment transport and beach topography measurements (Figure 16). Sediment transport measurements are often (quasi-) continuous, whereas beach topography is generally only measured once or twice a day during low tide. Measured topographic changes in the intertidal zone thus reflect time-integrated sediment transport. However, instantaneous transport rates can be highly variable on a timescale of seconds and integrating them over time can be problematic. Sediment transport rates can be large over a matter of seconds and by averaging them over a tidal cycle errors are easily made (Duncan, 1964, Masselink *et al.*, 2009). Some studies succeeded in measuring topographic change in the swash zone over individual swash events (Waddell, 1976, Sallenger and Richmond, 1984, Baldock *et al.*, 2005, Turner *et al.*, 2008). However, continuously measuring topographic change is difficult in the remainder of the intertidal zone. Continuous bed level measurements can be carried out with acoustic equipment (C. Berni *et al.*, 2009, Emmanuel *et al.*, 2009), pressure sensors (C. Berni *et al.*, 2009), or the newly developed **ultrasonic sensors** (Turner *et al.*, 2008).

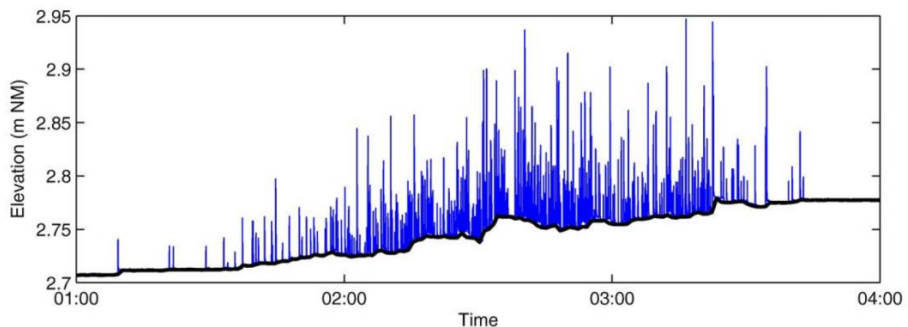


Figure 17. Example of bed level sensor measurements. The blue bars represent raw data from the bed level sensor and the thick line represents the one-minute averaged bed level relative to the mean sea level (NM). Measurements were carried out in the intertidal zone of a beach in southwestern France (from: Masselink *et al.*, 2009).

With such measurements the evolution of the bed level over time can be revealed, which is illustrated in Figure 17. From this example, it becomes clear that topographic changes can be large (more than 15 cm in this case) over a period of seconds to minutes (Masselink *et al.*, 2009). A downside of this measuring technique is that it measures the topography only very locally, however Masselink *et al.* (2009) solved this by installing 45 of these sensors in an array of 3 cross-shore profiles. Continuous bed level measurements are

thus a valuable addition to intertidal measurements, especially when multiple are installed along and across the beach.

Another drawback of only measuring the beach topography at low tide is that topographic changes may also result from wind-driven transport. Aeolian transport has been studied in the intertidal zone on various occasions (*e.g.* Sarre, 1989, Anthony *et al.*, 2009), but is rarely considered as a part of the sediment budget together with topography and underwater measurements. Some studies attributed significant erosion/accretion to transport by wind (*e.g.* Almeida *et al.*, 2012). These studies did not verify their findings with in-situ measurements of wind-driven transport though. The contribution of aeolian transport thus remains an uncertainty in the sediment budget of the intertidal zone.

2.6. Conclusion

The intertidal zone is among the most dynamic environments and constantly grows and erodes in response to waves, currents, and wind. Accurate measurements of sediment transport and resulting topographic changes are essential to understand the morphodynamics of the intertidal zone. In general, field investigations in the intertidal zone consist of measurements of flow velocity and SSC at one or a few locations across the beach and daily topography measurements of several cross-shore profiles. However, it appears to be difficult to relate sediment transport and topographic changes with such a measuring set-up. Measured sediment transport rates are often in a different order of magnitude or even in a different direction than transport rates derived from topographic changes. To improve sediment transport and topography measurements, it is recommended to:

1. Measure sediment transport at multiple locations along and across the intertidal zone. It is recognized that this is very costly and that research budgets do not always allow for this. However, it is very valuable to know sediment transport rates at multiple locations in the intertidal zone. Two measuring locations in the longshore direction already allow to investigate gradients in alongshore sediment transport and will result in a better approximation of the net sediment transport.

2. Measure suspended sediment transport over the entire water column at beaches with strong mixing of the sediment, such as beaches with strong tidal currents or energetic waves. This can be done with an array of

OBS or an ASM on micro- and meso-tidal beaches. On macro-tidal beaches, the SSC over the water column can be estimated based on acoustic backscatter.

3. Improve sensors to measure suspended sediment transport close to the bed and bed load transport and improve predictive formulas for sediment transport. It is currently difficult to measure sediment transport close to the bed for both suspended and bed load transport. Sand ripple profilers may partially solve this problem, but field experiments with this equipment are still scarce. In the meanwhile, predictive formulas are often used to estimate bed load transport, but these appear to be highly unreliable. Hence, it is recommended to improve both measuring techniques for near-bed transport in-situ and predictive formulas.

4. Measure the full beach topography on beaches with alongshore variability in beach topography, such as on beaches with cusps or nourishments. This can be done, for example, with static or mobile (airborne or terrestrial) laser scanning or photogrammetry from a UAV.

5. Correct (especially acoustic) measurements of SSC for grain size and turbulence. Measurements of SSC with optical or acoustic equipment are sensitive to grain size. Additionally, acoustic measurements are sensitive to turbulence. These measurements can be greatly improved when they are corrected for these parameters, especially the measurements with acoustic backscatter.

6. Measure beach topography over time. Sediment transport is usually measured continuously over a tidal cycle, whereas the beach topography is only measured at low tide which results in mismatches between the two. It is helpful to add continuous bed level measurements to an intertidal campaign in order to obtain a better relationship between them and to get a better understanding on the intertidal beach morphodynamics on a small scale (seconds to hours). If the beach topography is only measured during low tide, it is advised to investigate aeolian transport if wind conditions are energetic.

Chapter 3

Seasonal variations in intertidal beach topography

3.1. Introduction

The Belgian coast is densely populated and several areas are prone to coastal hazards such as erosion and marine flooding. The frequency and magnitude of these hazards are likely to amplify in the next decades due to sea level rise and climate change resulting in an increased threat for the people living along the coast (Nicholls *et al.*, 2011, de Winter *et al.*, 2013). It is important to get a better understanding of the hydrodynamic conditions resulting in storm erosion and post-storm beach recovery for efficient coastal protection. The intertidal zone plays an important role in storm impact and post-storm recovery. It is the zone where wave impact is largest and it acts as the pathway of sediment from the dry beach to the sub-tidal area.

Cross-shore topographic profiles have long been a source of information for the beach morphodynamics, providing insight into seasonal and long-term trends in beach morphology (*e.g.* Short and Trembanis, 2004, Quartel *et al.*, 2008). However, only few sites exist where a long-term dataset (covering multiple years) of beach profiles with a relatively short sampling interval (monthly) is available (Short and Trembanis, 2004, Ruggiero *et al.*, 2009). This limits our understanding of beach morphodynamics on a medium (*i.e.* seasonal to monthly) scale.

A number of studies were carried out at micro- and meso-tidal beaches (Masselink and Pattiaratchi, 2001, Short and Trembanis, 2004, Quartel *et al.*, 2008, Ruggiero *et al.*, 2009) but only a few studies were dedicated to the monthly dynamics of macro-tidal beaches (Corbau *et al.*, 1999, Sénéchal *et al.*, 2015) especially to beaches with a featureless intertidal zone. Findings of

these studies suggest that a seasonal trend in beach morphology exists (Masselink and Pattiaratchi, 2001, Ruggiero *et al.*, 2009) but that this seasonality is mainly driven by the occurrence of storm events as opposed to more energetic average conditions (Corbau *et al.*, 1999, Quartel *et al.*, 2007, Sénéchal *et al.*, 2015). The aim of this study is to understand the intertidal beach dynamics on a seasonal to monthly scale and to quantify the spatial and temporal variability of the intertidal beach topography for a tide-dominated sandy coast.

3.2. Methods

This study was carried out at two study sites along the Belgian coast: Groenendijk and Mariakerke (Figure 2 and Figure 18). The distance between the study sites is only 15 km, so it can be assumed that they are subject to the same hydrodynamic forcing. Mariakerke is a managed beach with a seawall and groins and regular beach and underwater nourishments. The most recent nourishment (beach and shoreface) was carried out in 2014 (Houthuys, 2012). On the contrary, Groenendijk is a relatively natural beach where no protective measures have been taken. The natural trend of the beach at Mariakerke is erosive ($-8 \text{ m}^3/\text{m}/\text{yr}$), but thanks to the nourishments the beach has been growing over the past decades ($+4 \text{ m}^3/\text{m}/\text{yr}$). The beach at Groenendijk has been growing steadily over the past decades ($+18 \text{ m}^3/\text{m}/\text{yr}$, Houthuys, 2012). The coastline orientation is 54° at Mariakerke and 65° at Groenendijk.

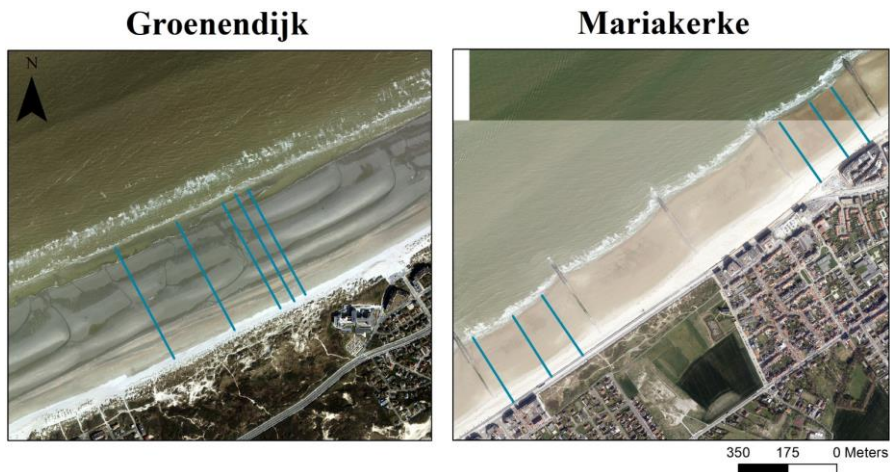


Figure 18. Location of the cross-shore profiles at Groenendijk and Mariakerke.

The topography of five cross-shore profiles at Groenendijk and six cross-shore profiles at Mariakerke was measured monthly since February 2017 for Groenendijk and September 2015 for Mariakerke (Figure 18). Measurements were carried out around the middle of each month, but are lacking for July and October 2016, July, August, and November 2017, and July and August 2018 (Figure 8). At Groenendijk the distance between profiles was approximately 250 m with two additional profiles at 50 m from the most eastern profile. At Mariakerke, the distance between profiles was approximately 150 m with 1 km in between two sets of three profiles. Profiles extended from the dunes/seawall to the low water line. The profiles were surveyed with an RTK-GPS which has an accuracy of 2-3 cm for the x, y and z coordinates combined. The beach volume of the intertidal area, the area between NLW and NHW, was calculated using trapezoidal rules which is a technique for approximating the definite integral (Figure 19).

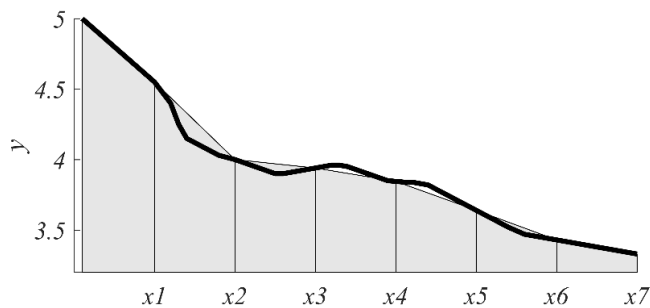


Figure 19. Calculating the beach volume using trapezoidal rules.

Beach volume changes were compared to hydrodynamic conditions that were measured continuously by an offshore wave buoy (Westhinder) and a tide gauge at Ostend by Coastal Division (Appendix A). Hydrodynamic data is lacking for some periods of up to one month (*e.g.* January 2016 and January 2017).

Haerens *et al.* (2012) described five storm thresholds for significant erosion along the Belgian coast. These thresholds are a maximum significant offshore wave height > 4 m; a water level > 5 m TAW; a storm duration > 12 hr; a total induced wave energy $> 6.5e+05$ J/m²; and a wind direction between W and NW. For this study energetic events are considered with lower thresholds: a maximum significant wave height > 3.75 m when the water level > 4 m TAW.

3.3. Results

The intertidal beach at Mariakerke is 160 m wide, gently-sloping (2%), and concave (Figure 20). At Groenendijk the intertidal beach is 290 m wide, gently-sloping (1%), and characterized by three ridges and runnels. The intertidal beach morphology was stable at both Mariakerke and Groenendijk. Especially at Mariakerke the shape of the beach did not change over the investigated period. At Groenendijk the ridges and runnels were sometimes very pronounced, while other times the intertidal beach morphology was more smooth. The ridges were always located at approximately the same location though. The standard deviation of the intertidal beach topography was up to 5 cm at Mariakerke and up to 25 cm at Groenendijk.

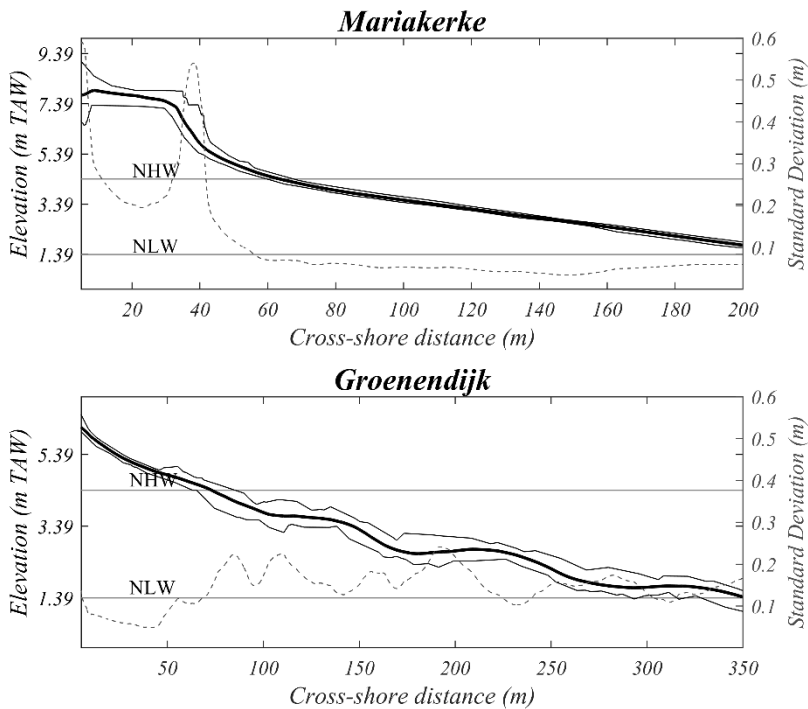


Figure 20. Mean (thick black line), envelope (black lines), and standard deviation over time (dashed grey line) of the topography of a representative cross-shore beach profile for Mariakerke and Groenendijk.

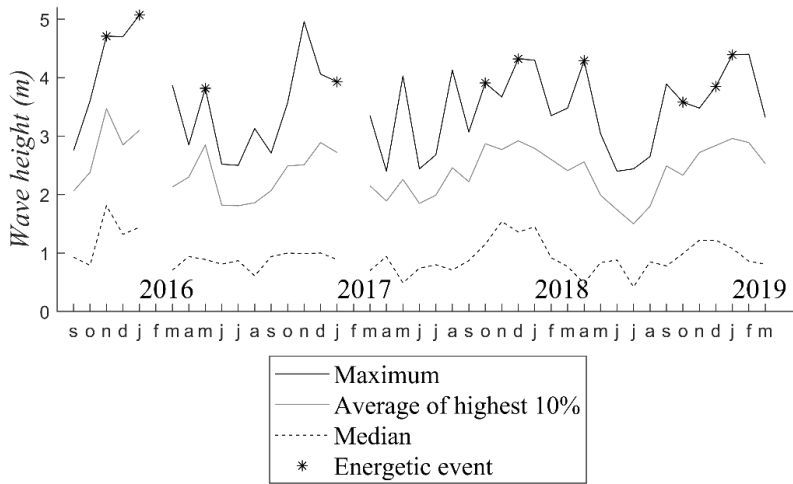


Figure 22. Time series of monthly maximum, average of highest 10%, and median significant wave height from September 2015 to March 2019. Note: data gaps are due to malfunctioning of the wave buoy.

Table 2. Hydrodynamic conditions during the events identified as energetic, with the conditions exceeding the Haerens et al. (2012) storm thresholds in bold.

	Duration (hr)	Max. significant wave height (m)	Max. water level (m TAW)
November 2015	6	4.70	4.34
January 2016	11.5	5.13	5.26
May 2016	2.5	3.86	4.31
	1	3.83	4.32
January 2017	8	4.66	5.47
	1	3.99	6.19
October 2017	3.5	4.23	4.78
December 2017	4	5.09	4.75
April 2018	1	3.78	5.14
October 2018	2	3.82	4.57
December 2018	2	4.01	5.43
January 2019	9	4.58	4.79

Table 3. Months with and without an energetic event showing beach erosion, stability, or accretion. Numbers indicate percentages.

	% of months <u>with</u> energetic event		% of months <u>without</u> energetic event	
	Mariakerke	Groenendijk	Mariakerke	Groenendijk
Erosion	56	60	19	25
Stability	33	0	19	25
Accretion	11	40	62	50

Table 4. Pearson correlation matrix of the monthly volume changes at Mariakerke, profiles numbered 1-6 from west to east (top), and at Groenendijk, profiles numbered 1-5 from west to east (bottom). Correlations > 0.5 are indicated in bold.

Mariakerke						
	1	2	3	4	5	6
1	1					
2	0.27	1				
3	0.16	0.62	1			
4	0.50	0.49	0.09	1		
5	0.33	0.41	0.68	0.09	1	
6	0.22	0.44	0.61	0.17	0.32	1

Groenendijk					
	1	2	3	4	5
1	1				
2	0.66	1			
3	0.18	0.46	1		
4	-0.16	-0.25	0.06	1	
5	0.29	0.18	0.17	-0.15	1

Intertidal beach volume changes were averaged for all profiles at Mariakerke and Groenendijk. However, it appears that the alongshore variability in topographic change is large. The correlation between profiles (R^2) is up to 0.68, but is generally much lower and can even be negative (Table 4). The topographic response to the incoming hydrodynamics is thus highly variable over a short distance (50-250 m). At Mariakerke, the profiles directly east (1 and 4) and the profiles directly west (3 and 6) of the groins show a relatively similar behavior, with correlations around 0.50.

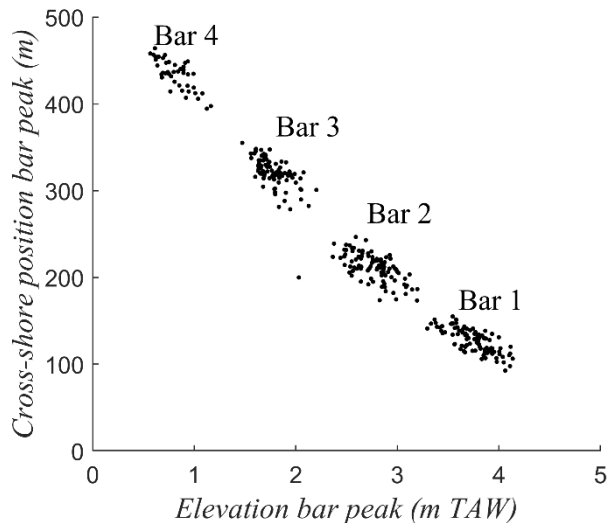


Figure 23. Cross-shore position and elevation of the peak of the bars for all profiles at Groenendijk and all surveys combined.

In Figure 23 the position and elevation of the bars (*i.e.* the peaks in beach topography) are shown for all profiles and all surveys at Groenendijk. Four separate groups of peaks can be identified of which three are located in the intertidal zone and one is located just below the NLW line at 0.8 m TAW. The lateral movement of the bars was limited to 70 m in the cross-shore direction. The average cross-shore position of the bars was similar for all five profiles, *i.e.* at 127 m, 212 m, 322 m, and 433 m from the dunes.

In contrast to the intertidal beach volume, the absolute height and the position of the bars displayed a seasonal cycle (Figure 24). The absolute bar height was calculated as the elevation of the top of the ridge minus the elevation of the bottom of the runnel at the landward side of the ridge. The bars built up during autumn and winter and became lower in spring. The second bar from the dunes was on average 42 cm high in January and 25 cm in June, for example. During energetic events (5 in total) the bars generally became higher as well. The relative position of the bars was calculated as the position of the bars compared to their average position. The bars moved onshore during autumn and winter and offshore during spring and summer. The seasonal difference in bar position was 20 m, on average. The bars thus move onshore and became more pronounced during energetic conditions, while the beach morphology is smoothed during calm conditions.

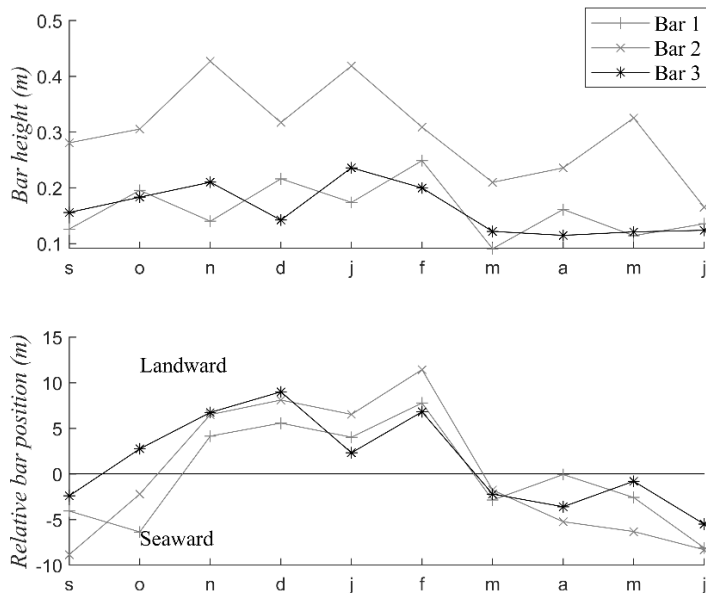


Figure 24. Top: Absolute height of the bars in the intertidal zone (i.e. the elevation of the ridge compared to the elevation of the landward runnel). Bottom: Relative position of the bars compared to the average position. Data is averaged over time. No surveys were carried out in July and August.

3.4. Discussion

3.4.1. Seasonal vs. event-driven topographic changes

The intertidal beach volume does not show a seasonal cycle, while the hydrodynamic conditions are clearly more energetic in winter than in summer. This contradicts previous observations of a seasonal cycle in beach morphology (Masselink and Pattiaratchi, 2001, Ruggiero *et al.*, 2009). Instead, intertidal beach volume changes seem to be event-driven. Erosion is observed during months with energetic events with offshore waves > 3.75 m. Beach growth is generally observed during the other months. This confirms other studies that pointed out that a seasonality in beach morphology is mainly driven by the larger amount of energetic events in winter, as opposed to the average conditions being more energetic (Corbau *et al.*, 1999, Quartel *et al.*, 2007, Sénéchal *et al.*, 2015).

Not all months with energetic events showed the same morphological outcome (Figure 21). Partly, this is caused by differences in the specific

hydrodynamic conditions, such as wave direction, wave energy, and water level, of the events. The storm conditions that generally lead to erosion of the intertidal zone along the Belgian coast have previously been described by Haerens *et al.* (2012). Differences in topographic response to hydrodynamic forcing may also be due to the pre-event beach state, which can make the beach more or less susceptible for erosion (Reyes *et al.*, 1999, Morton, 2002, Haerens *et al.*, 2012). Also, beach volume is an indicator for morphological change, but might not always be representative. Sediment can be transported down the beach profile without the beach volume changing. Furthermore, stability or accretion of the beach during months with energetic events may indicate a fast beach recovery. For example, in January 2016 no significant erosion was observed while an energetic event occurred, but this event took place almost one month before the next survey and the beach might have recovered in this month.

In general, energetic events had no long-lasting effects and recovery happened within one or two months. This may be attributed to the fact that the observed events were relatively small, as none of the events matched all thresholds for significant storm erosion proposed by Haerens *et al.* (2012). For larger storms it is known that recovery can take multiple years (Maspataud *et al.*, 2009).

As opposed to the beach volume, the bars at Groenendijk did show a seasonal cycle. They were smoothed and moved seaward during spring and summer, whereas they became more pronounced and moved onshore during autumn and winter. This is similar to the findings of Simmonds *et al.* (1996), who compared topographic surveys to numerical model results for the beach at Nieuwpoort (Figure 2). However, it must be noted that no storm events were covered. These would likely serve as a bulldozer and flatten the intertidal zone (Wright, 1982). The ridges and runnels at Groenendijk are formed by standing long waves (Simmonds *et al.*, 1996). Hence, the position of the bars depends on the wavelength of these long waves in combination with the wavelength of the short waves (O'Hare and Huntley, 1994, Simmonds *et al.*, 1996). As a result, the position of the bars was relatively fixed and similar for all the investigated profiles.

3.4.2. Alongshore variability in topographic response

Mariakerke and Groenendijk did not always respond to energetic events in a similar way, in fact, their response was sometimes opposite. This is possibly due to differences in beach characteristics. The beach at Groenendijk is wider and wave energy is more dispersed, which makes the beach less susceptible to storm erosion (Qi *et al.*, 2010). However, the shorter time series of

topographic data at Groenendijk, which covers only five energetic events were observed, does not allow for a more in-depth comparison between Mariakerke and Groenendijk.

Besides differences between Mariakerke and Groenendijk, a strong alongshore variability in topographic response to the incoming hydrodynamics was observed within both study sites (Table 4). This is in agreement with previous studies (Swales, 2002, Theuerkauf and Rodriguez, 2012) and can be attributed to the complex alongshore beach morphology (Theuerkauf and Rodriguez, 2012) with the ridges and runnels at Groenendijk and the groins at Mariakerke. It was noted that the profiles close to the groins respond more similar to hydrodynamic forcing than the profiles in the middle. The alongshore variability in topographic response to hydrodynamic forcing may be attributed to differences in beach morphology, such as slope or beach width, or alongshore variability in hydrodynamics. It is known that groins can affect the local hydrodynamics (Rocha *et al.*, 2013), while at Groenendijk the bars influence the currents and wave breaking.

3.4.3. Long-term trends in beach topography

The beach volume at Mariakerke gradually increased over the investigated period ($+2 \text{ m}^3/\text{m}/\text{year}$; Figure 25, left), which is in agreement with long-term studies ($+4 \text{ m}^3/\text{m}/\text{yr}$, Houthuys, 2012). This growth can be attributed to previous nourishments in this area (Houthuys, 2012). However, the beach at Groenendijk showed a trend of erosion ($-7 \text{ m}^3/\text{m}/\text{year}$; Figure 25, right), which strongly disagrees with previous studies that reported long-term accretion for this region ($+18 \text{ m}^3/\text{m}/\text{year}$, Houthuys, 2012). Houthuys (2012) investigated yearly topographic changes over multiple decades though, while here only two years were investigated. Possibly, the investigated years were characterized by more energetic hydrodynamic conditions or the natural sediment supply was less than in previous years.

The yearly beach volume changes quantified in this study were in the same order of magnitude as the average variation around the long-term trend found by Houthuys (2012). Yearly beach volume changes can be much larger, up to $50 \text{ m}^3/\text{m}/\text{year}$, when major storm events occur though (Houthuys, 2012). Storm events in this range occur approximately every 5 years in Belgium (Haerens *et al.*, 2012) but did not occur during the investigated period. From previous studies it is known that a large yearly variation can be typical for beaches with human interference and that these beaches can be less stable than natural beaches (Sénéchal *et al.*, 2016). Here, the beach volume variations at Mariakerke were of a similar order of magnitude as the variations at Groenendijk.

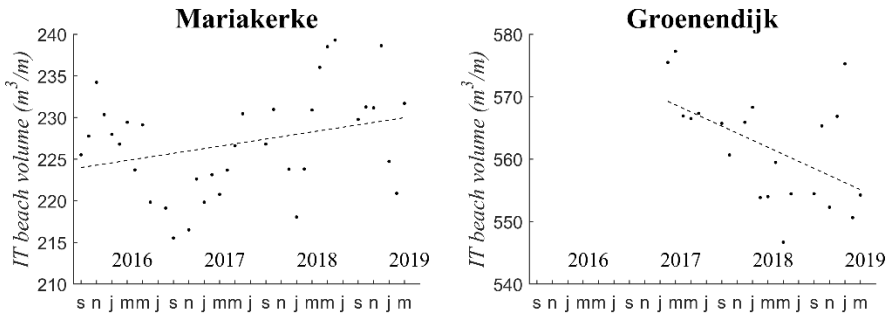


Figure 25. Total intertidal (IT) beach volume for Mariakerke and Groenendijk with the linear trend indicated by a dashed line.

3.5. Conclusion

This study investigated the spatial and temporal variability in beach topography for two macro-tidal beaches. At Mariakerke, a beach that is characterized by a featureless intertidal zone, six cross-shore topographic profiles were measured monthly over a period of 3.5 years. At Groenendijk, where ridges and runnels are present, the beach topography of five cross-shore profiles was measured over more than 2 years. The resulting datasets allowed to determine the range of topographic changes that take place on a monthly scale.

It was found that topographic changes can be large over one month, at least up to $15 \text{ m}^3/\text{m}/\text{month}$ at Mariakerke and $25 \text{ m}^3/\text{m}/\text{month}$ at Groenendijk. The standard deviation of the beach topography is 5 cm at Mariakerke and 25 cm at Groenendijk. This difference is due to the lateral movement of the bars at Groenendijk. These move onshore and become more pronounced during energetic conditions due to long wave activity. During calm conditions they move seaward and are smoothed. Nevertheless, their position is relatively fixed because of the wavelength of the long waves. Absolute volume changes are larger at Groenendijk than at Mariakerke, but relative changes compared to the total intertidal beach volume are in the same order of magnitude. The topographic response to the incoming hydrodynamics is highly variable between the profiles due to the complex beach morphology at both study sites.

No clear seasonal trend in the intertidal beach volume is observed. Topographic changes are rather event-driven, with erosion during months when the offshore wave height exceeded 3.75 m. However, not all months with energetic events showed erosion. This can be attributed to differences in

conditions between the events, the pre-event beach profile, and a fast recovery of the beach. This recovery was often within one or two months, but it must be noted that no major storm events occurred during the investigated period. It seems that the barred beach at Groenendijk is less susceptible to storm erosion thanks to the wide beach. Accretion is generally observed during months without energetic events.



Chapter 4

Intertidal beach dynamics in relation to nearshore hydrodynamics on a monthly scale*

4.1. Introduction

Beaches are among the most dynamic environments where topographic changes can be large over a short period of time. In particular the intertidal beach is very dynamic, as it is subject to most of the wave breaking and swash action. Besides wave effects, the intertidal zone is also exposed to tidal currents and wind. The relation between forcing and morphological response for the intertidal beach has been studied extensively in the past (*e.g.* Ahrens and Hands, 1998, Masselink *et al.*, 2009, Meyer, 1936, Philips *et al.*, 2017). However, as multiple processes act on the intertidal beach it is difficult to relate them to morphological changes. As a result, there are still important knowledge gaps when it comes to intertidal beach morphodynamics.

Most studies on the dynamics of the intertidal beach cover a short period (*i.e.* days to weeks) during which hydrodynamics, sediment transport, and beach topography are measured (*e.g.* Cartier and Héquette, 2013, Masselink *et al.*, 2008, Sedrati and Anthony, 2007). However, topographic changes on such a timescale are generally small, especially during calm, accretive, conditions. This makes it difficult to detect change (*e.g.* Bagnold, 1940, Woodroffe, 2007). To study beach accretion the topography should be

* Published as: Brand, E., Montreuil, A-L., Dan, S., Chen, M., 2018. Macro-tidal beach morphology in relation to nearshore wave conditions and suspended sediment concentrations at Mariakerke, Belgium. *Regional Studies in Marine Science*, 24, 97-106

monitored over several months. Studies to the intertidal beach morphodynamics on this scale are scarce though (Maspataud *et al.*, 2009). This is mainly due to the limited amount of detailed, high quality topographic datasets covering a long time span (Short and Trembanis, 2004). Some research over a longer period was conducted on the morphodynamics of macro-tidal beaches characterized by a bar morphology (*e.g.* Aarninkhof *et al.*, 2005, Philips *et al.*, 2017). For these beaches it was reported that landward sediment transport takes place under calm conditions, while seaward sediment transport occurs during storm events. However, research on non-barred, macro-tidal beaches is lacking.

From wave basin experiments it has long been known that wave steepness, the ratio of wave height over wavelength, affects the beach morphology (*e.g.* Meyer, 1936, Saville, 1950). It has been reported that sediment is transported onshore when the wave steepness is small and offshore when it is large. More recently the relation between wave steepness and beach morphology was reaffirmed by in-situ measurements, from which beach slope (Masselink *et al.*, 2009, Sunamura and Horikawa, 1974), wave direction (Masselink *et al.*, 2010), and wind speed (Morton *et al.*, 1994) have been found to influence the relation between wave steepness and beach morphology. However, most of these field measurements were carried out over a short period.

The aim of this study is to investigate the relation between wave steepness and beach morphology over a long period of time for a macro-tidal, non-barred beach. In total more than 1.5 years of monthly cross-shore topographic profiles are available for this study. Furthermore, field measurements of nearshore hydrodynamics and SSC were carried out for half a year. This data was supplemented with continuous wave buoy and tide gauge measurements.

4.2. Methods

4.2.1. Hydrodynamics and sediment dynamics

Three underwater measuring frames were equipped to measure wave characteristics and SSC. At section 100 a frame was placed at -8 m TAW and at section 104 frames were placed at -8 and -5 m TAW (Figure 26). Three measuring campaigns of approximately two months each were carried out in autumn 2015 (23 September – 14 November), spring 2016 (12 March – 10 May), and autumn 2016 (16 October – 29 November; Table 5).

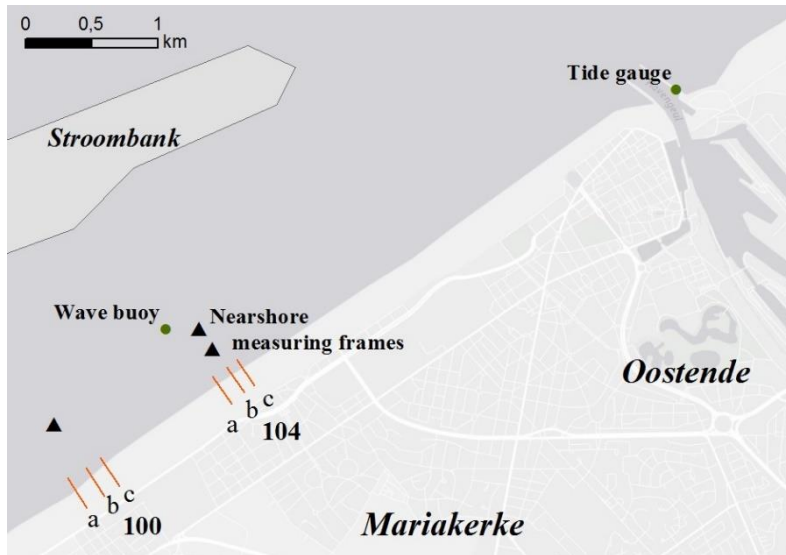


Figure 26. Map of the study area with the location of the cross-shore profiles and hydrodynamic measurements indicated.

Table 5. Timetable of topographic profiles with the hydrodynamic measurements for the three campaigns.

	Hydrodynamic measurements	Duration (days)	Topographic profiles
Autumn '15	23 Sep. – 14 Nov.	53	14 Sep., 12 Oct., 13 Nov.
Spring '16	12 Mar. – 10 May	59	23 Mar., 11 Apr., 11 May
Autumn '16	16 Oct. – 29 Nov.	44	16 Sep., 14 Nov., 16 Dec.

SSC was measured with three OBS at 40, 60, and 80 cm above the sea floor (Figure 27). The measurements were set at 4 Hz for 10 minutes every hour. OBS use an infra-red light beam to measure turbidity. To convert turbidity to SSC a calibration with sediment samples collected near the study site was performed. Some OBS experienced biofouling because of the presence of organisms such as algae and barnacles. Therefore not all OBS data towards the end of campaigns could be used. Noise was removed and the SSC data from the OBS at different heights were averaged.

An Acoustic Wave And Current profiler (AWAC) to measure wave characteristics and water level was added to the -8 m TAW frame at section 104. It was mounted looking up at 1.4 m above the bed and measured with a frequency of 2 Hz every 2 hours for 20 minutes. The AWAC uses acoustic

surface tracking algorithms to estimate the distance to the water surface using the echo of the vertical beam. Wave direction is calculated by combining the surface tracking algorithms with orbital velocity measurements that are sampled in a cell near the surface.

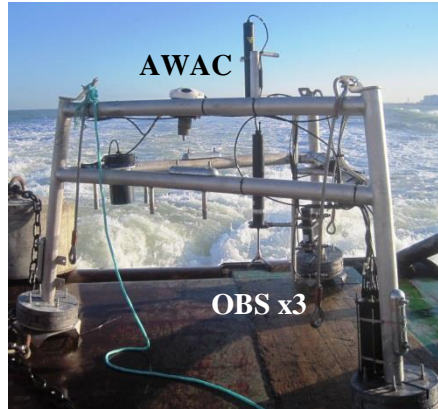


Figure 27. One of the measuring frames with the AWAC at the top and the three OBS at the bottom.

The quality of all data was checked and outliers were removed. After that, wave steepness was calculated using the shallow water approximations (Masselink et al., 2011):

$$L = T\sqrt{gh}$$

$$\text{Wave steepness} = H/L$$

where L is wavelength; h is water level; g is the gravitational acceleration; T is wave period; and H is wave height. In this case significant wave period (T_{sig}) and significant wave height (H_{sig}) were used.

Wave steepness was compared to intertidal beach topography. More than 1.5 year of topography data was available, whereas the nearshore measuring campaigns had a total duration of 6 months. Therefore, the measuring campaigns were supplemented with wave and water level data from a wave buoy and tide gauge from Coastal Division for the period from September 2015 to May 2017. This data is continuous, but there were some gaps of up to one month. Waves were measured every 30 minutes and water level every 5 minutes, so water level was averaged over intervals of 30 minutes. The distance between the nearshore measuring frames and the wave buoy is 250

m and the distance between the frame and the tide gauge is 4 km (Figure 26). The water depth is 8.0 m TAW at the wave buoy, whereas it is 2.3 m TAW at the tide gauge. The difference was added to the water level measurements to calculate wave steepness. The wave steepness from the buoy is compared to the wave steepness from the frame in Figure 28. Wave steepness from the wave buoy is slightly higher (6%) than from the frame. This might be due to inaccuracies in the calculated water level. The correlation between them is strong, which demonstrates that data from the wave buoy can be used in the case of no measurements from the frames.

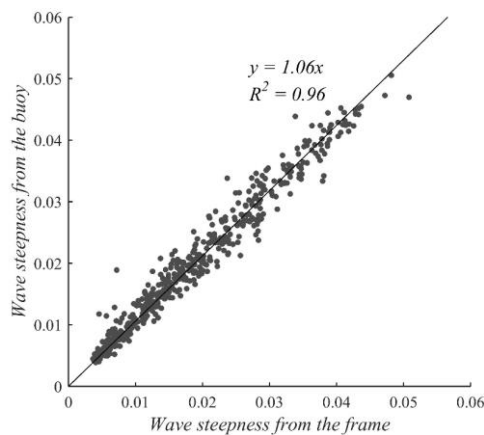


Figure 28. Wave steepness from the wave buoy compared to wave steepness from the nearest frame (section 104, -8 m TAW). The wave steepness is 2-hour averaged.

4.2.2. Topography

Three cross-shore topographic profiles at sections 100 and 104 (Figure 26) were measured every month from September 2015 to May 2017 by Coastal Division. The topography was measured with an RTK-GPS, which has an accuracy of 2-3 cm for the x, y, and z coordinates combined. No surveys were done in July and October 2016 and the topography was measured twice per month following storm events in January 2016 and from January to March 2017. This resulted in a total of 23 topographic surveys. In general, there was one topographic survey at the beginning, one halfway, and one at the end of each nearshore measuring campaign (Table 5). The distance between the profiles was approximately 150 m. Profiles a and c were located approximately 75 m away from groins. The profile length was up to 300 m from the seawall to the low water line.

The volumes of the intertidal and dry beach were calculated based on the topographic profiles. The intertidal beach corresponds to the zone between the NHW and NLW line and the dry beach covers the area from NHW to the seawall (Haerens *et al.*, 2012, Houthuys, 2012). Volumes were calculated for each profile separately using trapezoidal rules after which the volumes were averaged per section.

4.3. Results

4.3.1. Temporal variability of hydrodynamics and SSC

The hydrodynamic conditions showed a strong variability over the three campaigns (Figure 29 and Table 6). The first campaign in autumn 2015 was relatively calm. Wave height and wave steepness were small with an average significant wave height of 0.5 m. The second campaign in spring 2016 started calm, but towards the end more energetic conditions were observed with peaks in wave height reaching 2.0 m. The third campaign in autumn 2016 was the most energetic. The average wave height was 0.7 m and peaks reached 2.4 m. The wave period was similar for all campaigns with an average of 4.4 s. The maximum water level varied between + 3.7 m TAW during neap tide and +5.6 m TAW during spring tide for all campaigns and no storm surges occurred. Wave steepness was 0.015 on average and ranged from 0.005 to 0.040. The time series of SSC was characterized by a large variability, ranging from 0 to 5000 mg/l averaged over 6-hour periods. SSC were low during the first campaign in autumn 2015 (270 mg/l on average), almost twice as high during the second campaign (510 mg/l), and largest during the third campaign (1250 mg/l). An example of the flow velocity is given in Appendix B, for the first measuring campaign.

Table 6. Average and maximum significant wave height, average significant wave period, average wave steepness, and average SSC for the three campaigns.

	Autumn '15	Spring '16	Autumn '16
Average H_{sig} (m)	0.48	0.56	0.67
Max H_{sig} (m)	1.91	2.04	2.36
Average T_{sig} (s)	4.20	4.17	4.81
Average wave steepness	0.013	0.015	0.016
Average SSC (mg/l)	270	510	1250

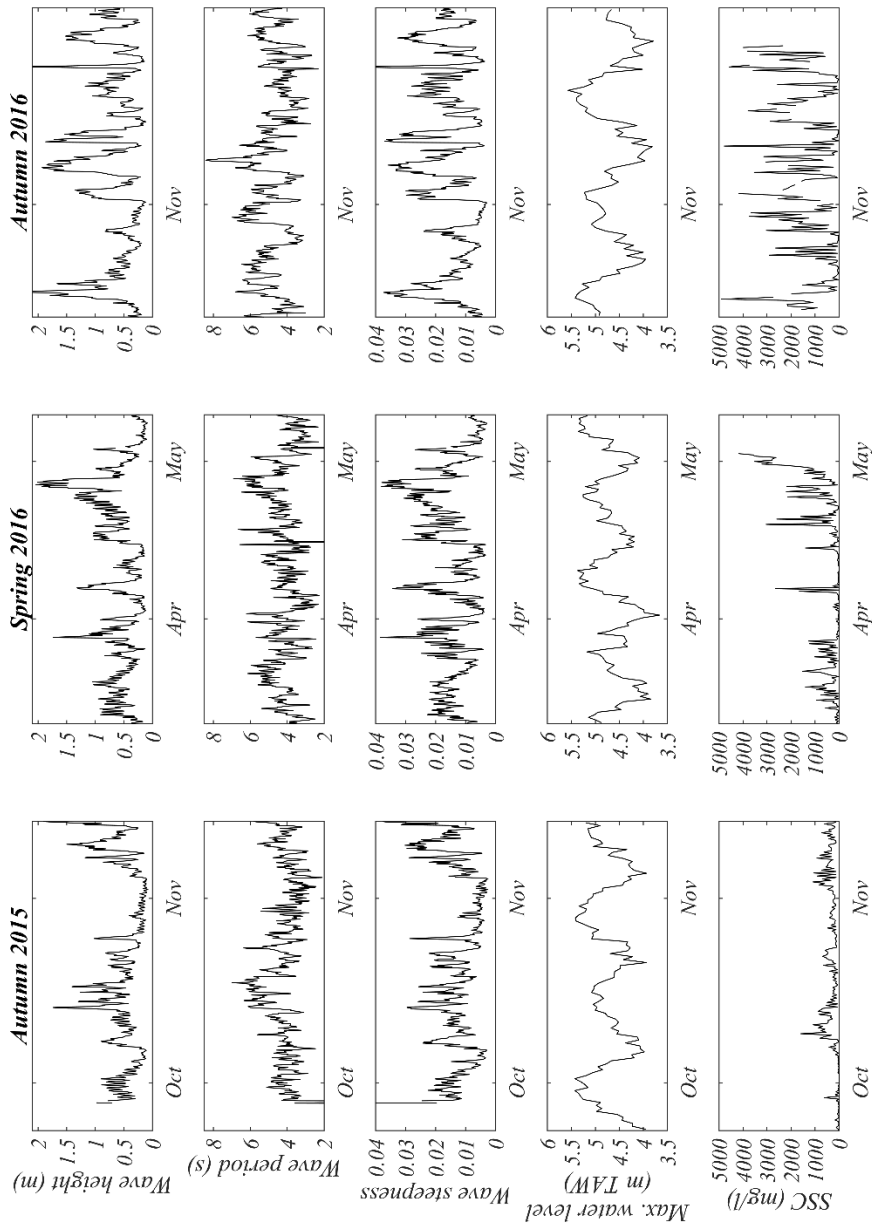


Figure 29. Time series of significant wave height, significant wave period, wave steepness, maximum water level, and SSC for the three measuring campaigns (for the frame at -8 m TAW at section 104, averaged over a 6-hour period). SSC data is not considered when biofouling occurred on the OBS.

4.3.2. Beach morphology and temporal variability of beach volume

Cross-shore topographic profiles were measured at three locations (a, b, and c) at two beach sections (100 and 104, Figure 26). At both sections the profile shape was concave with a gently sloping (1-2°), featureless intertidal beach (*i.e.* absence of bar and/or berm; Figure 30). The highest part of the dry beach (elevation > 7 m TAW) was relatively flat but its slope located around 40 m was steep (maximum slope of 16°). Profiles a, b, and c were characterized by a similar morphology, although profile a indicated a wider beach at both sections.

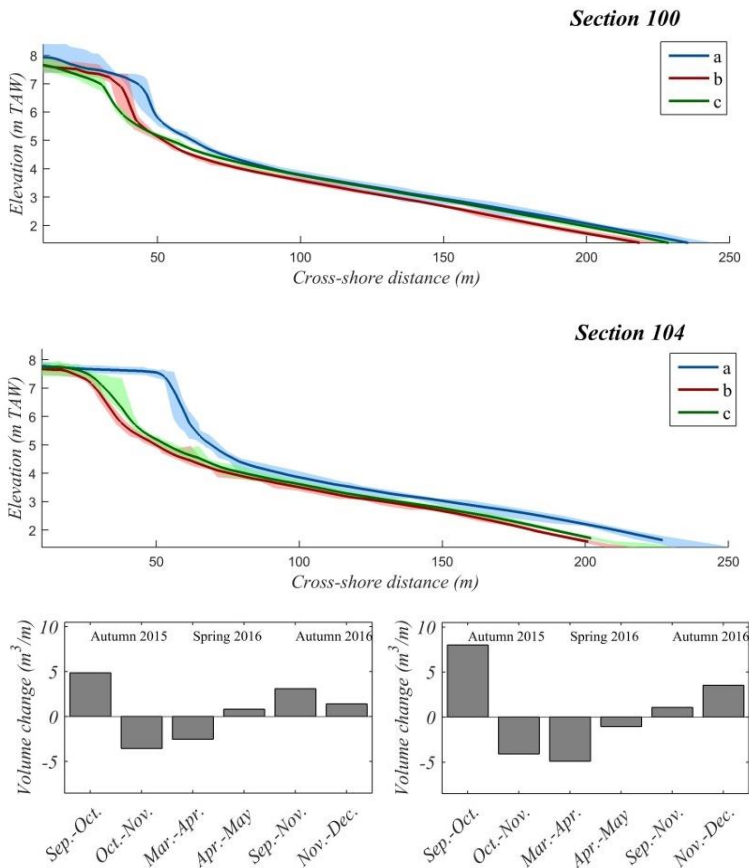


Figure 30. Beach topography and topographic changes. Top/middle: envelopes and average profiles for profiles a, b, and c. Bottom: monthly intertidal beach volume changes for both sections. Top and bottom left correspond to section 100, middle and bottom right to section 104.

At both sections the monthly variation in beach morphology was large with intertidal volume changes up to $7 \text{ m}^3/\text{m}$ (Figure 30). During the first campaign in autumn 2015 the biggest sand gain was observed over the first month ($5 \text{ m}^3/\text{m}$ at section 100 and $7 \text{ m}^3/\text{m}$ at section 104), whereas over the second month erosion was observed at both sections. During the second campaign the beach eroded, especially during the first month. The beach was relatively stable during the second month of this campaign. During the third campaign accretion occurred (approximately $6 \text{ m}^3/\text{m}$ over the campaign for both sections).

4.3.3. The relation between wave steepness, SSC, and morphological change

A comparison was made between wave steepness, SSC and intertidal beach volume change to study the effect of hydrodynamic forcing and sediment supply on beach topography. The lowest 10%, highest 10%, mean and median wave steepness and SSC were calculated for each period between topographic profiles. It was found that the mean was representative for the conditions that prevailed, so for further analysis monthly-averaged wave steepness and SSC were used.

A positive linear relationship was found between wave steepness and intertidal beach volume change (Figure 31, top left). Erosion was observed when the wave steepness was smaller than 0.015, whereas accretion was observed when it was larger than 0.015. This relationship was found to be significant with an R^2 of 0.67 and a p-value of 0.004 (< 0.1).

A positive linear relationship was also found between SSC and intertidal beach volume change (Figure 31, top right). Erosion occurred when SSC were low, whereas accretion occurred when SSC were high. An exception was the period between September and October 2015 when accretion occurred while wave steepness was small and SSC was low. However, the topographic profiles of September were surveyed before the nearshore campaign started. Based on the wave buoy data it seems that in the days between the topographic survey and the start of the campaign the wave conditions were very energetic with peaks in wave steepness up to 0.44. This suggests that the beach profiles surveyed in September were not representative for the beach profiles at the start of the campaign, thus the period between September and October 2015 was excluded from further analysis. Without this period, the R^2 of the relationship between SSC and intertidal beach volume change was 0.70 and the p-value was 0.002 (< 0.1), this means that the found relationship is significant.

A linear relationship was also found between wave steepness and SSC (Figure 31, bottom) with SSC increasing over wave steepness. For the

monthly-averaged relationship the R^2 was 0.74 and the p-value was 0.003 (< 0.1). When averaged over a three-day period instead of a month it becomes clear that this relationship is especially strong for wave steepness from 0.012 to 0.016. The increase in SSC over wave steepness in this phase is twice as strong as when the wave steepness is below 0.012 and five times stronger than when wave steepness is larger than 0.016.

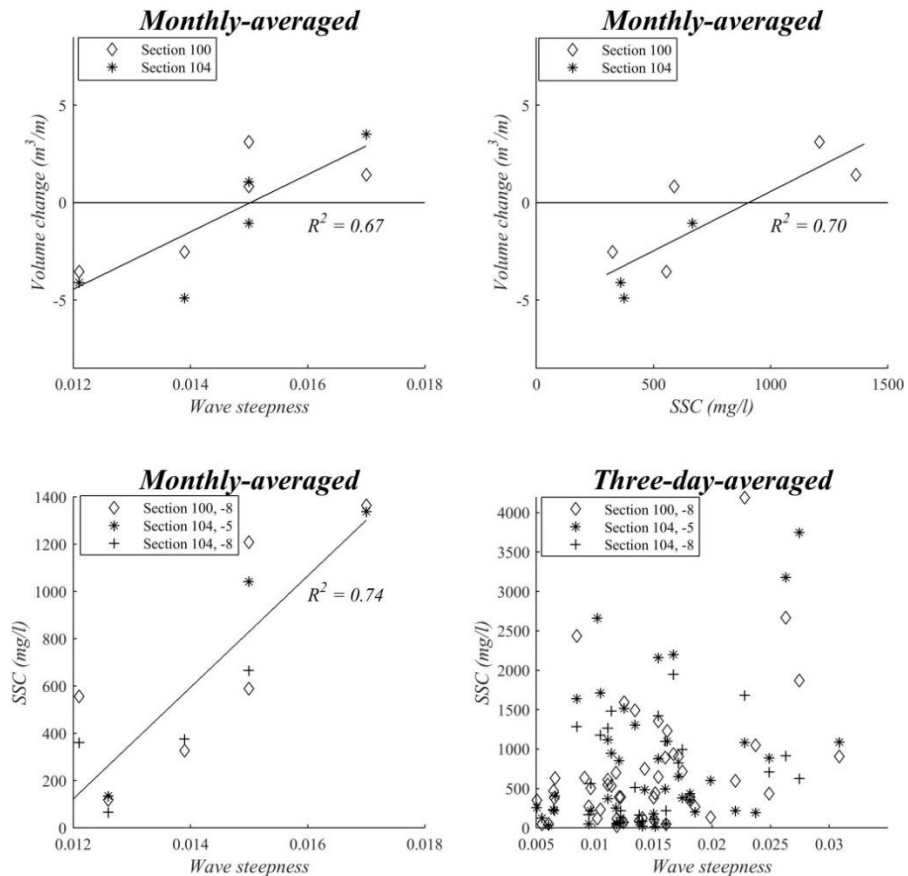


Figure 31. Comparison between monthly-averaged wave steepness and intertidal beach volume change (top left); SSC and intertidal beach volume change (top right); wave steepness and SSC (bottom left); and between three-day-averaged wave steepness and SSC (bottom right).

Topographic profiles were surveyed for more than 1.5 year, whereas the nearshore measuring campaigns had a total duration of 6 months. Therefore,

monthly volume changes were also compared to wave steepness based on 1.5 year of wave buoy and tide gauge measurements. From this analysis, three trends are observed (Figure 32). Firstly, there was a negative linear relationship between wave steepness and intertidal beach volume when wave steepness was smaller than 0.013. This relationship had an R^2 of 0.65 and a p-value of 0.172 (> 0.1) for both sections combined (0.79 and 0.016 for section 100 and 0.69 and 0.109 for section 104, respectively). This relation was thus not significant, but it is clear that for a low wave steepness (< 0.010) accretion is observed, whereas for a wave steepness of 0.010-0.013 erosion is observed.

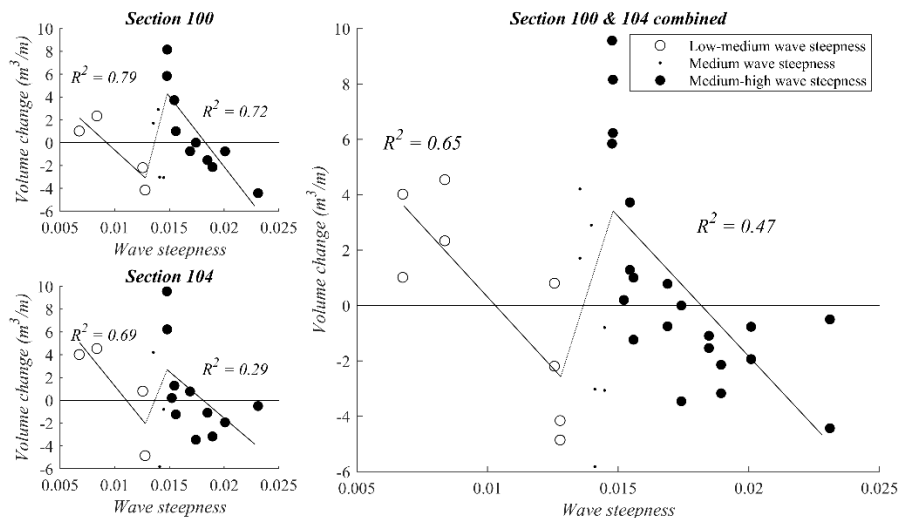


Figure 32. Volume change of the intertidal zone over wave steepness based on wave buoy and tide gauge data, for sections 100 and 104 separately (left, top and bottom respectively) and both sections combined (right).

Secondly, there was a negative linear relationship between wave steepness and intertidal beach volume when wave steepness was large (*i.e.* > 0.015). This trend had an R^2 of 0.47 and a p-value of 0.086 (< 0.1) for both sections combined (0.72 and 0.001 for section 100 and 0.29 and 0.002 for section 104, respectively), which makes this relationship significant. Accretion was observed when wave steepness was between 0.015 and 0.018, whereas erosion was observed when wave steepness was larger than 0.018.

Thirdly, there was a positive linear relationship for a wave steepness of 0.013 to 0.015 (not shown here). This trend connects the trends for low and high wave steepness and it corresponds to the trend that was found in Figure

31. This trend had an R^2 of 0.60 and a p-value of 0.029 (< 0.1) and was thus significant (0.56 and 0.095 for section 100 and 0.24 and 0.496 for section 104, respectively). A transition from erosive to accretive beach behavior was observed at a wave steepness of 0.014. This is close to the observed transition at a wave steepness of 0.015 that was found in Figure 31.

4.3.4. The effect of beach slope, wave direction, wave energy, and wind on the intertidal beach morphology

Beach slope, wave direction, wave energy, and wind are known to affect the relation between wave steepness and beach volume change in previous studies. However, at Mariakerke no effect of beach slope on the intertidal beach volume was found as is demonstrated in Figure 33 (top left). This might be due to the limited variation in slope, which only ranged from 1.05 to 1.17°.

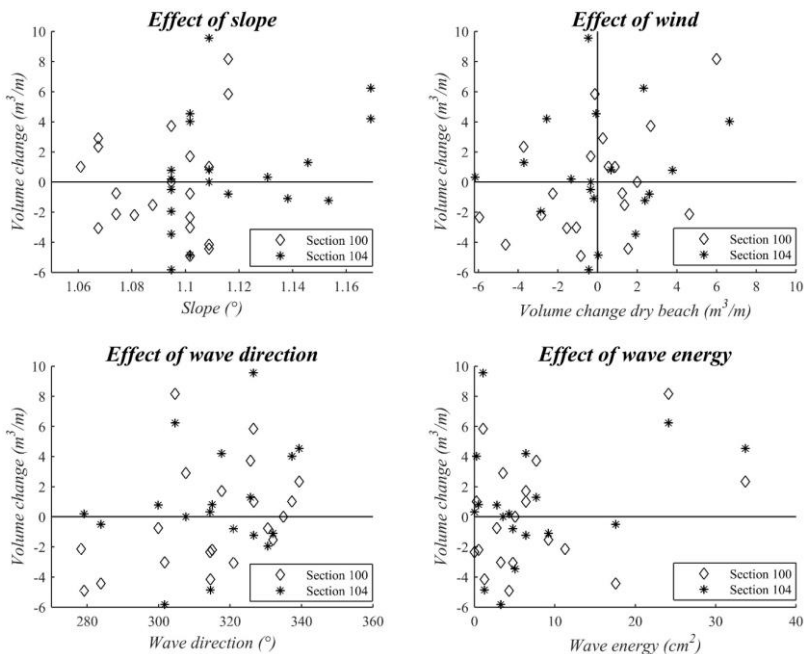


Figure 33. Volume change of the intertidal beach over beach slope (top left), volume change of the dry beach (top right), wave direction (bottom left), and wave energy (bottom right). All points are monthly averages.

The effect of wind-driven sand transport was investigated by comparing volumetric changes of the dry and intertidal beach (Figure 33, top right). The

dry and intertidal beach volume showed the same trend suggesting that the wind was unlikely responsible for transporting sand from the dry to the intertidal beach or vice versa. The effect of wave direction was also investigated (Figure 33, bottom left). Haerens *et al.* (2012) found that waves from the W-NW were most erosive. In this study erosion was indeed observed for waves from the W-NW, but no clear relationship between wave direction and intertidal beach volume could be distinguished. The effect of wave energy was also investigated (Figure 33, bottom right). As opposed to the observations of Haerens *et al.* (2012) there was not more erosion when the wave energy was large.

4.4. Discussion

The results suggest that the intertidal beach exhibits normal behavior with accretion when the waves are calm (wave steepness < 0.010) and erosion when the waves become more energetic (wave steepness > 0.010). However, when the wave steepness is between 0.013 and 0.015, a sudden increase in beach volume was observed. The relationships that were found between wave steepness and beach volume change in this study (Figure 32) were moderate, with an R^2 of 0.47 to 0.65 (for both sections combined), and characterized by some scatter. Part of this scatter might be due to the monthly averaging of the topographic change and wave steepness. Also, along-shore variation in beach topographic change is generally not revealed by measuring cross-shore profiles. Furthermore, beach topography is not only affected by the wave steepness, but also by other factors, such as the effect of wind and the wave direction, that have been discussed in section 4.4. Although the investigated forcing factors were not directly related to changes in intertidal beach topography, they may have caused some of the scatter in the relationships between wave steepness and intertidal beach volume change.

Despite some scatter, most relationships found in this study were significant. The only exception was the relationships between wave steepness and beach volume change when wave steepness was small (< 0.013), which was due to a limited number of observations in this range of wave steepness. The reversed trend for medium wave steepness, however, was strong. This trend has not been observed in previous studies that examined the effect of wave steepness on beach morphology (*e.g.* Ahrens and Hands, 1998, Johnson, 1949) and will be discussed hereafter.

4.4.1. The critical wave steepness distinguishing erosion and accretion

The boundary between accretive and erosive largely depends on the beach and wave characteristics. Values of 0.01 (Masselink *et al.*, 2010) up to 0.02-0.06 (Johnson, 1949) have previously been reported. Larson (1988) obtained a predictive criterion for this boundary:

$$\frac{H_0}{L_0} = 115 \left(\frac{\pi \omega_f}{gT} \right)^{1.5}$$

where ω_f is the fall velocity (0.041 m/s here for a D_{50} of 310 μm) and T is the average significant wave period (4.17 s here). According to this criterion the boundary for Mariakerke beach is at an offshore wave steepness of 0.020. This results in a boundary of 0.013 for nearshore steepness. This is close to the value that was found in this study (0.010) and thus it confirms the relation that was found between wave steepness and beach volume change.

4.4.2. The effect of nearshore suspended sediment supply on beach morphological changes

The reversed trend in beach morphology over wave steepness could not be explained by traditional factors such as wave direction and wind. SSC, on the other hand, increased remarkably fast when wave steepness was between 0.012 and 0.016. The cross-shore currents are flood dominant in the research area and therefore the current-driven suspended sediment transport is directed onshore (Brand *et al.*, 2017). An increase in SSC will therefore lead to an increase in onshore sediment transport. Most probably this explains why the intertidal beach volume is positively related to wave steepness when it is between 0.013 and 0.015.

4.4.3. The origin of the nearshore suspended sediment

The suspended sediment was probably not supplied by local beaches, because SSC was most often higher at -8 m TAW than at -5 m TAW (on average 1050 mg/l compared to 830 mg/l for section 104). Also it is likely that the sediment was not stirred up near the frames because the waves do not break yet in this zone. Furthermore, the sediment is probably not brought in by longshore currents, because this would mean that for medium wave steepness the beach in the southwest erodes whereas the beach at Mariakerke grows. This is rather unlikely because of the relative uniformity of the shoreline (Deronde *et al.*, 2008).

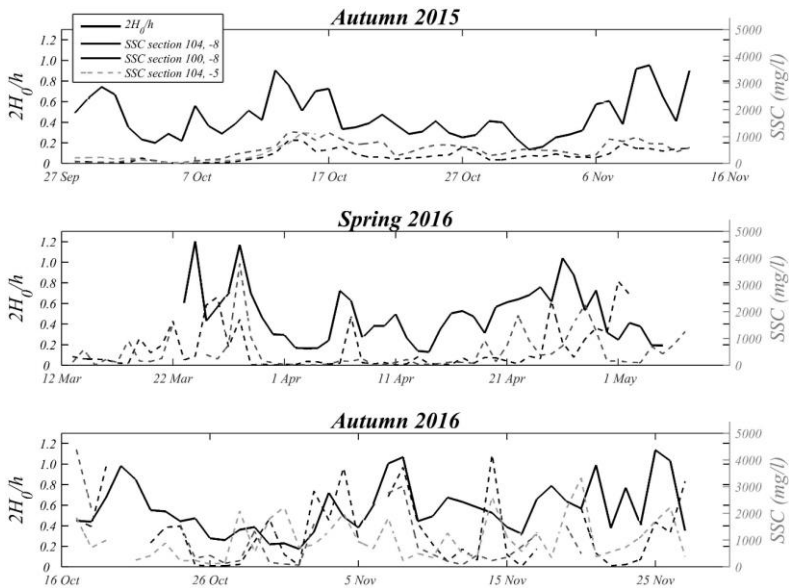


Figure 34. Time series of $2H_0/h$ and SSC from the three frames (averaged over the three OBS) for all nearshore measuring campaigns.

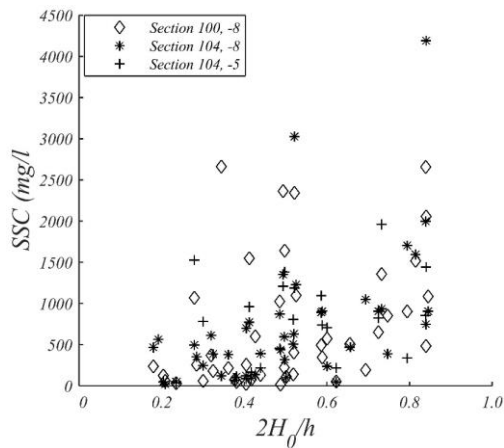


Figure 35. SSC versus $2H_0/h$ for the three nearshore measuring frames averaged over a three-day period.

Instead, the origin of the sediment was most likely from the Stroombank, a sand bank in front of the coast (Figure 26). Wave breaking over this bank starts when $2H_0 > h$ (H_0 is offshore wave height and h is water level at the

sandbank). It was found that $2H_0/h$ and SSC indeed follow a similar pattern over time (Figure 34 and Figure 35). Moreover, they are exponentially related with an R^2 of 0.33. Wave breaking over the bank occurred 10 % of the time so it is likely that the suspended sediment at Mariakerke beach originates from the sandbank. More research is needed to confirm the origin of the suspended sediment though.

4.4.4. Conceptual model of morphological change in relation to wave steepness and SSC

Four beach states were defined based on the observations of wave steepness and intertidal beach volume change. These four states are presented in a conceptual model (Figure 36). The first state is the calm accretive state, characterized by a wave steepness smaller than 0.010. In this state waves transport sediment shoreward and the beach grows. Onshore sediment transport by currents is limited, because the SSC is low.

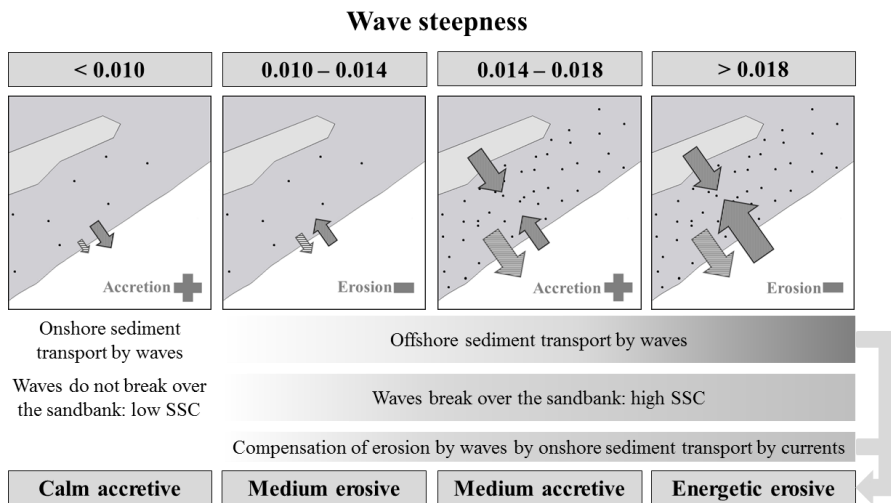


Figure 36. Conceptual model of suspended sediment transport and intertidal beach morphological response over wave steepness. Dark grey arrows represent net sediment transport by waves, striped arrows represent net sediment transport by currents.

The second state is the medium erosive state when the wave steepness is between 0.010 and 0.014. In this state the beach starts to be eroded by waves. Although waves start breaking over the sandbank and SSC rise, onshore sediment transport by currents is too small to compensate the erosion by

waves and the beach erodes. The third state is the medium accretive state when the wave steepness is between 0.014 and 0.018. Waves erode the beach, but SSC are large. Onshore sediment transport by currents compensates offshore sediment transport by waves and the beach grows. The fourth beach state is the energetic erosive state characterized by a wave steepness larger than 0.018. In this state SSC no longer rise and wave erosion becomes dominant over onshore transport induced by currents again. These four beach states are mainly based on monthly averages of wave steepness and monthly intertidal beach volume changes and it should be noted that other parameters, such as longshore sediment transport and wave direction, might influence the intertidal beach morphodynamics.

4.5. Conclusion

An extensive dataset of 1.5 years of intertidal beach topography and nearshore hydrodynamics and SSC was collected to examine the relation between wave steepness and morphological change for a macro-tidal, sandy beach. The monthly-averaged wave steepness that was covered ranged from 0.005 to 0.025 and the monthly-averaged SSC ranged from 300 to 1400 mg/l.

Linear correlation analysis was used to investigate the relation between morphology, wave steepness, and SSC. Accretion was observed when wave steepness was smaller than 0.010 and erosion was observed when wave steepness was between 0.010 and 0.013. This relationship was not significant though, due to a limited amount of data in this range. An opposite and significant trend was observed when wave steepness was medium (0.013-0.015), with erosion by small waves and accretion by large waves. Traditional factors such as wave energy, wave direction, beach slope, and wind could not explain this opposite trend. SSC, on the other hand, increased remarkably fast when wave steepness was in this range. Shoreward suspended sediment transport was driven by flood dominant cross-shore currents resulting in (partial) compensation of wave erosion. When wave steepness was larger than 0.015 the beach morphology was negatively related to wave steepness again, with erosion from a wave steepness of 0.018.

Based on these results four beach states can be identified: calm accretive, medium erosive, medium accretive, and energetic erosive. It is thus concluded that variations in intertidal beach morphology of macro-tidal beaches depend not only on wave steepness but also on current magnitude and direction and SSC.

Chapter 5

Intertidal beach morphodynamics on a daily scale *

5.1. Introduction

The intertidal zone is a key area for the beach morphodynamics, as it serves as the pathway of sediment from the subtidal zone to the dunes and vice versa (Aagaard *et al.*, 2005, Biauxque and Sénéchal, 2019, de Vries *et al.*, 2019). Generally, the intertidal beach erodes during storms, while sediment is transported back to the beach during calm conditions (Masselink and Hughes, 2003). A persisting challenge is to unravel the exact forcing factors that control beach erosion and accretion, as multiple forcing factors (*e.g.* waves, tidal currents, and wind) act simultaneously on the intertidal beach.

It is generally acknowledged that wave steepness, *i.e.* wave height over wavelength, is an important driving factor for topographic change in the intertidal zone (*e.g.* Meyer, 1936, Sunamura and Horikawa, 1974, Ahrens and Hands, 1998, Masselink *et al.*, 2009, Philips *et al.*, 2017). Onshore sediment transport is commonly observed when wave steepness is small, whereas offshore transport is observed when wave steepness is large. In contrast to the effect of waves, the effect of tide remains uncertain though. A considerable amount of studies to intertidal beach morphodynamics has been carried out on microtidal beaches, where tides generally play a passive role in sediment transport and topographic change (*e.g.* Wright and Short, 1984, Davis, 1985). The morphodynamics of macro-tidal beaches has been studied to a lesser extent, but it has been recognized that the role of tidal currents may be

* Submitted as: Brand, E., Montreuil, A-L., Houthuys, R., Chen, M., 2019. Relating tidal currents, waves, and natural sediment supply to changes in intertidal beach topography on macro-tidal, sandy beaches. *Mar. Geol.*, under review

significant (Wright *et al.*, 1982, Masselink and Hegge, 1995, Voulgaris *et al.*, 1998, Sipka and Anthony, 1999, Masselink and Pattiaratchi, 2000, Cartier and Héquette, 2011). It has been observed that the effect of tidal currents may vary over a spring-neap tidal cycle and can be reinforced by wind forcing (Anthony *et al.*, 2004). It has also been acknowledged that the tide is responsible for shifts in the position of the shoaling wave, surf, and swash zone across the beach. Variations in tidal amplitude enhance or limit the movement of these zones, and could thus weaken or amplify the impact of waves on the intertidal beach (Masselink and Short, 1993, Levoy *et al.*, 2000, Kroon and Masselink, 2002). However, the relative importance of tide in macro-tidal beach morphodynamics remains uncertain.

Furthermore, the effect of short-term (*i.e.* daily) variations in (natural) sediment supply on the intertidal beach dynamics has rarely been studied, due to difficulties related to measuring sediment transport (Aagaard, 2014). Earlier, studies based on geological evidence have proven that the exchange of sediment between the nearshore and the beach is an important element of the sediment budget of beaches (*e.g.* Beets *et al.*, 1992, Stive and DeVriend, 1995, Cowell *et al.*, 2001, van Heteren *et al.*, 2011). Studies on the effect of monthly to seasonal variations in sediment supply endorse this fact (Dubois, 1989). Nevertheless, field investigations of the effect of short-term variations in sediment supply to sandy beaches remain scarce (Aagaard, 2014).

To improve our knowledge of the intertidal beach morphodynamics on a daily scale, this study aimed to investigate and determine the relative importance of the impact of waves, tidal currents, and variations in (natural) sediment supply on the intertidal beach topography. This was done based on extensive field measurements to be able to perform a statistical analysis on the importance of the forcing factors. In total, six fortnight measuring campaigns were carried out during which the marine forcing and SSC were measured at the low water line. Cross-shore topographic profiles was measured every day at low tide.

5.2. Methods

Six fortnight measuring campaigns were carried out to investigate the effect of marine forcing on the intertidal beach topography at Mariakerke and Groenendijk (Table 7). Flow velocity, water level, wave conditions, and SSC were measured continuously with a frame (Figure 37 and Figure 38) that was placed on the NLW line at Mariakerke and on top of the lowest bar (+1.90 m TAW) at Groenendijk. The beach topography of five cross-shore profiles

from the toe of the dunes/dike to the low water line (Figure 37) was measured every day during low tide. The campaigns were designed to cover both energetic and calm conditions (Table 7) and to each cover a full spring-neap tidal cycle. The name of each campaign corresponds to the season (*i.e.* spring, summer, or winter) and the study site (*i.e.* flat = developed site Mariakerke; barred = natural site Groenendijk).

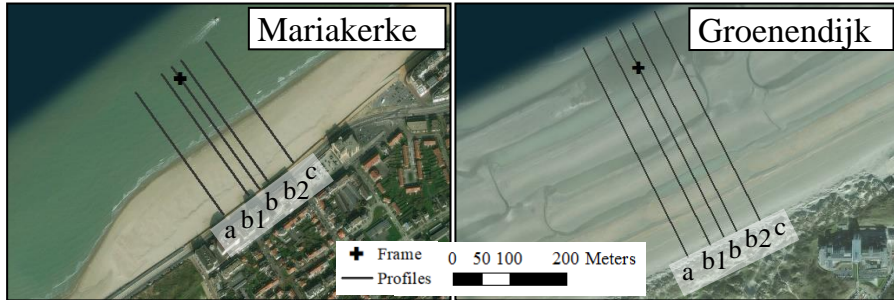


Figure 37. Maps of the study sites with the intertidal frame and cross-shore topographic profiles indicated.

Table 7. Overview of the intertidal measuring campaigns. (Note that ‘flat’ here corresponds to the developed site Mariakerke and ‘barred’ corresponds to the natural site Groenendijk).

Campaign	Location	Date
Spring - flat	Mariakerke	13 – 24 March 2017
Summer - barred	Groenendijk	8 – 19 May 2017
Winter - flat	Mariakerke	7 – 20 November 2017
Winter - barred	Groenendijk	23 January – 2 February 2018
Summer - flat	Mariakerke	16 – 26 April 2018
Autumn - barred	Groenendijk	31 October – 13 November 2018

5.2.1. Hydrodynamics and sediment dynamics

The measuring frame (Figure 38) was equipped with an OBS at 35 cm above the bed to measure turbidity at a frequency of 1 Hz. Turbidity was converted to SSC based on a calibration with in-situ samples. Furthermore, two ADCPs (Aquadopp model) were mounted on the frame to measure profiles of flow velocity with a 5 cm interval. One was mounted looking up at 50 cm above the bed and measured at 1 Hz and the other was looking down at 60 cm above the bed and measured at 4 Hz. Additionally, an ECM was mounted at 50 cm

above the bed. This sensor was set to measure flow velocity and pressure at 8 Hz for 1 minute every 10 minutes, from which significant wave height and period were calculated as the mean wave height/period (trough to crest) of the highest one third of the waves.

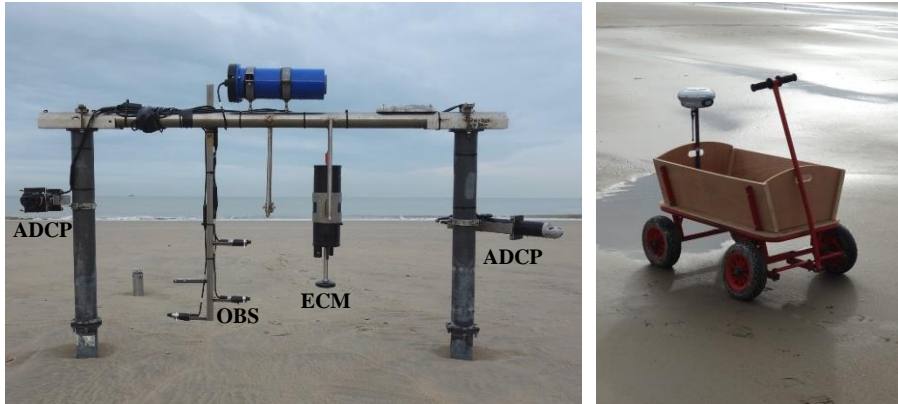


Figure 38. Left: The intertidal measuring frame (1 m high, 2.2 m wide) with (from left to right) the down-looking ADCP, the OBS, the ECM, and the up-looking ADCP. Right: The RTK-GNSS mounted on a beach cart.

The data was treated by removal of the obvious outliers and of the data when the equipment was exposed to the air. The tidal water level was extracted from the water level measurements with a least squares harmonic analysis (Pawlowicz *et al.*, 2002). The daily maximum tidal water level was determined. From the wave measurements wave steepness was calculated as $Wave\ steepness = H/L$. Wavelength was calculated from the significant wave period and height depending on the water depth and wave height with the dispersion equation (Masselink *et al.*, 2011):

$$L = gT^2 \tanh(2\pi h/L)/2\pi$$

or the shallow water approximations (Masselink *et al.*, 2011):

$$L = T\sqrt{gh}$$

The bed shear stress was calculated for tidal currents (subscript c) and waves (subscript w) separately according to Dufois *et al.* (2008):

$$\tau_c = \rho C_d u^2$$

$$\tau_w = 0.5\rho f_w U_b^2$$

with:

$$f_w = 0.00251 \exp(5.21(A/k_s)^{-0.19})$$

with (De Swart, 1974):

$$A = U_b T / (2\pi)$$

$$k_s = 2.5 D_{50}$$

where ρ is the water density, C_d is the drag coefficient (= 0.003 for sandy beds) and u is the flow velocity. In this study the hourly-averaged flow velocity was used to calculate the current-induced bed shear stress. U_b is the near bed orbital velocity and D_{50} is the grain size on the intertidal beach. The average D_{50} over the intertidal zone was used for each campaign.

Wave direction and wind conditions were acquired from a wave buoy at -8 m TAW (Raversijde, 1 km from Mariakerke) and wind station (Oostende) from Meetnet Vlaamse Banken (Appendix A).

5.2.2. Beach topography

The beach topography was measured once per day during low tide. Five cross-shore profiles were surveyed: one central profile (b), two profiles at 25 m from the central profile (b1 and b2), and two distant profiles 75 m from the central profile (a and c, Figure 37). At Mariakerke, the profiles a and c were 75 m away from groins that bounded the study area at each side. The topography was measured with a Real-Time Kinematic Global Navigation Satellite System (RTK-GNSS), which has an accuracy of 2-3 cm for the x, y, and z coordinates combined, mounted on a cart (Figure 38).

The volume of the intertidal beach was calculated from the topographic profiles. The intertidal beach was defined as the area between NHW and NLW. Volumes were calculated for each profile separately using trapezoidal rules. The volumes of all profiles (a, b1, b, b2, and c) were averaged and daily volume changes were calculated. Due to poor RTK-GNSS signal or deviation of the measurements from the planned profile lines, volumes are lacking for approximately 3 days each campaign.

5.2.3. Relating forcing and response: principal component analysis

A Principal component analysis (PCA) was applied to determine the common variation of multiple marine forcing factors and topographic change. This method has previously been applied successfully in coastal research to identify forcing factors for morphological changes (*e.g.* Suanez and Stéphan, 2006, Montreuil *et al.*, 2013, Fabbri *et al.*, 2017). A PCA was applied on wave steepness, maximum tidal water level, and current direction to determine which factor, waves or tide, was the most important factor determining the main current direction. Furthermore, a PCA was applied on wave steepness, wave direction, maximum tidal water level, SSC, and intertidal beach volume change, to investigate the relationship between marine forcing and topographic response. SSC was chosen as a proxy for the natural sediment supply, because the majority of the suspended sediment is brought to the beach from the nearshore, as will be shown in the results. Principal components were calculated and the correlations between each principal component, the forcing factors, and the topographic response were computed. In this study correlations above 0.5 were deemed relevant and correlations between 0.3 and 0.5 were also considered.

5.3. Results

5.3.1. Hydrodynamics and sediment dynamics

The investigated hydrodynamics covered a wide variety of conditions over the six campaigns (Figure 39 and Table 8). The wave conditions were calm during the Summer-barred and Summer-flat campaigns, with an average wave height of 0.22 m and 0.21 m, respectively, and an average wave steepness of 0.018. The conditions were more energetic during the other campaigns, especially during the Winter-flat campaign when peaks in wave height (steepness) reached 1.46 m (0.068). The average wave period over all campaigns was 3.7 s, with a minimum of 2.2 s and a maximum of 6.1 s. The offshore wave direction was W to NNW, varying between 260° and 340°. The wind conditions showed a similar pattern as the waves, with strong winds generating large waves. Wind speeds varied between 3 and 12 m/s and a direction between S (85°) and NW (325°).

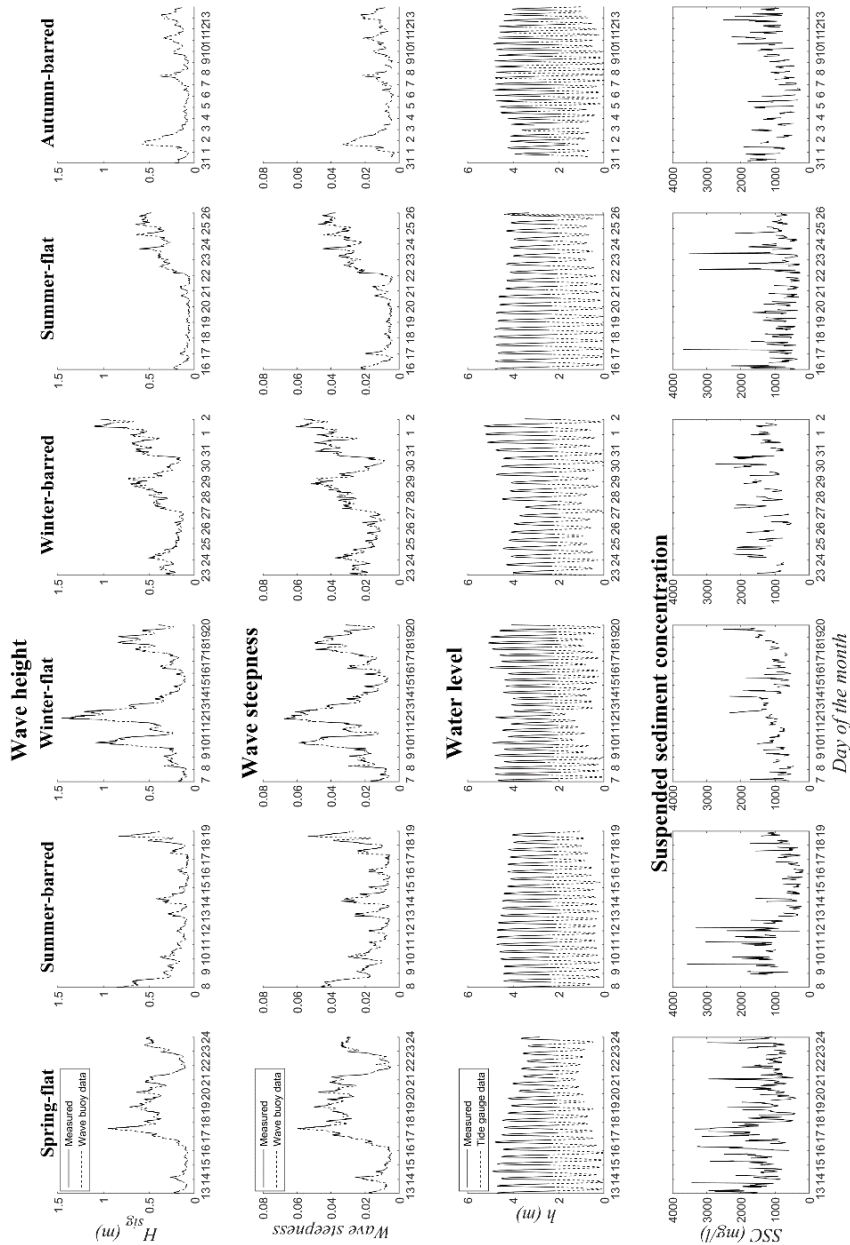


Figure 39. 30-minute-averaged hydrodynamics: significant wave height, wave steepness, water level, and SSC for all the campaigns. The measured water level is supplemented with tide gauge data from Oostende Harbor for low tide.

The water level showed clear spring-neap tidal variations during all the campaigns (Figure 39). Haerens *et al.* (2012) defined a storm threshold for water level of 5 m TAW. This threshold was exceeded twice during the Winter-flat campaign and three times during the Winter-barred campaign. The highest water level was observed during the Winter-barred campaign, when a peak in water level reached 5.28 m TAW.

The 30-minute-averaged SSC ranged from 200 mg/l up to 3500 mg/l (Figure 39). During the Spring-flat campaign the SSC started high (around 2000 mg/l), while waves were only 0.1-0.3 m, but this was most likely resulting from the disposal of dredged material southwest of Mariakerke on 13 March (visual observations during the measurements).

Table 8. Overview of the average (avg) and maximum (max) hydrodynamic conditions and SSC for all campaigns

		Spring- flat	Summer- barred	Winter- flat	Winter- barred	Summer- flat	Autumn- barred
Wave height (m)	avg	0.31	0.22	0.42	0.39	0.21	0.17
	max	0.95	0.85	1.46	1.10	0.65	0.55
Wave steepness	avg	0.024	0.018	0.028	0.028	0.018	0.011
	max	0.059	0.054	0.068	0.060	0.048	0.028
Water level (m)	Max	4.91	4.72	5.09	5.28	4.84	4.88
SSC (mg/l)	avg	1325	733	1056	1275	839	1035
Bed shear stress (N/m ²)	waves	5.34	3.71	7.01	6.63	3.49	2.87
	currents	0.06	0.06	0.08	0.08	0.07	0.07

The occurrence of calm versus energetic waves and neap versus spring tide during the campaigns is summarized in Table 9. A wave steepness of 0.013 is used as the theoretical boundary for energetic conditions based on the monthly morphodynamics. All conditions are covered, but calm hydrodynamic conditions (neap tide and low waves) are less common than energetic conditions (spring tide and large waves).

Table 9. Occurrence of hydrodynamic conditions.

	Neap tide (max. water level < 4 m)	Spring tide (max. water level > 4 m)
Calm waves (steepness < 0.013)	14%	28%
Energetic waves (steepness > 0.013)	26%	32%

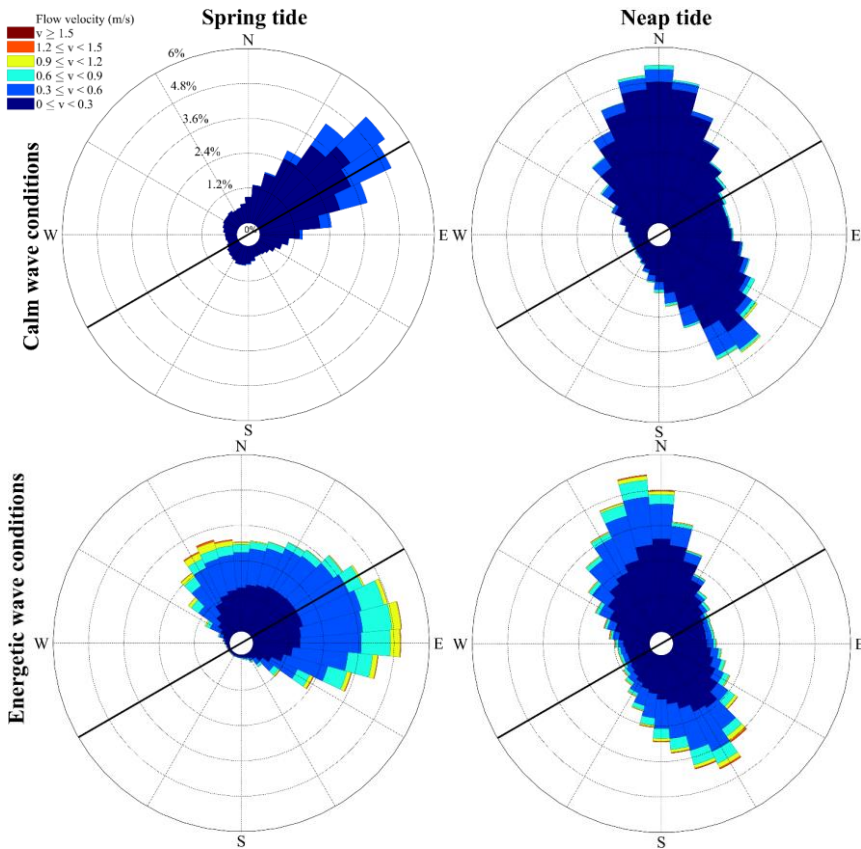


Figure 40. Typical current roses for spring vs. neap tide (left vs. right) and calm vs. energetic conditions (top vs. bottom). Currents were measured at 35 cm above the bed at Mariakerke and currents are not included for water levels < 2.39 m TAW. The shoreline orientation is indicated by the black line. Each current rose represents one tidal cycle.

5.3.2. Current direction

Figure 40 shows four typical current roses for spring and neap tidal cycles under calm and energetic wave conditions. During spring tide (left) the alongshore oriented tide-generated currents dominated, whereas during neap tide (right) cross-shore oriented wave-generated currents were dominant. Besides the effect of tide, the current direction was also influenced by the wave conditions with more cross-shore oriented currents when wave conditions were more energetic (bottom). The observations at 35 cm above the bottom were representative for the water column, except that seaward currents were stronger close to the bottom, whereas shoreward currents were stronger in the water column as a result of wave action.

The alongshore currents were especially strong during the flood phase with an average speed up to 0.4 m/s (35 cm above the bed, Figure 41). During the ebb phase the average alongshore current was almost zero at the low water line. Fluctuations in the alongshore current were mainly observed during energetic wave conditions as a result of waves, especially during low tide when waves were breaking near the frame (Figure 41, bottom). The difference in alongshore flow velocity between spring and neap tide was large at Mariakerke, while it was small at Groenendijk. This contrast may be explained by the presence of the groins at Mariakerke which likely affect the current pattern or the larger flow section (wider intertidal beach) at Groenendijk.

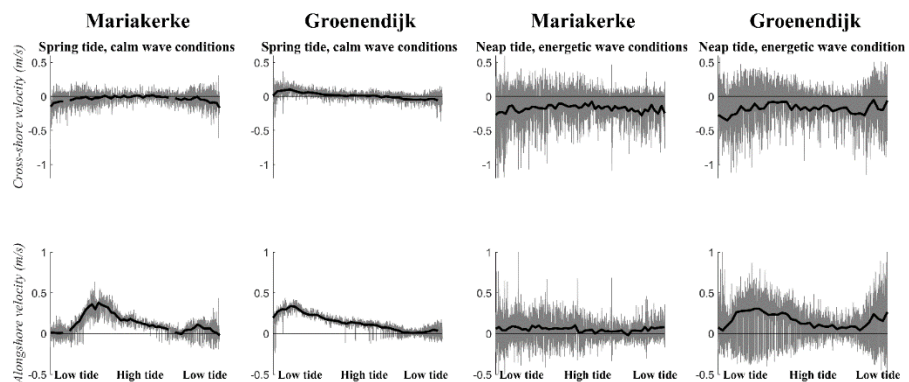


Figure 41. Cross-shore (top) and alongshore (bottom) flow velocity at 35 cm above the bed over one tidal cycle during spring tide & calm wave conditions (left) vs. neap tide & energetic wave conditions (right), with the measured flow velocity in grey and the 10-minute averaged flow velocity in black.

The 10-minute averaged cross-shore oriented current was almost zero when wave conditions were calm, whereas it was 0.2 m/s and seaward oriented when waves were energetic. The current velocity was measured at 35 cm above the bed and because the measurements represent processes in the shoaling and breaking zone the current direction is away from the shore as a result of undertow. The fluctuations in cross-shore flow velocity were much larger when waves were energetic than when they were calm as a result of waves.

Table 10. Correlations between daily dominant current direction, daily-averaged wave steepness, maximum tidal water level, and the first principal component for both study sites combined. High correlations are bold (>0.5) and underlined ($0.3-0.5$).

	Mariakerke 1 st principal component	Groenendijk 1 st principal component
Dominant current direction	0.76	0.60
Wave steepness	<u>-0.43</u>	-0.54
Maximum tidal water level	<u>0.49</u>	0.53
Percentage of variation explained	54 %	62 %

A PCA was applied to assess the effect of waves and tide on the current pattern. The analysis included the dominant current direction, maximum tidal water level, and wave steepness. The PCA shows that the dominant current direction, wave steepness, and maximum tidal water level are all strongly correlated to the first principal component (Table 10). The current direction becomes more positive, thus more alongshore (NE) oriented, when it is spring tide and when wave conditions are calm. They become cross-shore oriented during neap tide and energetic waves conditions. The PCA shows that both waves and tide influence the current direction equivalently.

5.3.3. Natural sediment supply to the beach

SSC was compared to wave steepness (Figure 42) and a clear relationship was observed between them. The measured SSC increased fast when wave steepness was small (< 0.025). They were linearly related with an R^2 of 0.40 and a p-value of $6.22e^{-5}$ (< 0.10). When wave steepness was larger than 0.025 the increase in SSC over wave steepness declined with 70%. However, the relationship between SSC and wave steepness was still linear, with an R^2 of 0.13 and a p-value of 0.07 (< 0.10). Wave steepness and SSC follow a similar

pattern but often lagged in time. It becomes clear that peaks in wave steepness and SSC may coincide (e.g. Winter-flat), but that there is an average time lag of 1.3 tidal cycles (Figure 42, bottom). At the start of the Spring-flat campaign the SSC was large even though wave conditions were calm. This was however explained by a disposal of sediment that happened on 13 March southwest of Mariakerke.

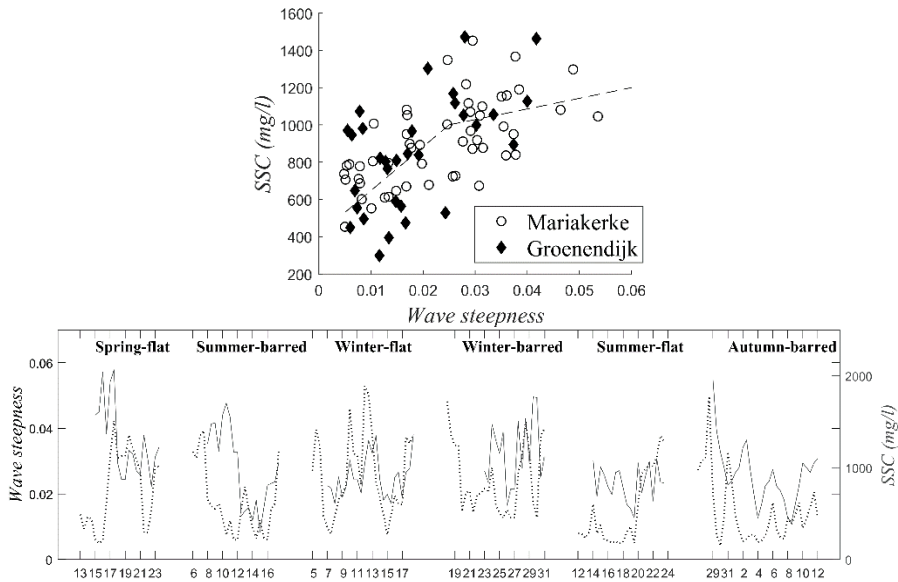


Figure 42. Top: Comparison between SSC and wave steepness when both are averaged over a tidal cycle. Data that was affected by the nearby sediment disposal during the Spring-flat campaign was removed. Bottom: Time series of SSC (grey line) and wave steepness (black, dotted line) for all campaigns. Wave steepness was supplemented with data from the wave buoy at Raversijde to illustrate the wave conditions before the campaign.

5.3.4. Beach topography

The topography of five cross-shore profiles (Figure 37) was measured every day at low tide (Figure 43, bottom). At Mariakerke, the profile shape was concave with a gently-sloping, featureless intertidal beach (*i.e.* absence of bars and/or a berm). The highest part of the dry beach (> 7 m TAW) was relatively flat but a steep slope was located at 50 m from the dike. The standard deviation of the beach topography was highest around this steep slope. At Groenendijk, the intertidal beach was characterized by four intertidal bars located at 3.8, 2.8, 1.8 and 0.9 m TAW.

The standard deviation of the daily topographic change in the intertidal zone was in the order of 1-20 cm (Figure 43, middle) and daily intertidal beach volume changes were large with peaks up to 5 m³/m (Figure 43, top). Accretion was observed during the Summer-barred (+6.19 m³/m in total), Spring-flat (+5.23 m³/m in total), and Summer-flat (+4.49 m³/m in total) campaigns. Little net change was observed over the Winter-barred campaign (+1.09 m³/m in total), although the standard deviation of the beach topography was high (up to 8 cm), especially at the bars. Net erosion was observed during the Winter-flat campaign (-3.28 m³/m in total), with most erosion occurring on 11 November. At Groenendijk, the bars were flattened and migrated onshore during calm conditions (Summer-barred, autumn-barred), whereas they became steeper during energetic conditions (Winter-barred), similar to the findings of Simmonds *et al.* (1996).

5.3.5. Relationship between hydrodynamics, SSC, and beach topography

A PCA was applied to investigate the intertidal beach morphodynamics at Mariakerke and Groenendijk. The correlations between intertidal beach volume, wave steepness, offshore wave direction, maximum tidal water level, SSC (a proxy for natural sediment supply), and each principal component were calculated. Wave direction was not related to any of the variables, including the intertidal beach volume, and therefore the final PCA was applied without considering wave direction. In Table 11 and Figure 44 the first two principal components of the PCA are presented. The first principle component accounts for 36-51% of the variance and the second principal component accounts for 28% of the variance.

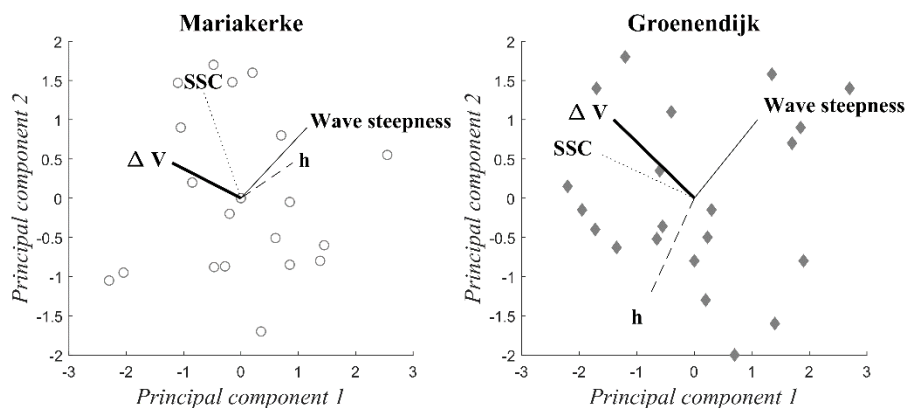


Figure 44. A PCA biplot between volume change and hydrodynamic forcing factors: wave steepness, maximum tidal water level, and SSC.

Table 11. Correlations between daily intertidal beach volume change, daily-averaged wave steepness, maximum water level, daily-averaged SSC, and the first two principal components for Mariakerke and Groenendijk. High correlations are bold (>0.5) and underlined ($0.3-0.5$).

	1 st principal component		2 nd principal component	
	Mariakerke	Groenendijk	Mariakerke	Groenendijk
Intertidal beach volume	-0.60	-0.54	0.26	0.52
Wave steepness	0.56	<u>0.41</u>	0.52	0.52
Maximum tidal water level	<u>0.47</u>	-0.29	0.26	-0.62
SSC	-0.33	-0.62	0.77	0.30
Percentage of change explained	36 %	51 %	28 %	28 %

The first principal component explains most of the topographic change observed in the intertidal zone. For both sites it shows that the beach volume decreases when wave steepness increases and/or when the natural sediment supply decreases and vice versa. At Mariakerke, the first principal component also shows that the beach erodes (the volume decreases) when the maximum water level is large. At Groenendijk, the maximum water level is not related to the first principal component.

The second principal component mainly shows the relation between sediment supply and wave steepness. SSC increase along with wave steepness (as illustrated in Figure 42). Besides wave steepness and SSC, the second principal component is significantly related to the intertidal beach volume and the water level at Groenendijk. It shows that the intertidal beach volume decreases when the tidal range increases, similar to the tidal influence that was described by the first principal component at Mariakerke. The second principal component also shows that the beach volume increases when wave steepness and thus sediment supply increases.

The intertidal beach thus erodes when wave steepness is large, sediment supply is limited, and when the tidal range is large, while the beach grows under opposite conditions. However, the effect of wave steepness is twofold: on the one hand large waves erode the intertidal zone, while on the other hand large waves result in an increase in sediment supply and thus in beach growth. Intertidal beach volume changes and wave steepness are compared in Figure 45. A third order polynomial relationship was fitted based on the monthly beach morphodynamics. The relationship is rather weak and characterized by substantial scatter that can largely be attributed to the tidal range. However, it shows that the intertidal beach volume increases for a wave steepness between 0.010 and 0.030. This is similar to the range for which SSC increases over wave steepness.

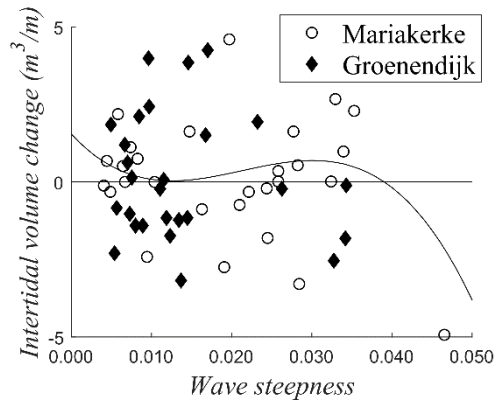


Figure 45. Daily intertidal beach volume change compared to daily-averaged wave steepness.

Two differences in intertidal beach morphodynamics were observed between the developed beach of Mariakerke and the barred beach of Groenendijk. At Mariakerke the effect of tide is stronger than at Groenendijk, which is most likely due to the groins that influence the tidal currents. At Groenendijk the effect of variations in sediment supply is larger than at Mariakerke. This is in agreement with previous studies that showed the large impact of natural sediment supply at Groenendijk (Deronde *et al.*, 2008, Houthuys, 2012). In spite of these differences, the PCA results for both Mariakerke and Groenendijk are very similar. Although there are obvious differences in beach morphology between Groenendijk and Mariakerke, both beaches are classified as dissipative (Deronde *et al.*, 2008), which probably explains their comparable behavior.

5.4. Discussion

Wave steepness and tidal conditions are the main drivers for topographic change based on the PCA. The beach response to wave steepness is similar to previous studies with accretion for small and erosion for large wave steepness (Meyer, 1936, Sunamura and Horikawa, 1974, Masselink *et al.*, 2010). Strong erosion was observed under high water levels before, but this mainly concerned storm surges instead of tidal variations in water level (Haerens *et al.*, 2012). Only few studies identified the tide as a driver for topographic change, especially for alongshore transport of bedforms (*e.g.* Levoy *et al.*, 2000, Anthony *et al.*, 2004).

5.4.1. The effect of tide on the beach topography

A possible effect of tidal range on beach topography has been described by Masselink and Short (1993). They argued that tidal range and wave height determine the relative importance of swash, surf zone, and shoaling wave processes, which in turn affects beach topography. Surf zone and swash conditions prevail in the intertidal zone when the relative tidal range (tidal range over wave height: TR/H_b) is low, whereas shoaling waves prevail when the relative tidal range is high. In this study the relative tidal range varied between 1 and 22, which is a relatively large variation. However, no relation between relative tidal range and intertidal beach volume change was found. This suggests that the relative importance of wave processes is not the cause for erosion during spring tide. This is in agreement with the results of Anthony *et al.* (2004) for a nearby study area in Northern France.

Tidal currents can significantly contribute to bed shear stress, thus enhancing local erosion (*e.g.* Bartholdy and Aagaard, 2001). In this study it was found that current-induced bed shear stress varied between 0.05 and 0.10 N/m^2 . This may be sufficiently large to get sediment in motion (Shields, 1936, Soulsby, 1997, Kobayashi *et al.*, 2008). However, no significant differences in bed shear stress between spring and neap tide were observed. Additionally, the current-induced bed shear stress was small compared to the wave-induced bed shear stress. The wave-induced bed shear stress mostly varied between 2.5 and 25 N/m^2 . It is thus highly unlikely that tide-generated currents stirred a significant amount of sediment and are thus not the cause of the increased erosion observed during spring tide.

Tidal currents did not erode significant amounts of sediment, but they did play an important role in transporting the sediment. Sediment that was stirred by waves was transported cross-shore by waves during neap tide. Net transport was onshore when waves were calm and offshore when waves were energetic. Alongshore tide-generated currents dominated during spring tide, similarly to other tide-dominated beaches (*e.g.* Reichmüth and Anthony, 2007). At the low water line mainly NE directed currents were observed. This is in agreement with previous observations close to Groenendijk, where sediment transport in NE direction was observed at multiple locations across the intertidal zone based on sand tracer experiments (Voulgaris *et al.*, 1998) and to previous observations of a net gradient of sediment transport towards the NE along the Belgian coast (Deronde *et al.*, 2006, Houthuys, 2011, Verwaest *et al.*, 2011). The finding of sediment being transport away from the beach by tidal currents contradicts the findings of Reichmüth and Anthony (2007), who did not attribute sediment transport to tidal currents at two

macro-tidal study sites in northern France. Sedrati and Anthony (2007), on the other hand, did attribute alongshore transport of sediment that was stirred by waves to alongshore currents on a different study site in northern France. Probably, these disagreements are due to the magnitude of the alongshore currents that were investigated, which was twice as large (up to 0.6 m) in this study and the study of Sedrati and Anthony (2007) as the magnitude of the alongshore currents observed by Reichmüth and Anthony (2007).

Strong tide-generated currents were previously observed in the intertidal zone of macro- and mega-tidal beaches. It was noticed that the magnitude of these currents strongly varied over a spring-neap tidal cycle and that wave-generated currents can be subordinate to tidal currents during spring tide (Anthony *et al.*, 2004), comparable to the observations in this study. Previous studies also found that the current direction was influenced by wave direction (Voulgaris *et al.*, 1998, Sedrati and Anthony, 2007) and wind speed (Anthony *et al.*, 2004, Sedrati and Anthony, 2007). The effect of wind speed and wave direction on the current direction was tested with the PCA, but was found to be negligible in this study. This might be due to rather constant W to NNW wave direction and the limited wind speed. In this study the maximum wind speed was 12 m/s, whereas Anthony *et al.* (2004) encountered wind speeds up to 15 m/s. Although strong tidal currents were observed previously, it remained unclear what their effect on the intertidal beach topography was. This was investigated in this study with PCA, from which it has become clear that the impact of tide can be large and may even be equivalent to that of waves.

5.4.2. Sediment supply to the beach

Besides wave and tidal conditions, variations in SSC were significantly correlated to changes in intertidal beach topography. Previously, the importance of sediment supply from the nearshore as a driving factor for topographic change was stressed for a monthly scale. In this study, the time lag that was observed between wave steepness and SSC (Figure 42, bottom) clearly suggests that a large part of the suspended sediment does not originate from local resuspension, but is indeed supplied from elsewhere. The Belgian coast is characterized by strong (tidal) currents in the nearshore area (Haerens *et al.*, 2012, Brand *et al.*, 2017). Hence, the source of this sediment may be the northern part of the French coast or the Flemish Banks, a complex of subtidal sand banks in front of the Belgian coast. However, it may also originate from the local shoreface (Houthuys, 2012). The SSC increased over wave steepness until the latter reached 0.025 (Figure 42, top). This point

coincides with the point where the positive relationship between wave steepness and intertidal beach volume becomes negative (Figure 45).

5.4.3. Summary of the observed intertidal beach morphodynamics

Waves and tidal currents were identified as the main drivers for topographic change. The amount of sediment supplied to the beach was found to be a secondary driver. It is noted that in-situ measurements in the intertidal zone are prone to inaccuracies. The current direction, for example, was only measured at the mean low water line, which was justified by the observations of Voulgaris *et al.* (1998) of rather homogeneous sediment transport (and thus current) directions across the intertidal zone at a nearby site. Furthermore, the observed topographic changes are affected by RTK-GNSS inaccuracies and alongshore variability in topographic change (Theuerkauf and Rodriguez, 2012). Nevertheless, the results are qualitatively in agreement with previous studies in nearby areas, such as Voulgaris *et al.* (1998) and Anthony *et al.* (2004) and the obtained relationships between hydrodynamics and intertidal beach topography are significant (p -value < 0.10) thanks to the large dataset that was investigated.

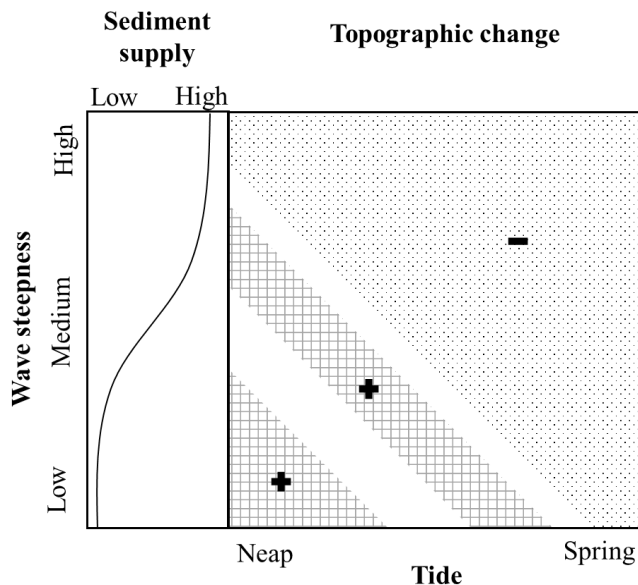


Figure 46. Conceptual summary of the combined effects of waves through wave steepness, tide, and sediment supply on the intertidal beach volume, with checkered, white, and spotted indicating accretion, stability, and erosion respectively.

In Figure 46 the combined effect of waves, tidal conditions, and natural sediment supply on the intertidal beach topography is summarized. The beach grows when wave steepness is small, whereas it erodes when wave steepness is large. During spring tide more erosion is observed than during neap tide, because strong tide-generated currents can transport sediment away from the beach. When wave steepness is medium an increase in sediment supply to the beach is observed. This sediment supply results in accretion (or less erosion) of the intertidal beach. This study thus highlights that the optimal conditions for beach growth are calm wave conditions, neap tide, and/or a large sediment supply to the beach.

5.5. Conclusion

The combined effect of waves, tidal currents, and sediment supply on the beach topography was examined based on extensive field measurements. With the dataset collected from six fortnight campaigns it was reaffirmed that wave steepness is an important driver for topographic change. Accretion was observed when wave steepness was small (< 0.010), whereas erosion was observed when wave steepness was large (> 0.010).

Besides wave impact, tidal currents also strongly influenced the intertidal beach topography. Currents were cross-shore and wave-dominated during neap tide, while strong tide-induced alongshore currents were observed during spring tide. These strong flood tidal currents were accompanied by erosion of the intertidal beach. It was hypothesized that the spring tidal currents transported locally eroded sediment away from the beach, thus enhancing erosion of the intertidal zone. The effect of the tidal currents on the beach topography was significant and equivalent to the effect of waves.

Topographic changes in the intertidal zone were also related to daily variations in natural sediment supply. Accretion was intensified when sediment supply was large. Daily variations in sediment supply were strongly related to the wave conditions. High SSC (up to 3500 mg/l) were observed during or following energetic conditions, with an average time lag of 1.3 tidal cycles. The effect of waves was thus twofold: larger waves were primarily erosive, but they also played a role in beach growth through reinforced sediment supply. The effect of variations in sediment supply on the intertidal beach topography was subordinate to the erosive effect of wave steepness and tidal currents.

The morphodynamics of a developed site (Mariakerke) was compared to that of a natural site (Groenendijk). It was found that the groins at the

developed site enhanced the erosive effect of tidal currents. At the natural site the sediment supply to the beach was larger and the beach was more susceptible to variations in this supply than the developed site. In spite of these differences both beaches respond in a similar way to hydrodynamic forcing.

This study thus highlights that on macro-tidal beaches tidal currents can thus be equally important as waves in shaping the beach topography and the effect of waves can be twofold: on the one hand are larger waves primarily erosive, but on the other hand they can also play a role in beach growth through reinforced sediment supply.

Chapter 6

Sediment transport in the intertidal zone*

6.1. Introduction

The intertidal zone is highly dynamic, as it is subject to waves, tidal currents, and wind. Its dynamics has frequently been examined by relating hydrodynamic forcing directly to morphological response (Anthony *et al.*, 2004, Reichmüth and Anthony, 2007, Austin *et al.*, 2010). Sediment transport processes have been investigated to a lesser extent due to the complex motions and scales involved: from seconds to tidal cycles and beyond. Thus, most studies to sediment transport have been qualitative (Aagaard *et al.*, 2005, Sedrati and Anthony, 2007, Turner *et al.*, 2008) and only few have been successful in quantifying sediment transport in the intertidal zone (*e.g.* Tonk and Masselink, 2005). Accurate measurements of sediment transport are crucial to improve our understanding and modelling capacities of the intertidal morphodynamics (Masselink *et al.*, 2008).

The high impact of breaking waves, rapidly changing bed levels, and variations in water level make it challenging to measure sediment transport in the intertidal zone. However the advance of sophisticated sensors such as high frequency OBS and acoustic backscatter sensors now allows to examine sediment transport more accurately and at an appropriate scale (Aagaard *et al.*, 2012). At the same time, equipment has been developed to measure the beach topography with a high spatial resolution. This provides more accurate

* Published as: Brand, E., De Sloover, L., De Wulf, A., Montreuil, A-L., Vos, S., Chen, M., 2019. Cross-shore Suspended Sediment Transport in Relation to Topographic Changes in the Intertidal Zone of a Macro-Tidal Beach (Mariakerke, Belgium). *Journal of Marine Science and Engineering*, 7, 1-16

estimations of beach volume changes compared to cross-shore profile measurements (Theuerkauf and Rodriguez, 2012). Therefore, sediment transport measurements can be appropriately validated.

In general, it is acknowledged that cross-shore sediment transport processes on beaches are controlled by the balance between onshore transport due to wave skewness/asymmetry and offshore transport by undertow (Voulgaris *et al.*, 1996, Masselink *et al.*, 2008). However, sediment transport has been investigated most extensively on micro- to meso-tidal beaches, where waves are the dominant forcing (Sedrati and Anthony, 2007). Only a few studies have been specifically dedicated to the measurements of sediment transport on macro-tidal beaches and the associated intertidal bars (i.e. ridges and runnels, Cartier and Héquette, 2015). As a result, the role of tidal currents in sediment transport remains unclear.

This study presents a comprehensive set of records of (cross-shore) sediment transport and topographic response for a sandy, macro-tidal beach along the Belgian coast. Surveys were collected over two fortnight periods under low and moderate wave energy conditions (maximum wave heights of 0.7 and 1.5 m). The aim is to highlight the role of cross-shore sediment transport processes in the dynamics of a tide-dominated beach. As it was previously found that bed load only comprised 20% of the total load along the Belgian coast (Voulgaris *et al.*, 1996), the focus of this study is on suspended sediment transport.

6.2. Methods

6.2.1. Data acquisition – hydrodynamics and sediment transport

This study was carried out at the beach of Mariakerke in Belgium (Figure 2 and Figure 47). Two fortnight measuring campaigns (7–20 November 2017 and 16–26 April 2018) were carried out to investigate marine forcing, sediment transport, and resulting topographic changes. Flow velocity, water level, wave conditions, and SSC were measured with a frame at the NLW line (Figure 47). The full beach topography was surveyed with a permanent TLS and the topography of five cross-shore profiles (Figure 47) was measured with an RTK-GNSS. Wind conditions were measured at the airport of Ostend, approximately 1 km from the study site.

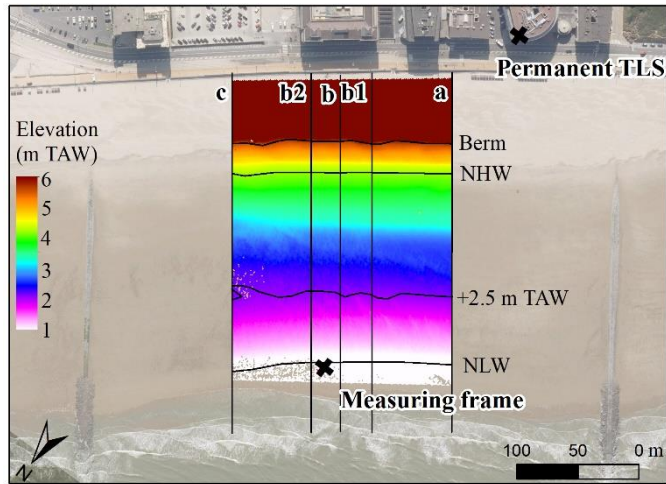


Figure 47. DEM of the study site with the position of the intertidal measuring frame, cross-shore topographic profiles, the permanent TLS, and the berm, NHW, 2.5 m, and NLW line.

The measuring frame (Figure 48) was equipped with three OBS to measure turbidity, a proxy for SSC, at 10 cm (4 Hz), 30 cm (1 Hz), and 50 cm (1 Hz) above the bed. Furthermore, two ADCPs (Aquadopp model) were mounted on the frame to measure profiles of flow velocity and acoustic backscatter, another proxy for SSC. Both were mounted at 70 cm above the bed and measured 9 cells of 5 cm, but one was looking up (1 Hz) and one was looking down (4 Hz). Additionally, an upward-looking ADCP was deployed in the sand which measured profiles with 14 cells of 30 cm (1 Hz, 5 minute bursts) to cover the part of the water column above 1.2 m. During the November 2017 measuring campaign an ECM was mounted 50 cm above the bed. This sensor was set to measure flow velocity and pressure (8 Hz, 1 minute every 10 minutes) from which wave height and wave period were calculated. During the April 2018 measuring campaign the ECM was replaced by a pressure sensor (10 Hz). Additionally a LISST (LISST-100x, 1 Hz, 10 seconds every 1 minute) was mounted on the frame at 75 cm above the bed to survey the grain size of the suspended sediment. The LISST was only operational during the first week of the April 2018 campaign.



Figure 48. Left: The intertidal measuring frame (1 m high, 2.2 m wide) with the down-looking ADCP, up-looking ADCP (not on the frame), three OBS, ECM, and up-looking ADCP. Right: the LISST

The data was treated by removal of the data when the equipment was exposed to the air and the obvious outliers. Flow velocity was converted to cross- and alongshore flow velocity to determine on- and offshore sediment transport rates. The cross-shore sediment flux was calculated by multiplying SSC and flow velocity. The mean and oscillatory component of the cross-shore suspended sediment transport were also calculated separately to investigate the contribution of mean currents versus the contribution of waves ($\overline{u \cdot c} = \overline{u} \cdot \overline{c} + \overline{u' \cdot c'}$, where u is flow velocity and c is SSC). The total suspended load per tidal cycle was calculated by vertically integrating the sediment transport over the water column and by integrating the transport over the tidal cycle. It was converted to a volume using a sediment density of 2000 kg/m^3 (typical density of wet sand).

Sediment transport was compared to the velocity skewness (U_{sk}) that was calculated from the cross-shore flow velocity (u_{cross}): $U_{sk} = \langle u_{cross}^3 \rangle / \langle u_{cross}^2 \rangle$ (Bailard and Inman, 1981). Positive and negative velocity skewness are indicative of onshore and offshore transport, respectively, as it is assumed that sediment transport is proportional to u^3 . Sediment transport was also compared to wave steepness, to investigate the effect of wave conditions on suspended sediment transport. Wave steepness was calculated as *Wave steepness* = H/L . Wavelength was calculated depending on the water depth and wave height with the dispersion equation: $L = gT^2 \tanh(2\pi h/L) / 2\pi$ or the shallow water approximations: $L = T\sqrt{gh}$, (Masselink *et al.*, 2011). In this study significant wave period (T_{sig}) and height (H_{sig}) were used.

Turbidity measured by the OBS was converted to SSC with a calibration based on in-situ samples (Appendix C). The acoustic backscatter from the ADCP (Amp) was corrected for acoustic spreading and water absorption (Lohrmann, 2001): $EI = 0.43Amp + 20 \log(R) + 2a_w R$, where R is the range along the acoustic beam and a_w is the water absorption (1.0637 dB/m here). EI , the range normalized echo intensity (dB), was converted to SSC based on the OBS measurements in the lowest part of the water column. The relationship between tidally-averaged SSC based on acoustic backscatter and optical backscatter (Figure 49) was significant with a p-value of $1.44e-5$ (< 0.05 , R^2 of 0.45), although instantaneous differences were large.

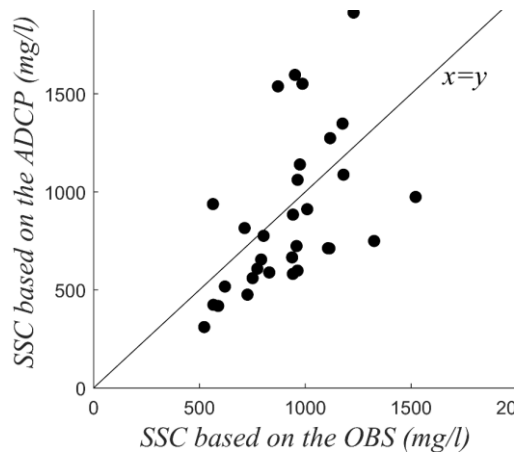


Figure 49. Tidally-averaged SSC at 30 cm above the bed based on ADCP vs OBS measurements.

6.2.2. Data acquisition – beach topography

TLS, or LiDAR, has been used successfully to survey the beach topography (Van Gaalen *et al.*, 2011, Fabbri *et al.*, 2017, Vos *et al.*, 2017). TLS is a highly automated active remote sensing technique, composed of an Electromagnetic Distance Measuring (EDM) technique to derive a backscatter based distance by measuring the circulation time of a pulse or the wavelength difference of a continuous wave. The coordinates of a point on the reflecting surface are determined by transmitting signals from a measuring instrument of which the orientation and the coordinates are known or fixed in three dimensions. Additional background information on TLS can be found in Appendix D.

A time-of-flight-pulse-based Riegl® VZ-2000 terrestrial LiDAR was installed on a 42 m high building near the study area (Figure 50) and data was

acquired similar to (Vos *et al.*, 2017). The permanent TLS scanned the intertidal and dry beach on an hourly basis over a period of one year. The scanner was installed on a stable frame and protected by weather-proof housing. The scan data was calibrated using a truth set of reference points to enhance the accuracy and precision. The point density of the permanent TLS data varies between more than 250 points/m² in the southwestern part of the dry beach and 1 point/m² in the northeastern part of the intertidal beach. It appears that the useful range of the scanner is limited to 200 m. The vertical accuracy (root mean square error) of the TLS data was found to be 1–3 cm.

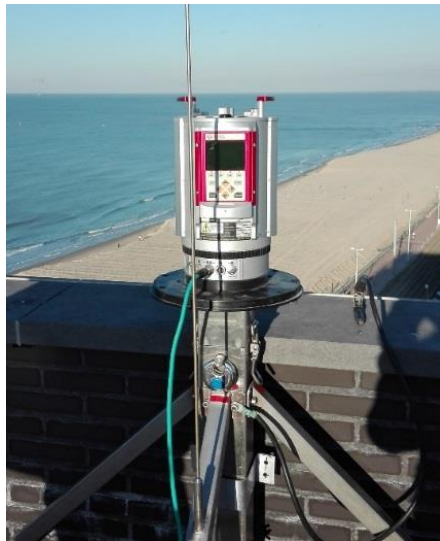


Figure 50. Set-up of the permanent TLS at the study site.

The 3D point cloud data from the permanent TLS was interpolated to a rasterized (1×1 m) Digital Elevation Model (DEM) using Inverse Distance Weighting (IDW). DEMs of Differences (DoDs) were generated by subtracting the DEMs of subsequent days. For each day the volume of the intertidal zone was calculated. The intertidal zone was defined as the area between NLW line and the toe of the berm (+5.30 m TAW). It was chosen to extend the area above the NHW line because it was assumed that the narrow strip between the NHW line and the berm was dominated by hydrodynamic forcing.

Wet areas of the beach yield poor reflection of the laser scan signal, which sometimes resulted in a lack of data in the lowest part of the intertidal zone. Beach topography was therefore also measured with RTK-GNSS during low

tide to fill the gaps in permanent TLS data. Five cross-shore profiles were surveyed: one central profile (b), two profiles at 25 m from the central profile (b1 and b2), and two distant profiles 75 m from the central profile and 75 m away from the groins (a and c, Figure 47). The RTK-GNSS profiles were measured at an interval of 1 m in the cross-shore direction with a vertical accuracy of 2–4 cm (Taaouati and Nachite, 2011). The volume of the intertidal beach was calculated from the topographic profiles. Volumes were calculated for each profile separately using trapezoidal rules. The volumes of all profiles (a, b1, b, b2, and c) were averaged and daily volume changes were calculated.

6.3. Results

6.3.1. Hydrodynamics, SSC, and grain size of the suspended sediment

The hydrodynamic conditions and SSC during the two periods of data collection (November 2017 and April 2018) are summarized in Figure 51. The wave conditions were energetic in November with peaks in wave height of 1.46 m in the intertidal zone, corresponding to an offshore measured wave height of 3.15 m, while peaks in wave steepness reached 0.075. The average wave height over the two weeks was 0.42 m. In April the waves were calm with an average and maximum wave height of 0.21 m and 0.65 m respectively. The water level exceeded the storm threshold of 5 m TAW that was defined for the Belgian coast (Haerens *et al.*, 2012) on 16 November when the water level reached 5.01 m TAW. This threshold was approached on 10 and 19 November, when the water level reached 4.91 and 4.98 m TAW, respectively.

Currents were directed onshore with a large alongshore component during flood, while ebb currents were directed offshore. Flow velocity was highest at approximately 1.5 m above the bed (2.9 m TAW), which corresponds to 1/3 of the high water level. Strong offshore and southwesterly directed currents were observed when waves were energetic (> 0.6 m). The average SSC was 1056 mg/l in November and 839 mg/l in April. SSC was especially high when energetic waves occurred, such as between 10 and 14 November. SSC was on average 500-1000 mg/l higher during the flood phase than during the ebb phase. Generally, the suspended sediment was well-mixed over the water column, but SSC were highest near the bed when waves were energetic.

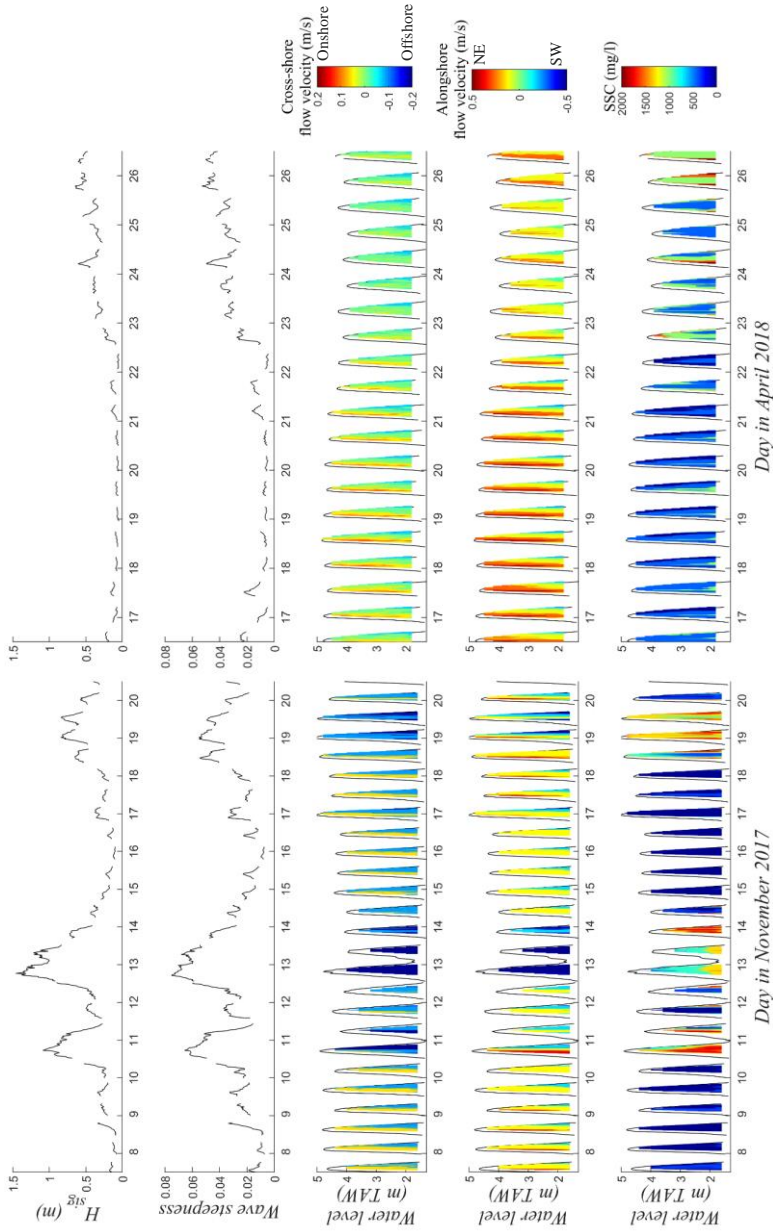


Figure 51. 30-minute-averaged significant wave height (H_{sig}) and wave steepness, cross-shore (positive velocities indicate onshore flow, negative offshore) and alongshore flow velocity (positive velocities indicate NE flow, negative SW) and SSC over depth (in m TAW) for November (left) and April (right).

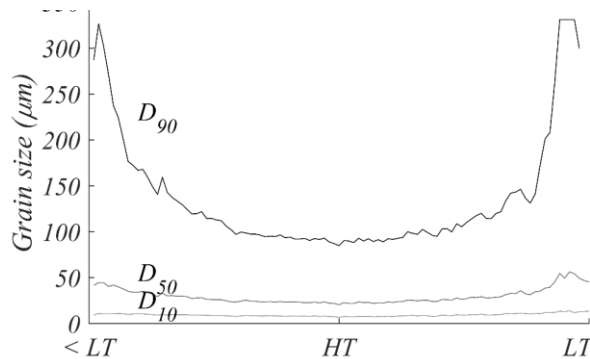


Figure 52. 5-minute-averaged grain size of the suspended sediment over one tidal cycle (LT = Low Tide, HT = High Tide, 18 April 2018). Grain size of the smallest 10% (D_{10}), the largest 10% (D_{90}), and the median grain size (D_{50}).

During calm conditions the median grain size (D_{50}) of the suspended sediment was 33 μm (Figure 52). The grain size of the smallest and largest 10 % of the grains (D_{10} and D_{90}) were 9 and 137 μm . The grain size of the suspended sediment was largest around low tide as waves were breaking near the frame. The sediment on the beach was coarser than the sediment in suspension, with a D_{10} of 197 μm , a D_{50} of 297 μm , and a D_{90} of 450 μm . This discrepancy in grain size makes it highly likely that most of the suspended sediment is transported to the frame from elsewhere and is not locally eroded during calm conditions. Only around low tide the grain size of the sediment in suspension suggests local erosion of sediment. During low tide, approximately 15 % of the grains in suspension is larger than the D_{10} of the sediment on the beach.

6.3.2. Suspended sediment transport

Mean and oscillatory cross-shore suspended sediment transport are presented in Figure 53 for the first week of the November 2017 campaign which showed the largest variability in hydrodynamic conditions. The first days (7–10 November) were tide-dominated with calm waves and spring tide conditions. Mean transport dominated and was onshore during flood and offshore during ebb. Oscillatory transport was onshore because of wave asymmetry (larger onshore than offshore flow velocities) and was especially large around low tide when waves were breaking near the measuring frame. On 10-11 and 12-13 November the conditions were wave-dominated, with wave heights exceeding 1 m. Mean transport still dominated but was mainly offshore because of strong undertow, the return flow of the waves. Oscillatory transport was still directed onshore but was stronger than for tide-dominated

conditions. It was relatively constant indicating that waves were constantly breaking at the NLW line. Figure 53 illustrates the sediment transport at 10 cm above the bed, but is representative for the entire water column.

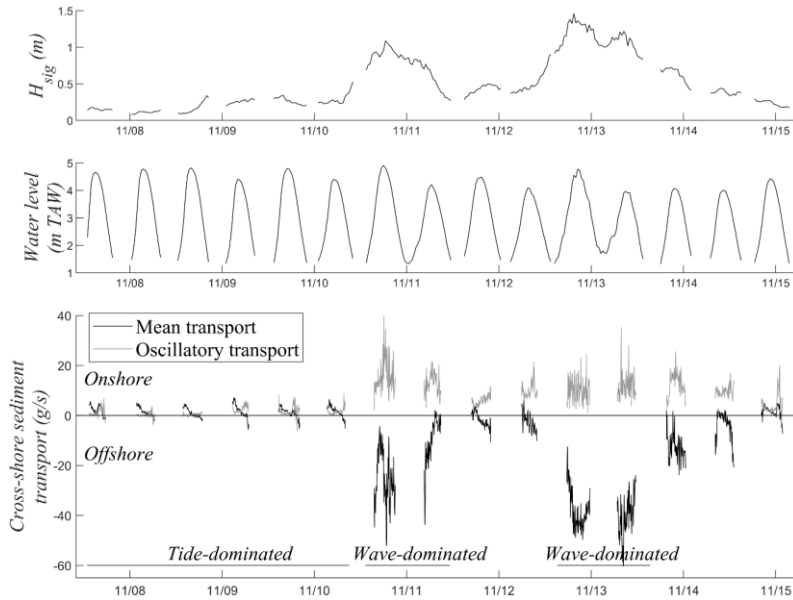


Figure 53. Mean and oscillatory cross-shore suspended sediment transport at 10 cm above the bed over the first week of the November campaign (bottom) with the significant wave height and water level for reference (top and middle).

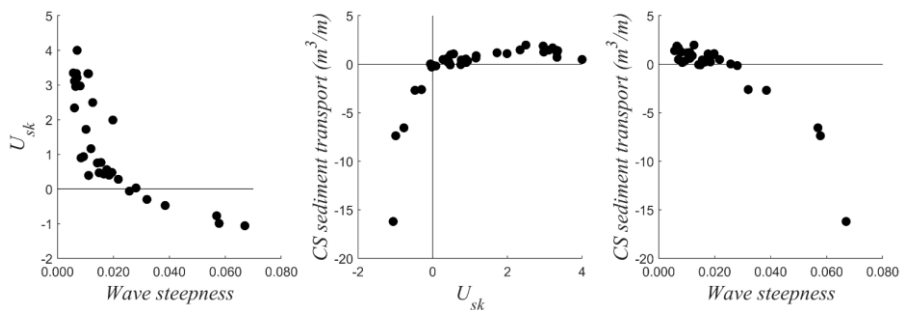


Figure 54. Comparison between velocity skewness (30 cm above the bed), wave steepness, and cross-shore sediment transport. Each point represents one tidal cycle. Cross-shore sediment transport was calculated over the lowest 1 m of the water column and is averaged for the 3 OBS.

The cross-shore suspended load per tidal cycle was compared to the velocity skewness and wave steepness (Figure 54). The velocity skewness was positive when waves were small because of the shape of the incident waves. The velocity skewness became negative when waves became larger (wave steepness > 0.025) due to the strong undertow. Net transport was offshore when the velocity skewness was negative, whereas transport was onshore when the velocity skewness was positive. Consequently, sediment transport was onshore when wave steepness was small and offshore when wave steepness was large.

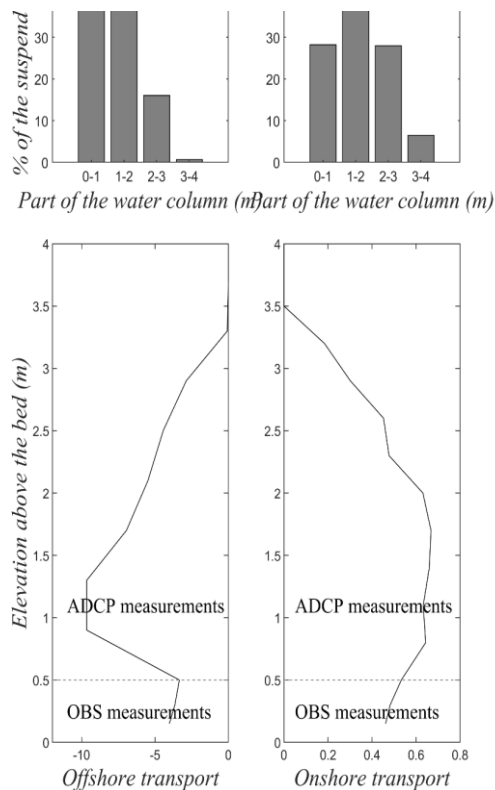


Figure 55. Total cross-shore suspended load over a tidal cycle. Top: Distribution of the transport over the water column for offshore (left) and onshore (right) transport events. Bottom: Examples of the cross-shore suspended sediment load over depth for one tidal cycle when transport was maximum offshore (left) and onshore (right). Note that the x-axis are uneven.

To investigate the sediment transport over the water column, cross-shore suspended sediment transport was tidally-integrated. This was done for slices of 1 m (Figure 55, top) and slices of 30 cm (the maximum cell size of the ADCPs; Figure 55, bottom) of the water column. The distribution of the total suspended load over the water column per slice of 1 m is shown for offshore and onshore transport events. Suspended sediment transport was the largest between 1 and 2 m above the bed. Sediment transport was more homogenous during calm conditions and more concentrated near the bottom during energetic conditions. The maximum offshore transport was significantly larger than the maximum onshore transport (9.7 vs. 0.7 m³/m/m depth). The suspended sediment transport peaked at 1 m above the bed during offshore transport events. During such events the SSC was largest near the bed, while offshore flow velocities were highest at 1-1.5 m above the bed. During onshore transport events the suspended sediment load was well-mixed over the water column. A small peak in transport was observed at 1.5 m above the bed. The total suspended load decreased towards the top of the water column (> 2 m), because it represents a smaller period of time.

6.3.3. Topographic change

Figure 56 and Figure 57 represent the net topographic change over the two fortnight measuring campaigns (red = erosion, green = accretion) and the daily volume changes of the intertidal zone, respectively. Bed level changes in the intertidal zone were in the order of centimeters to decimeters over the fortnight periods. Wind-driven topographic changes of several decimeters were also observed on the upper beach above the berm. In November the intertidal beach predominantly eroded, with a loss of sediment of 18.6 m³/m over the campaign. Strongest erosion was observed on 12 November, while most other days the beach was stable or even grew. In April the intertidal beach gradually built-up, gaining 5.1 m³/m over the campaign.

An alternating pattern of erosion and accretion was detected from daily DoDs when the suspended load was large. Figure 58 shows the zones of maximum accretion and erosion for the three days with most offshore sediment transport (10, 12, and 19 November; left) and the three days with most onshore transport (17, 18, and 19 April; right). The erosion and accretion pattern was compared to the beach slope, which was subdivided into sloping (> 1°) and relatively flat (< 1°). Erosion was observed at the bottom of the slopes during offshore transport events, while accretion was observed at the top of these slopes. During onshore transport events accretion was observed at the bottom of slopes and erosion at the top. A part of the sediment that was eroded from the intertidal zone during energetic conditions was deposited just

below the NLW line. This sediment was returned to the beach during calm conditions.

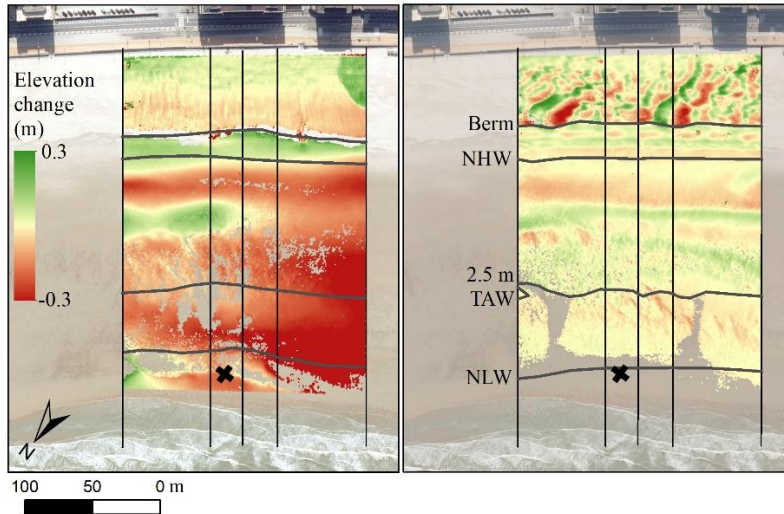


Figure 56. DoD of the first and last survey for the November (left) and April (right).

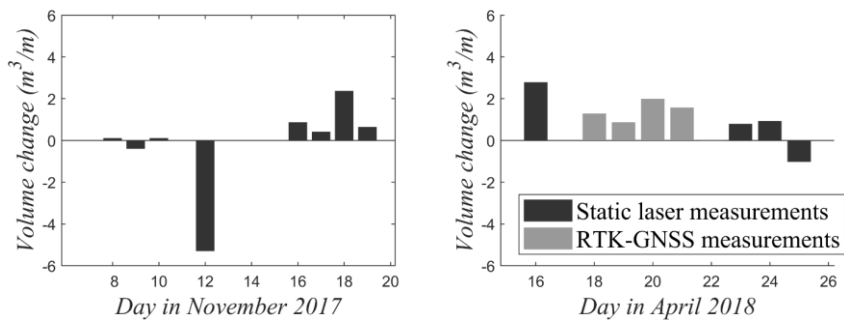


Figure 57. Daily intertidal beach volume changes (NLW – toe of the berm) for the November (left) and April (right) campaign. Measurements are lacking for 7, 11, 13-15 November and 17 April.

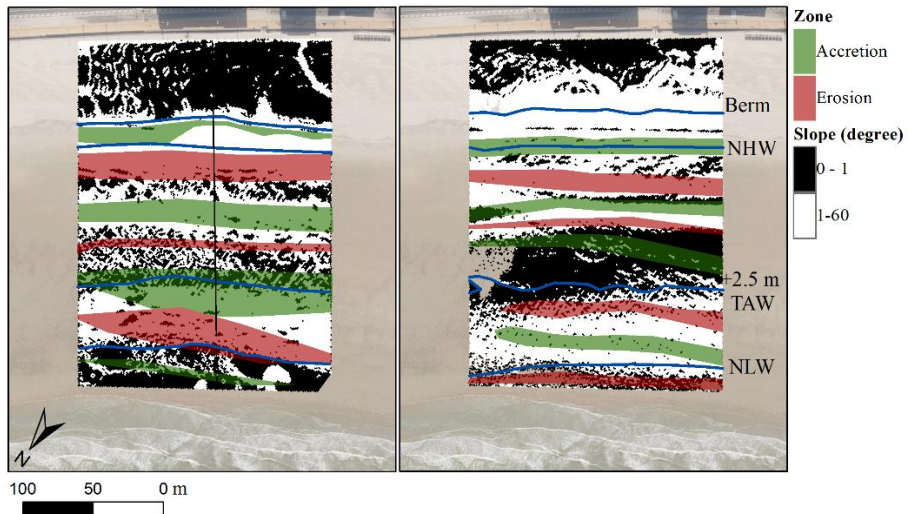


Figure 58. Beach slope (left = November, right = April) with zones of maximum erosion/accretion indicated for days when considerable offshore (left) or onshore (right) suspended sediment transport was measured by the frame.

6.4. Discussion

Sediment was transported to the beach by tidal currents and by wave-induced oscillatory transport under calm conditions (wave steepness < 0.025). Sediment was transported offshore by strong undertow during energetic conditions. The dominance of mean transport over oscillatory transport is in agreement with previous observations on the Belgian and other macro-tidal coasts (Voulgaris *et al.*, 1996, Austin *et al.*, 2009). However, the mean cross-shore transport by tidal currents may have been enhanced by the groins, which divert the tidal currents to more cross-shore. The suspended sediment was well-mixed over the water column, resulting in a peak of sediment transport at 1.5 m above the bed. Other studies usually observe highest suspended sediment transport rates close to the bed (Kraus, 1987, Tonk and Masselink, 2005, Cartier and Héquette, 2015). However, most studies to suspended sediment transport have been on wave-dominated beaches, while on macro-tidal beaches tidal currents play an important role in keeping sediment in suspension and transporting sediment.

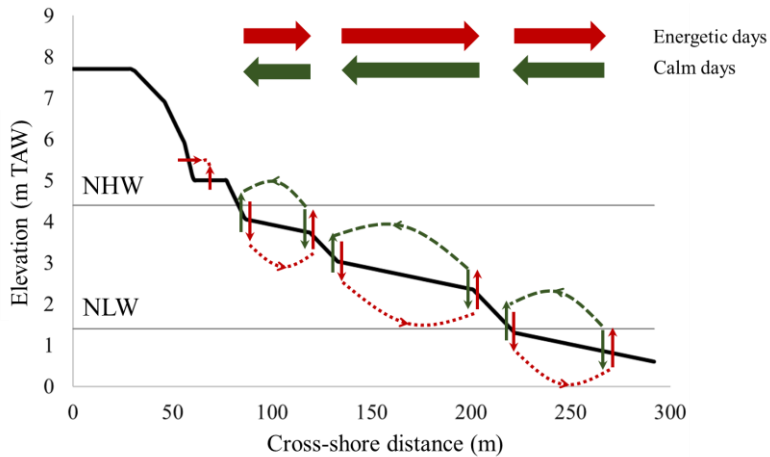


Figure 59. Schematized cross-shore beach profile with sediment transport and resulting topographic change during energetic (red, dotted) and calm (green, dashed) days.

Schematized sediment transport and topographic response across the intertidal zone is shown in Figure 59. It appears that morphological features are developed during energetic conditions around 80 m, 120 m and 210 m cross-shore distance. The beach morphology is smoothed during calm conditions. It was previously found that intertidal bars (*i.e.* ridges and runnels) are formed along the Belgian coast by standing long waves (Simmonds *et al.*, 1996). This type of bar system is exclusive to dissipative, macro-tidal beaches with sufficient sediment supply and a fetch-limited wave climate, which are common along the North Sea coast (Simmonds *et al.*, 1996, Van Houwelingen *et al.*, 2006, Cartier and Héquette, 2015). Here, long waves (period > 10 s) were over 40 cm during energetic conditions, while they were 5 cm on average during calm conditions. Most likely, the coupling between short and long waves lead to positions of sediment convergence and divergence (O'Hare and Huntley, 1994), which resulted in bar formation. However, they never fully develop due to the presence of the groins (Deronde *et al.*, 2008).

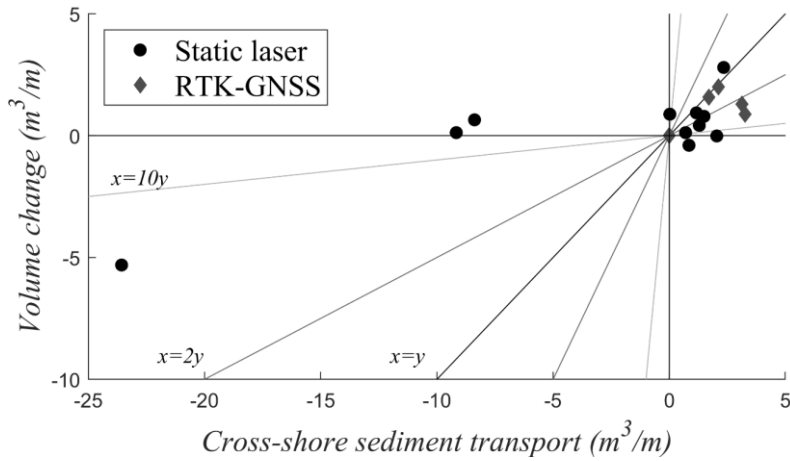


Figure 60. Cross-shore sediment transport per m beach width compared to the observed intertidal beach volume change. Points represent one day each. Lines represent a 1:1 relationship between cross-shore sediment transport and beach volume change (black) and 2x (dark grey) and 10x (light grey) over- and underestimation of the volume change.

The total cross-shore suspended sediment load is compared to intertidal beach volume changes in Figure 60. Topographic changes suggest the same transport direction as the underwater measurements for 81% of the time. Generally, they are also in the same order of magnitude (75%) or even less than 2 times over- or underestimated (38%) by the suspended sediment load. The suspended sediment load was on average 1.4 times larger than the observed topographic change for calm conditions (onshore sediment transport). Energetic conditions were less frequent than calm conditions, but based on the limited observations it can be concluded that the total suspended load does not predict beach changes very well. Erosion of the intertidal zone occurred only during 1 out of the 3 days with offshore transport, whereas the beach was stable during the other 2 days. Reasons for differences between the measured sediment transport and observed volume changes include exchange of sediment with the dry beach, gradients in alongshore sediment transport, bed load transport, sediment transport by swash action, measurement inaccuracies, and human interference (Appendix E).

It was assumed that all sediment entering or leaving the intertidal zone passed the low water line. However, undermining of the berm was observed when waves were high (Figure 62). This resulted in an input of sediment from the upper beach to the intertidal zone. This was reaffirmed by the presence of sand accumulation near the toe of the berm (around 5.1 m TAW) during

energetic conditions (Figure 58). Under these conditions the water level reached 4.8-5.0 m TAW and waves reached the toe of the berm.

Figure 61 shows hourly observations of the toe of the berm on 12 November when the maximum water level reached 4.8 m TAW. The elevation of the toe of the berm increased with 14 cm during high tide. This corresponded to a deposited volume of 0.88 m³/m, which explains 17% of the total change in the intertidal zone.

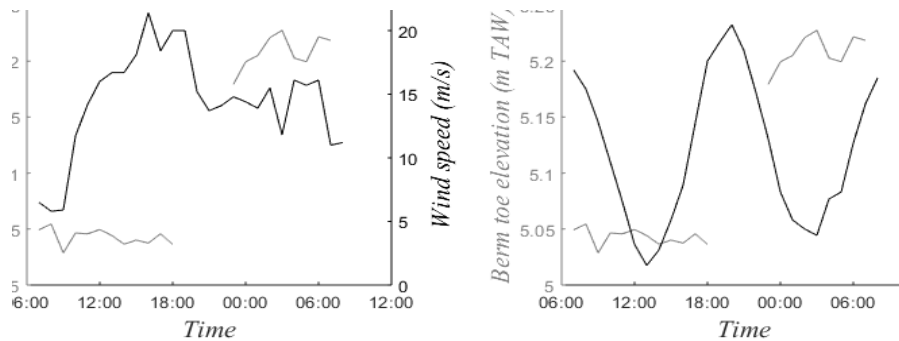


Figure 61. Hourly elevation of the toe of the berm (average of the five cross-shore profiles) compared to the wind speed and the water level on 12/13 November.

Sediment exchange between the intertidal zone and the upper beach may also result from wind activity. Wind-driven transport in the intertidal zone has been investigated on various occasions (Sarre, 1989, Anthony *et al.*, 2009), but rarely as a part of the sediment budget. Some studies attributed significant intertidal beach erosion/accretion to transport by wind (Almeida *et al.*, 2012), but aeolian transport remains uncertain in the sediment budget when relating topographic changes to underwater transport. Here, aeolian sand transport was quantified based on the hourly observations of the toe of the berm on 12 November (Figure 61). This was the most energetic day with wind speeds up to 22 m/s blowing onshore, which were optimal conditions for sand transport in the intertidal zone as observed in the field. Sediment transported by the wind was deposited in front of the berm, resulting in a rise of the berm toe of 4 cm while the intertidal zone was not affected by hydrodynamic processes (Figure 61, second low tide). This corresponds to a deposited volume of 0.25 m³/m (5% of the total change). Sediment transport from the intertidal zone to the upper beach was even smaller, as the majority of the wind-blown sediment was intercepted by the berm.



Figure 62. Ground photograph of the berm following the high water of 12 November.

Sediment exchange between the intertidal zone and the upper beach by aeolian transport and by waves undermining the berm was thus limited. Sediment exchange between the study site and adjacent beaches was most likely significant though, but could not be investigated with the current measuring set-up. It was demonstrated that gradients in alongshore sediment transport can result in significant topographic changes along the Belgian coast (Voulgaris *et al.*, 1998), similar to other sandy beaches (Tonk and Masselink, 2005, Sedrati and Anthony, 2007). Gradients in alongshore sediment transport will thus explain some of the differences between the measured sediment load and observed topographic changes.

Differences between the total suspended load and beach volume changes may also be explained by the sediment transport that was not covered by the measurements: bed load transport and transport under low water levels. It was presumed that the contribution of bed load transport was small based on (Voulgaris *et al.*, 1996) who argued that only 20% of the total load near the study site consisted of bed load transport. Sediment transport measurements were limited to a water depth of 40 cm (64% of the time). Part of the sediment transport under breaking waves (8% of the time) and the transport by swash (5% of the time) were not covered. The remainder of the time, the intertidal zone was not affected by hydrodynamic processes (23%). Previously, it was found that significant sediment transport can occur under low water levels (Hughes *et al.*, 1997, Voulgaris *et al.*, 1998, Aagaard, 2002, Houser *et al.*, 2006, Masselink *et al.*, 2009). Therefore, disagreements between the suspended load and observed topographic changes may thus be explained by hydrodynamic processes for the 13% of the time that was not covered by the measurements.

Despite these inaccuracies, a good relationship between sediment transport and topographic change was established under calm conditions. This

proves the added value of acoustic backscatter to survey sediment transport over the entire water column and the use of a permanent TLS to survey the beach topography with a high accuracy.

6.5. Conclusion

In order to improve our understanding and modelling capacities of the intertidal zone, a major focus of coastal research is to include sediment transport in studies about intertidal beach morphodynamics. This study investigated cross-shore sediment transport and resulting topographic changes for a tide-dominated, sandy beach on a daily scale. This was done based on in-situ measurements of the hydrodynamics, SSC, and beach topography.

The suspended sediment was generally well-mixed, but during energetic conditions the SSC was the highest near the bed. Flow velocity was highest at approximately 1.5 m above the bed. As a result, the suspended sediment transport was well-mixed over the water column with a peak in transport at approximately 1/3 of the (maximum) water column. This peak was most pronounced during energetic conditions due to strong flow velocities and higher SSC close to the bottom. During calm conditions ($H_{sig} < 0.3$ m) the suspended sediment was fine, with a D_{50} of 33 μm and a D_{90} of 137 μm . It can be expected that the suspended sediment is coarser during more energetic conditions.

Sediment transport by mean currents was dominant over oscillatory sediment transport. Mean sediment transport was onshore during calm conditions because of tidal currents and offshore during energetic conditions because of undertow. Oscillatory transport was always onshore because of the flood dominance of the waves. The combination of mean and oscillatory currents resulted in a positive velocity skewness and onshore sediment transport when waves were small (wave height < 0.6 m or wave steepness < 0.025). The velocity skewness was negative and sediment transport was offshore when waves were large.

Changes in beach topography showed an alternating pattern of erosion and accretion. Morphological features were formed during energetic conditions (for an offshore wave height up to at least 3.15 m) and smoothed during calm conditions. At least a part of the sediment that was eroded from the intertidal zone during energetic conditions was deposited just below the low water line. During calm conditions, this sediment was transported back to the intertidal zone.

A good relationship between measured sediment transport and intertidal beach volume changes was obtained by using acoustic backscatter to survey sediment transport over the full water column and a permanent TLS to accurately measure beach topography. The suspended load and daily intertidal beach volume changes were in the same direction and order of magnitude for 75% of the investigated days. Especially during calm days with onshore transport the relationship between the suspended load and intertidal beach volume changes was good, although the transport measurements overestimated the volume change (1.4 times). Energetic conditions were less well represented, but it seemed that the measured sediment transport greatly overestimated the volume changes observed in the intertidal zone. This was attributed to input of sediment from the dry beach, gradients in alongshore sediment transport, bed load transport, and transport by swash. The contribution of aeolian transport was found to be negligible (maximum 0.25 m³/m/day, corresponding to 5% of the total change) even though wind conditions were energetic (up to 22.6 m/s). Nevertheless, a good relationship between measured sediment transport and observed topographic changes was obtained, allowing to improve our understanding and to support modelling capacities of the intertidal zone.

Chapter 7

General conclusions and recommendations

7.1. Conclusions

The intertidal zone is very dynamic as it is subject to waves, tide, and wind. In general, the beach erodes when waves are energetic while it recovers during calm conditions. It is challenging to unravel the exact processes that govern beach erosion and recovery though. The main focus of this study was to improve our understanding of the relationship between hydrodynamic forcing and topographic response for tide-dominated, sandy beaches. Extensive field measurements were carried out in the nearshore, the intertidal zone, and on the dry beach on the natural, barred beach of Groenendijk and the managed, featureless beach of Mariakerke.

First, monthly beach profiles were analyzed to investigate the medium scale (seasonal to monthly) beach dynamics and to quantify the spatial variability in topographic changes. Second, these monthly profiles were compared to the nearshore hydrodynamics and sediment dynamics. Third, daily beach volume changes were compared to the hydrodynamics and sediment dynamics measured at the low water line during six fortnight measuring campaigns to get a more detailed understanding of the intertidal beach morphodynamics. These campaigns were designed based on a comprehensive literature review. Finally, sediment transport was quantified and related to daily topographic changes, to bridge the gap between hydrodynamic forcing and topographic response. In this chapter the conclusions of these studies are summarized and recommendations for future research and coastal management are given.

7.1.1. Beach dynamics

No clear seasonal trend in intertidal beach volume is observed from the monthly topographic surveys. Instead, monthly topographic changes seem event-driven, with erosion during events with an offshore wave height exceeding 3.75 m and accretion in between. However, not all months with energetic events are accompanied by erosion. This can be attributed to differences in specific event conditions, the pre-event beach profile, or a fast recovery of the beach. This recovery is often within one or two months, but it will likely take longer when major storm events occur.

Monthly beach volume changes can be large, at least up to $\pm 15 \text{ m}^3/\text{m}$ at Mariakerke and $\pm 25 \text{ m}^3/\text{m}$ at Groenendijk. Absolute volume changes are larger at Groenendijk than at Mariakerke but relative to the total intertidal beach volume they are of similar magnitude. Typical monthly variations in beach elevation are 5 cm at Mariakerke and 25 cm at Groenendijk. Intertidal beach volume changes on a daily scale can be up to at least $\pm 5 \text{ m}^3/\text{m}$ for both Mariakerke and Groenendijk under non-storm conditions and daily variations in beach elevation are typically in the order of a few centimeter. The topographic response to the incoming hydrodynamics is highly variable between the profiles due to the complex beach morphology at both study sites with the groins at Mariakerke and the ridges and runnels at Groenendijk.

The ridges and runnels at Groenendijk move onshore and become more pronounced under energetic conditions because of long wave activity while the beach morphology is smoothed during calm conditions. The bar position differs approximately 20 m and the bar height differs 15 cm between summer and winter. The intertidal zone at Mariakerke is usually featureless but a ridge and runnel morphology arises during energetic (non-storm) conditions. They never fully develop at Mariakerke because of the groins. They are smoothed during calm conditions.

7.1.2. Hydrodynamic forcing vs. topographic response

Wave steepness is found to be the main driver for topographic changes in the intertidal zone. The intertidal beach grows when wave steepness is small (< 0.010), while it erodes when wave steepness is large (> 0.018). This trend is opposite when wave steepness is medium (0.013-0.015), with erosion by small and accretion by large waves. Traditional factors such as wave energy, wave direction, beach slope, and wind cannot explain this. SSC in the nearshore, on the other hand, increases remarkably fast when wave steepness is in this medium range. The suspended sediment is transported shoreward from the nearshore to the intertidal zone by flood dominant currents, which results in (partial) compensation of wave erosion. This suspended sediment is

supplied from sources that are likely tens of kilometers away from the beach, such as the tidal banks in front of the coast, since a time lag of 1.3 tidal cycles exists between peaks in wave steepness and peaks in SSC. Besides this supply of sediment from other sources, it was found that part of the sediment that is eroded during energetic conditions is deposited just below the low water line and is transported back to the intertidal zone when wave steepness is small. In conclusion, the effect of waves is twofold: larger waves are primarily erosive, but they also play a role in beach growth through reinforced sediment supply. The effect of variations in sediment supply on the intertidal beach topography is subordinate to the erosive effect of wave steepness though.

Besides wave impact and the influence of variations in sediment supply, it was found that the tidal currents strongly influence the intertidal beach morphodynamics. Currents are cross-shore and wave-dominated during neap tide, while strong tide-induced alongshore currents are observed during spring tide. These spring tidal currents are accompanied by erosion of the intertidal beach. It is hypothesized that spring tidal currents transport sediment that is locally eroded by waves away from the beach, thus enhancing erosion of the intertidal zone. The effect of the tidal currents on the beach topography is of the same magnitude as the effect of waves. The relationship between hydrodynamic forcing and topographic response is summarized in a conceptual model of the intertidal beach morphodynamics (Figure 63).

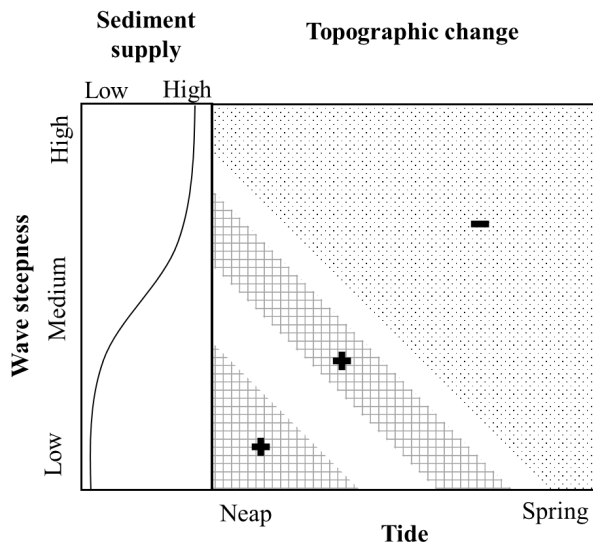


Figure 63. Conceptual model of the combined effects of waves through wave steepness, tide, and sediment supply on the intertidal beach volume.

In this study the natural, barred beach of Groenendijk was compared to the managed, featureless beach of Mariakerke. Both beaches respond fairly similar to hydrodynamic forcing, in spite of their differences in beach morphology. The groins at Mariakerke slightly enhance the erosive effect of tidal currents. At Groenendijk the natural sediment supply is larger and the beach is more susceptible to variations in this supply. Furthermore, the beach at Groenendijk is slight more stable and less susceptible to erosion by energetic events thanks to the wider intertidal zone.

7.1.3. Sediment transport

The suspended sediment is mainly transported by mean currents: tidal currents transport sediment onshore during calm conditions, while undertow (and most likely alongshore tidal currents) transports sediment offshore during energetic conditions. Oscillatory transport is of smaller magnitude and is always onshore because of the flood dominance of the waves.

The suspended sediment is generally well-mixed, but during energetic conditions the SSC is highest near the bed. Flow velocity is highest at approximately 1.5 m above the bed. As a result, the suspended sediment transport is rather uniform over the water column with a peak in transport at approximately 1/3 of the (maximum) water column. This peak is most pronounced during energetic conditions due to strong currents and high SSC close to the bottom.



Figure 64. The Groenendijk study site.

7.2. Recommendations

7.2.1. Recommendations for coastal management

Based on this extensive research of intertidal beach morphodynamics, it is suggested for coastal management purposes to:

1. Survey the beach with a high spatial resolution, especially when the alongshore variability in beach morphology is large, such as at Groenendijk where ridges and runnels are present, and at Mariakerke where the groins affect the beach morphology.

2. Investigate the sediment transport near the sandbanks. It is hypothesized that they are an important source of sediment for the Belgian beaches and therefore they might play an important role in the resilience of the beach and in the protection against beach erosion and coastal flooding.

3. Carry on with the monthly topographic surveys and to add beach surveys prior to and immediately after an energetic event. The monthly cross-shore beach profiles already provided valuable insight in the beach morphodynamics. However, the dataset for Groenendijk is still too small to draw any definite conclusion on a seasonal cycle in beach topography or the response to energetic events. Pre- and post-storm (offshore waves > 3.75 m) beach surveys are necessary because beach recovery can take place within one month.

7.2.2. Recommendations for the design of intertidal measuring campaigns

Accurate measurements of sediment transport and resulting topographic changes are essential to understand the morphodynamics of the intertidal zone. In general, field investigations in the intertidal zone consist of measurements of flow velocity and SSC at one or a few locations across the beach and daily topography measurements of several cross-shore profiles. However, it appears to be difficult to relate sediment transport and topographic changes with such a measuring set-up. Measured sediment transport rates are often in a different order of magnitude or even in a different direction than transport rates derived from topographic changes. Based on an extensive literature review, the following recommendations are highlighted to improve sediment transport and beach topography measurements:

1. Measure sediment transport at multiple locations along and across the intertidal zone. It is recognized that this is very costly and that research budgets do not always allow for this. However, it is very valuable to know sediment transport rates at multiple locations in the intertidal zone. Two measuring locations in the longshore direction already allow to investigate gradients in alongshore sediment transport and will result in a better approximation of the net sediment transport.

2. Measure suspended sediment transport over the entire water column at beaches with strong mixing of the sediment, such as beaches with strong tidal currents or energetic waves. This can be done with an array of OBS or an ASM on micro- and meso-tidal beaches. On macro-tidal beaches, the SSC over the water column can be estimated based on acoustic backscatter.

3. Improve sensors to measure suspended sediment transport close to the bed and bed load transport and improve predictive formulas for sediment transport. It is currently difficult to measure sediment transport close to the bed for both suspended and bed load transport. Sand ripple profilers may partially solve this problem, but field experiments with this equipment are still scarce. In the meanwhile, predictive formulas are often used to estimate bed load transport, but these appear to be highly unreliable. Hence, it is recommended to improve both measuring techniques for near-bed transport in-situ and predictive formulas.

4. Measure the full beach topography on beaches with alongshore variability in beach topography, such as on beaches with cusps or nourishments. This can be done, for example, with static or mobile (airborne or terrestrial) laser scanning or photogrammetry from a UAV.

5. Correct (especially acoustic) measurements of SSC for grain size and turbulence. Measurements of SSC with optical or acoustic equipment are sensitive to grain size. Additionally, acoustic measurements are sensitive to turbulence. These measurements can be greatly improved when they are corrected for these parameters, especially the measurements with acoustic backscatter. Laboratory studies could provide valuable insights in the influence of grain size on acoustic backscatter intensity under controlled conditions.

6. Measure beach topography over time. Sediment transport is usually measured continuously over a tidal cycle, whereas the beach topography is

only measured at low tide which results in mismatches between the two. It is helpful to add continuous bed level measurements to an intertidal campaign in order to obtain a better relationship between them and to get a better understanding on the intertidal beach morphodynamics on a small scale (seconds to hours). If the beach topography is only measured during low tide, it is advised to investigate aeolian transport if wind conditions are energetic.

7.2.3. Recommendations for future research

In this thesis, the hydrodynamic forcing factors that govern beach erosion and recovery were identified and cross-shore sediment transport was investigated. It was found that the most important forcing factors are wave steepness, tidal currents, and sediment supply for macro-tidal beaches. The role of some, less important, parameters is still unclear though. For example, it is recognized that wave direction and wind-driven currents are likely to affect the intertidal zone, but their influence remains a topic for future research. Also, the effect of wind-driven transport when the intertidal zone is exposed (Figure 65) was deemed insignificant, but was only investigated based on one energetic event with onshore wind. The significance of wind-driven transport is uncertain for other conditions. The intertidal beach volume was chosen as a proxy for intertidal beach topography in this study but other proxies might give additional insights. Thus, further research on proxies for beach topography, such as beach width and beach slope, is advised.



Figure 65. Wind-driven sediment transport in the intertidal zone at Groenendijk.

A reasonably good relationship between cross-shore sediment transport and topographic changes was obtained. However, gradients in alongshore sediment transport may also exist and force topographic changes in the intertidal zone. It is likely that sediment is transported away from the beach

by strong alongshore currents during spring tide but the contribution of alongshore sediment transport to topographic changes has yet to be investigated. Furthermore, based on this research and previous studies the contribution of bed load transport was deemed small. It would be interesting to quantify the bed load transport in the future. Also, it would be worthwhile to measure sediment transport in the swash zone as field studies to sediment transport resulting from swash action are scarce.





Bibliography

- Aagaard, T., 2002. Modulation of surf zone processes on a barred beach due to changing water levels, Skallingen, Denmark. *Mar. Geol.*, 18, 25-38
- Aagaard, T., Davidson-Arnott, R., Greenwood, B., Nielsen, J., 2004. Sediment supply from shoreface to dunes: linking sediment transport measurements and long-term morphological evolution. *Geomorphology*, 60, 205-224
- Aagaard, T., Kroon, A., Andersen, S., Møller Sørensen, R., Quartel, S., Vinther, N., 2005. Intertidal beach change during storm conditions; Egmond, The Netherlands. *Mar. Geol.*, 218, 65-80
- Aagaard, T., Hughes, M., Baldock, T., Greenwood, B., Kroon, A., Power, H., 2012. Sediment transport processes and morphodynamics on a reflective beach under storm and non-storm conditions. *Mar. Geol.*, 326-328, 154-165
- Aagaard, T., 2014. Sediment supply to beaches: Cross-shore sand transport on the lower shoreface. *J. Geophys. Res. Earth Surf.*, 119: 913-926
- Aarninkhof, S.G.J., Ruessink, B.G., Roelvink, J.A., 2005. Nearshore subtidal bathymetry from time-exposure video images. *J. Geophys. Res.*, 110, 1-13
- Ahrens, J.P., Hands, E.B., 1998. Velocity parameters for predicting cross-shore sediment transport. *J. Waterw., Port, Coastal, and Ocean Eng.*, 124, 16-20
- Albers, T., von Lieberman, N., 2010. Morphodynamics of Wadden Sea Areas – Field Measurements and Modeling. *International Journal of Ocean and Climate Systems*, 1, 123-132
- Almeida, L.P., Vousdoukas, M.V., Ferreira, Ó, Rodrigues, B.A., Matias, A., 2012. Thresholds for storm impacts on an exposed sandy coastal area in southern Portugal. *Geomorphology*, 143-144, 3-12
- Andrade, F., Ferreira, M.A., 2006. A Simple Method of Measuring Beach Profiles. *J. Coast. Res.*, 22, 995-999
- Anthony, E.J., Levoy, F., Monfort, O., 2004. Morphodynamics of intertidal bars on a megatidal beach, Merlimont, Northern France. *Mar. Geol.*, 208, 73–100.
- Anthony, E.J., Ruz, M-H., Vanhée, S., 2009. Aeolian sand transport over complex intertidal bar-trough beach topography. *Geomorphology*, 105, 95-105

-
- Austin, M., Masselink, G., O'Hare, T., Russell, P., 2009. Onshore sediment transport on a sandy beach under varied wave conditions: Flow velocity skewness, wave asymmetry or bed ventilation? *Mar. Geol.*, 259, 86-101
- Austin, M., Scott, T., Brown, J., MacMahan, J., Masselink, G., Russell, P., 2010. Temporal observations of rip current circulation on a macro-tidal beach. *Cont. Shelf Res.*, 30, 1149-1165
- Bagnold, R.A., 1963. Mechanics of marine sedimentation. In: Hill, M.L. (ed.), *The Sea: Ideas and Observations*. New York: Wiley Interscience, 3, 507-528
- Bagnold, R.A., 1940. Beach formation by waves: some model experiments in a wave tank. *J. ICE*, 15, 27-52
- Bagnold, R.A., 1947. Sand movement by waves: some small-scale experiments with sand of very low density. *Journal of the Institution of Civil Engineers*, 5554, 447-469
- Bailard, J.A., Inman, D.I., 1981. An energetics bed load model for a plane sloping beach. *J. Geophys. Res.*, 86, 2035-2043
- Bailard, J. A., 1984. A simplified model for longshore sediment transport. *Proc., 19th Conf. on Coastal Engineering, B. L. Edge, ed., ASCE, Reston, VA*, 1454-1470
- Baldock, T.E., Barnes, M.P., Hughes, M.G., 2005. Field observations of instantaneous cross-shore free surface profiles and flow depths in the swash zone. *Proceedings of Coastal Dynamics 2005, ASCE*
- Bartholdy, J., Aagaard, T., 2001. Storm surge effects on a back-barrier tidal flat of the Danish Wadden Sea. *Geo-Marine Letters*, 20, 133-141
- Battisto, G.M., Friedrichs, C.T., Miller, H.C. and Resio, D.T., 1999. Response of OBS to mixed grain size suspensions during Sandy Duck'97. *Coastal Sediment Conference 99, ASCE, New York*, 297-312
- Bayram, A., Larson, M., Miller, H.C., Kraus, N.C., 2001. Cross-shore distribution of longshore sediment transport: comparison between predictive formulas and field measurements. *Coast. Eng.*, 44, 79-99
- Beets, D.J., van der Valk, L., Stive, M.J.F., 1992. Holocene evolution of the coast of Holland. *Mar. Geol.*, 103, 423-443
- Bell, P.S., Thorne, P.D., Williams, J.J., 1998. Acoustic measurements of sand ripple profile evolution under controlled wave conditions. In: *Proceedings of the 4th European Conference on Underwater Acoustics*, 1, 353-358
- Berni, J.A.J., Zarco-Tejada, P.J., Suarez, L., Fereres, E., 2009. Thermal and narrowband multispectral remote sensing for vegetation monitoring from an unmanned aerial vehicle. *IEEE Trans. Geosci. Remote Sens.*, 47, 722-738
- Berni, C., Mignot, E., Michallet, H., Dalla-Costa, C., Grasso, F., Lagauzère, M., 2009. Diversity of bed evolution at wave and tidal scales on Truc-Vert beach. *J. Coast. Res.*, Special Issue 56, 1726-1730

-
- Bernstein, D.J., Freeman, C., Forte, M.F., Park, J.Y., Gayes, P.T., Mitasova, H., 2003. Survey design analysis for three-dimensional mapping of beach and nearshore morphology. *Proceedings of the Coastal Sediment '03*, St. Petersburg, Florida, USA
- Bertin, X., Castelle, B., Chaumillon, E., Butel, R., Quique, R., 2008. Longshore transport estimation and interannual variability at a high-energy dissipative beach: St. Trojan beach, SW Oléron Island, France. *Cont. Shelf Res.*, 28, 1316-1332
- Biausque, M., Sénéchal, N., 2019. Seasonal morphological response of an open sandy beach to winter wave conditions: The example of Biscarosse beach, SW France. *Geomorph.*, 331, 157-169
- Brand, E., Chen, M., Montreuil, A-L., Dan, S., 2017. Intertidal beach recovery in relation to nearshore hydrodynamics, Mariakerke, Belgium. *HydroSenSoft 2017*, Madrid, March 2017
- Brand, E., Montreuil, A-L., Chen, M., 2019. The effect of turbulence and particle size on suspended sediment concentration measurements in the intertidal zone. *Coastal Sediments 2019, Tampa, St. Pete, Florida, USA*
- Butt, T., Russell, P., Puleo, J., Masselink, G., 2005. The application of Bagnold-type sediment transport in the swash zone. *Cont. Shelf Res.*, 24, 757-771
- Caldwell, J.M., 1956. Wave action and sand movement near Anaheim Bay, California. *U.S. Army Beach Erosion Board, Tech. Mem.*, 68, 21 pp.
- Cartier, A., Héquette, A., 2011. Variation in longshore sediment transport under low to moderate conditions on barred macrotidal beaches. *J. Coast Res. Special Issue*, 64: 45-49
- Cartier, A., Héquette, A., 2013. The influence of intertidal bar-trough morphology on sediment transport on macrotidal beaches, northern France. *Zeitschrift für Geomorphologie*, 57, 325-347
- Cartier, A., Héquette, A., 2015. Vertical distribution of longshore sediment transport on barred macrotidal beaches, northern France. *Cont. Shelf Res.*, 93, 1-16
- CERC (USACE Waterways Experiment Station's Coastal Engineering Research Center), 1984. *Shore protection manual*, U.S. Government Printing Office, Washington, DC.
- Ciavola, P., Taborda, R., Ferreira, O., Dias, J.A., 1997. Field measurements of longshore sand transport and control processes on a steep meso-tidal beach in Portugal. *J. Coast. Res.*, 13, 1119-1129
- Coco, G., Senechal, N., Rejas, A., Bryan, K.R., Capo, S., Parisot, J.P., Brown, J.A., MacMahan, J.H.M., 2013. Beach response to a sequence of extreme storms. *Geomorphology*, 204, 493-501
- Cohn, N., Anderson, D.L., Susa, T., Ruggiero, P., Honegger, D., Haller, M.C., 2014. Observations of Intertidal Bars Welding to the Shoreline: Examining the

-
- Mechanisms of Onshore Sediment Transport and Beach Recovery. *American Geophysical Union, Fall Meeting 2014*
- Cohn, N., Ruggiero, P., de Vries, S., Garcia-Medina, G., 2017. Beach growth driven by intertidal sandbar welding. *Coastal Dynamics 2017*, 1059-1069
- Corbau, C., Tessier, B., Chamley, H., 1999. Seasonal Evolution of Shoreface and Beach System Morphology in a Macrotidal Environment, Dunkerque Area, Northern France. *J. Coast. Res.*, 15, 97-110
- Cowell, P.J., Stive, M.J.F., Roy, S., Kaminsky, G.M., Buijsman, M.C., Thom, B.G., Wright, L.D., 2001. Shoreface sand supply to beaches. *Proceedings ICCE2000, Am. Soc. Civil Eng., New York*, 2495-2508
- Davis, R.A., 1985. Beach and nearshore zone. In: Davis, R.A. (ed.). *Coastal Sedimentary Environments. New York: Springer-Verlag*, 379-444
- Delacourt, C., Alleman, P., Jaud, M., Grandjean, P., Deschamps, A., Ammann, J., Cuq, V., Suanez, S., 2009. DRELIO: An Unmanned Helicopter for Imaging Coastal Areas. *J. Coast. Res.*, Special Issue 56, 1489-1493
- Delgado, I., Alcantara, C.J., Alejo, I., Alonso, I., Louzao, M., 2002. Influence of hydrodynamics and sedimentary characteristics of Barqueiro Ria on Arealonga beach dynamics. *J. Coast. Res.*, 36, 231-239
- Deronde, B., Houthuys, R., Debruyne, W., Fransaer, D., Van Lancker, V., Henriët, J., 2006. Use of airborne hyperspectral data and laserscan data to study beach morphodynamics along the Belgian coast. *J. Coast. Res.*, 22, 1108-1117
- Deronde, B., Houthuys, R., Henriët, J-P., Van Lancker, V., 2008. Monitoring of the sediment dynamics along a sandy shoreline by means of airborne hyperspectral remote sensing and LIDAR: a case study in Belgium. *Earth Surf. Process. Landforms*, 33, 280-294
- De Sloover, L., De Wulf, A., Stal, C., Verbeurgt, J., Vos, S., 2019. Case study of a hypertemporal terrestrial LiDAR to monitor a macrotidal beach: assessment of different calibration procedures. *19th International Multidisciplinary Scientific GeoConference SGEM 2019*, 1-8
- De Swart, D.H., 1974. Offshore sediment transport and equilibrium beach profiles. *Delft Hydraulics Laboratory publication*, 131
- De Vries, S., Gong, Y., Hoonhout, B., 2019. The role of sediment supply to the aeolian coastal dune system in contrasting areas. *Coastal Sediments 2019, Tampa*, 1240-1248
- De Winter, R.C., Sterl, A., Ruessink, B.G., 2013. Wind extremes in the North Sea Basin under climate change: an ensemble study of 12 CMIP5 GCMs. *J. Geophys. Res.: atmospheres*, 118, 1601-1612
- Dohmen-Janssen, M., Hanes, D.M., 2002. Sheet flow dynamics under monochromatic nonbreaking waves. *J. Geophys. Res.*, 107, 1-21

-
- Doody, J.P., 2012. Sand Dune Conservation, Management and Restoration. *Springer, Berlin, Germany*
- Downing, J.P., Sternberg, R.W., Lister, C.R.B., 1981. New instrumentation for the investigation of sediment suspension processes in the shallow marine environment. *Mar. Geol.*, 42, 19-34
- Dubois, R.N., 1989. Seasonal variation of mid-foreshore sediments at a Delaware beach. *Sedimentary Geology*, 61, 37-47
- Dufois, F., Garreau, P., Le Hir, P., Forget, P., 2008. Wave- and current-induced bottom shear stress distribution in the Gulf of Lions. *Cont. Shelf Res.*, 28, 1920-1934
- Duncan, J.R., 1964. The effects of water table and tidal cycle on swash-backwash sediment distribution and beach profile development. *Mar. Geol.*, 2, 186-197
- Eamer, J.B.R., Walker, I.J., 2013. Quantifying spatial and temporal trends in beach-dune volumetric changes using spatial statistics. *Geomorphology*, 191, 94-108
- Emery, K.O., 1961. A simple method of measuring beach profiles. *Limnology and Oceanography*, 6, 90-93
- Emmanuel, I., Parisot, J.P., Michallet, H., Barthélemy, E., Sénéchal, N., 2009. Sediment transport particular events and beach profile response. *J. Coast. Res.*, Special Issue 56, 1766-1770
- Esteves, L.S., Lisniewski, M.A., Williams, J.J., 2009. Measuring and modelling longshore sediment transport. *Est. Coast. Shelf Sci.*, 83, 47-59
- Fabbri, S., Giambastiani, B.M.S., Sisti, F., Scarelli, F., Gabbianelli, G., 2017. Geomorphological analysis and classification of foredune ridges based on Terrestrial Laser Scanning (TLS) technology. *Geomorphology*, 295, 436-451
- Fernández-Fernández, S., Baptista, P., Martins, V.A., Silva, P.A., Abreu, T., Pais-Barbosa, J., Bernardes, C., Miranda, P., Rocha, M.V.L., Santos, F., Bernabeu, A., Rey, D., 2016. Longshore Transport Estimation on Ofir Beach in Northwest Portugal: Sand-Tracer Experiment. *J. Waterw. Port. Coast. Eng.*, 142, 04015017
- Furgerot, L., Mouaze, D., Tessier, B., Perez, L., Haquin, S., Weill, P., Crave, A., 2016. Sediment transport induced by tidal bores. An estimation from suspended matter measurements in the Sée River (Mont-Saint-Michel Bay, northwestern France). *Comptes Rendus Geoscience*, 348, 432-441
- Gallagher, E.L., Elgar, S., Guza, R.T., 1998. Observations of sand bar evolution on a natural beach. *J. Geophys. Res.*, 103, 3203-3215
- Gao, S., Collins, M., 1991. A critique of the McLaren Method for defining sediment transport paths: discussion. *J. Sediment. Petrol.*, 61, 143-146
- Gao, S., Collins, M., 1992. Sand sediment transport patterns inferred from grain-size trends based upon definition of "transport vectors". *J. Sediment. Petrol.*, 80, 47-60

-
- Gao, S., Collins, M., 1994. Analysis of grain size trends, for defining sediment transport pathways in marine environments. *J. Coast. Res.*, 10, 70–78
- Gartner, J.W., 2004. Estimating suspended solids concentrations from backscatter intensity measured by acoustic Doppler current profiler in San Francisco Bay, California. *Mar. Geol.*, 211, 169-187
- Haerens, P., Bolle, A., Trouw, K., Houthuys, R., 2012. Definition of storm thresholds for significant morphological change of the sandy beaches along the Belgian coastline. *Geomorphology*, 143-144, 104-117
- Hails, J.R., 1974. A review of some current trends in nearshore research. *Earth-Sci. Rev.*, 10, 171-202
- Hanley, M.E., Hoggart, S.P.G., Simmonds, D.J., Bichot, A., Colangelo, M.A., Bozzeda, F., Heurtefeux, H., Ondiviela, B., Ostrowski, R., Recio, M., Trude, R., Zawadzka-Kahlau, E., Thompson, R.C., 2014. Shifting sands? Coastal protection by sand banks, beaches and dunes. *Coast. Eng.*, 87, 136-146
- Havinga, H., 1982. Bed Load Determination by Dune Tracking. *Dir. Water Management and Water Motion District South East, Rijkswaterstaat, The Netherlands*
- Hoefel, F., Elgar, S., 2003. Wave-induced sediment transport and sand bar migration. *Science*, 299, 1885-1887
- Houser, C., Greenwood, B., Aagaard, T., 2006. Divergent response of an intertidal swash bar. *Earth Surf. Process. Landforms*, 31, 1775-1791
- Houthuys, R., De Moor, G., Sommé, J., 1993. The Shaping of the French-Belgian North Sea Coast throughout Recent Geology and History. *Proceedings of the 8th Symposium on Coastal and Ocean Management, July 19-23, 1993, New Orleans, Louisiana*, 27-40
- Houthuys, R., 2011. A sedimentary model of the Brussels Sands, Eocene, Belgium. *Geologica Belgica*, 14, 1-2
- Houthuys, R., 2012. Morfologische trend van de Vlaamse kust in 2011. *Agentschap Maritieme dienstverlening en Kust. Afdeling Kust: Oostende*. 150 pp.
- Hughes, M.G., Masselink, G., Brander, R.W., 1997. Flow velocity and sediment transport in the swash zone of a steep beach. *Mar. Geol.*, 138, 91-103
- Huising, E.J., Gomes Pereira, L.M., 1998. Errors and accuracy estimates of laser data acquired by various laser scanning systems for topographic applications. *ISPRS Journal of Photogrammetry and Remote Sensing*, 53, 245-261
- Incoul, A., Nuttens, T., De Maeyer, P., Seube, N., Stal, C., Touzé, T., De Wulf, A., 2014. Mobile Laser Scanning of Intertidal Zones of Beaches using an Amphibious Vehicle. *INGEO 2014 – 6th International Conference on Engineering Surveying, Prague, Czech Republic, April 3-4*, 87-92
- Inman, D.L., 1949. Sediment trap studies of suspended material near the surf zone. *Scrpps Inst. Oceanogr. Q., Prog. Rep. to U.S. Army Corps Eng. BEB*, 2, 5-6

-
- Inman, D.L., Bagnold, R.A., 1963. Littoral processes. In: Hill, M.L. (ed.), *The Sea: Ideas and Observations*. New York: Wiley Interscience, 3, 507-528
- Jaffe, B.E., Sternberg, R.W., Sallenger, A.H., 1984. Role of suspended sediment in shore-normal beach profile changes. In: *Proc. 19th. Int. Coastal Eng. Conf., Houston, TX. ASCE, New York*, 1983-1996
- Jaud, M., Delacourt, C., Allemand, P., Deschamps, A., Cancouët, R., Ammann, J., Grandjean, P., Suanez, S., Fichaut, B., Cuq, V., 2011. Comparison of some very high resolution remote sensing techniques for the monitoring of a sandy beach. *AGU, Fall Meeting 2011*
- Johnson, J.W., 1949. Scale effects in hydraulic models involving wave motion. *Trans Amer. Geophys. Union*, 30, 517-525
- Kamphuis, J. W., 1991. Alongshore sediment transport rate. *J. Waterw. Port. Coastal. Ocean Eng., ASCE*, 117, 624-640
- Klein, J.T., Smit, M.J., Goosen, H., Hulsbergen, C.H., 1998. Resilience and Vulnerability: Coastal Dynamics or Dutch Dikes? *The Geographical Journal.*, 164, 259-268
- Kobayashi, N., Payo, A., Schmied, L., 2008. Cross-shore suspended sand and bed load transport on beaches. *J. of Geophys. Res.: Oceans*, 113, C07001
- Kolokythas, G.A., Silva, R., Delgado-Blanco, M.R., 2016. Morphological evolution of a bed profile induced by a storm event at the Belgian coast predicted by XBeach model. *Proceedings of the European Association of Remote Sensing Laboratories*, 3, 26-33
- Komar, P.D., Inman, D.L., 1970. Longshore sand transport on beaches. *J. Geophys. Res. (1896-1977)*, 75, 5914-5927
- Kraus, N.C., 1987. Application of Portable Traps for Obtaining Point Measurements of Sediment Transport Rates in the Surf Zone. *J. Coast. Res.*, 3, 139-152
- Kroon, A., Masselink, G., 2002. Morphodynamics of intertidal bar morphology on a macrotidal beach under low-energy wave conditions, North Lincolnshire, England. *Mar. Geol.*, 190, 591-608
- Lanckriet, T., Puleo, J.A., Waite, N., 2013. A Conductivity Concentration Profiler for Sheet Flow Sediment Transport. *J. of Ocean Engineering*, 38, 55-70
- Lanckriet, T., Trouw, K., Zimmerman, N., Wang, L., De Maerschalck, B., Delgado, R., Verwaest, T., Lebbe, L., Van Meir, N., Viaene, P., 2008. Potential implications of sea-level rise for Belgium. *J. Coast. Res.*, 24, 358-366
- Larson, M., 1988. Quantification of beach profile change. *Technical Report CERC-89-9, Coastal Engineering Research Center, Waterways Experiment Station, Vicksburg, Mississippi*.
- Le Roux, J.P., 1994. An alternative approach to the identification of sand sediment transport paths based on a grain-size trends. *Sedimentary Geology*, 94, 97-107

-
- Lebbe, L., Van Meir, N., Viaene, P., 2008. Potential implications of sea-level rise for Belgium. *J. Coast. Res.*, 24, 358–366.
- Levoy, F., Monthort, O., Rousset, H., 1994. Quantification of longshore transport in the surfzone on macrotidal beaches. Field experiments along the western coast of Cotentin (Normandy, France). In: ASCE (Ed.), in: *Proceedings of the 24th International Conference on Coastal Engineering, Kobe, Japan*, 2282-2296
- Levoy, F., Montfort, O., Larsonneur, C., 1997. Quantification des débits solides sur les plages macrotidales à l'aide de traceurs fluorescents, application à la côte ouest du Cotentin. *Oceanologica Acta*, 20, 811-822
- Levoy, F., Anthony, E.J., Monfort, O., Larsonneur, C., 2000. Morphodynamics of megatidal beaches in Normandy, France. *Mar. Geol.*, 171, 39-59
- Lohrmann, A., 2001. Monitoring sediment concentration with acoustic backscattering instruments. *Nortek Tech. Note*, 3, 1-5
- MacDonald, N.J., O'Connor, B.A., 1995. Changes in wave impact on the Flemish coast due to increased mean sea level. *Journal of Marine Systems*, 7, 133-144
- Maspataud, A., Ruz, M-H., Héquette, A., 2009. Spatial variability in post-storm beach recovery along a macrotidal barred beach, southern North Sea. *J. Coast. Res.*, 56, 88-92
- Masselink, G., 1992. Longshore variation of grain size distribution along the coast of the Rhône delta, Southern France: a test of "McLaren model". *J. Coast. Res.*, 8, 286-291
- Masselink, G., Short, A.D., 1993. The Effect of Tide Range on Beach Morphodynamics and Morphology: A Conceptual Beach Model. *J. Coast. Res.*, 9, 785-800
- Masselink, G., Hegge, B., 1995. Morphodynamics of meso- and macrotidal beaches: examples from central Queensland, Australia. *Mar. Geol.*, 129, 1-23
- Masselink, G., Hughes, M., 1998. Field investigation of sediment transport in the swash zone. *Cont. Shelf Res.*, 18, 1179-1199
- Masselink, G., Pattiaratchi, C., 2000. Tidal asymmetry in sediment resuspension on a macrotidal beach in northwestern Australia. *Mar. Geol.*, 163: 257-274
- Masselink, G., Pattiaratchi, C.B., 2001. Seasonal changes in beach morphology along the sheltered coastline of Perth, Western Australia. *Mar. Geol.*, 172, 243-263
- Masselink, G., Hughes, M.G., 2003. Introduction to coastal processes and geomorphology. *NY, Oxford University Press Inc.*
- Masselink, G., Russell, P., 2006. Flow velocities, sediment transport and morphological change in the swash zone of two contrasting beaches. *Mar. Geol.*, 227, 227-240

-
- Masselink, G., Austin, M., Tinker, J., O'Hare, T., Russell, P., 2008. Cross-shore sediment transport and morphological response on a macrotidal beach with intertidal bar morphology, Truc Vert, France. *Mar. Geol.*, 251, 141-155
- Masselink, G., Russell, P., Turner, I., Blenkinsopp, C., 2009. Net sediment transport and morphological change in the swash zone of a high-energy sandy beach from swash event to tidal cycle time scales. *Mar. Geol.*, 267, 18-35
- Masselink, G., Russell, P., Blenkinsopp, C., Turner, I., 2010. Swash zone sediment transport, step dynamics and morphological response on a gravel beach. *Mar. Geol.*, 274, 50-68
- Masselink, G., Hughes, M.G., Knight, J., 2011. Introduction to coastal processes & geomorphology – second edition. *London, UK: Hodder education*
- McLaren, P., 1981. An interpretation of trends in grain-size measures. *J. Sediment. Petrol.*, 51, 611-624
- McLaren, P., Bowles, D., 1985. The effects of sediment transport on grain-size distributions. *J. Sediment. Petrol.*, 55, 457-470
- McLean, S.R., Ribberink, J.S., Dohmen-Janssen, C.M., Hassan, W.N., 2001. Sand Transport in Oscillatory Sheet Flow with Mean Current. *J. Waterw. Port, Coastal and Ocean Eng.*, 127, 141-151
- Merckelbach, L.M., Ridderinkhof, H., 2006. Estimating suspended sediment concentration using backscatterance from an acoustic Doppler profiling current meter at a site with strong tidal currents. *Ocean Dyn.*, 56, 135-168
- Medvedev, V.C., Aibulatov, N.A., 1956. The use of 'labelled' sand to study the movement of material. *Izv. Akad. Nauk S.S.S.R., Ser. Geogr.*, 4, 99-102
- Meyer, R.D., 1936. A model study of wave action on beaches. *M.S. thesis in civil engineering, Univ. Calif.*
- Mikkelsen, O.A., Pejrup, M., 2001. The use of a LISST-100 laser particle sizer for in-situ estimates of floc size, density and settling velocity. *Geo-Marine Letters*, 20, 187-195
- Montreuil, A-L., Bullard, J.E., Chandler, J.H., 2013. Detecting seasonal variations in embryo dune morphology using a terrestrial laser scanner. *J. Coast. Res.*, 65, 1313-1318
- Morton, R.A., Paine, J.G., Gibeaut, J.C., 1994. Stages and durations of post-storm beach recovery, southeastern Texas Coast, U.S.A. *J. Coast. Res.*, 10, 884-908
- Morton, R.A., 2002. Factors controlling storm impacts on coastal barriers and beaches – a preliminary basis for near real-time forecasting. *J. Coast. Res.*, 18, 486-501
- Nauw, J.J., Merckelbach, L.M., Ridderinkhof, H., van Aken, H.M., 2014. Long-term ferry-based observations of the suspended sediment fluxes through the Marsdiep inlet using acoustic Doppler current profilers. *J. of Sea Res.*, 87, 17-29

-
- Nicholls, R.J., Woodroffe, C.D., Burkett, V., Hay, J., Wong, P.P., Nurse, L., 2011. Scenarios for coastal vulnerability assessment. *Treatise on Estuarine and Coastal Science*, 12, 289–303
- Nordstrom, K.F., Jackson, N.L., Allen, J.R., Sherman, D.J., 2003. Longshore sediment transport rates on a microtidal estuarine beach. *J. Waterw. Port, Coastal and Ocean Eng.*, 129, 1-4
- O'Hare, T.J., Huntley, D.A., 1994. Bar formation due to wave groups and associated long waves. *Mar. Geol.*, 116, 313-325
- Parisot, J.P., Capo, S., Castelle, B., Bujan, S., Moreau, J., Gervais, M., Réjas, A., Hanquiez, V., Almar, R., Marieu, V., Gaunet, J., Gluard, L., George, I., Nahon, A., Dehouck, A., Certain, R., Barthe, P., Le Gall, F., Bernardi, P.J., Le Roy, R., Pedreros, R., Delattre, M., Brillet, J., Sénéchal, N., 2009. Treatment of topographic and bathymetric data acquired at the Truc-Vert Beach during the ECORS Field Experiment. *J. Coast. Res.*, Special Issue 56, 1786-1790
- Pawlowicz, R., Beardsley, B., Lentz, S., 2002. Classical Tidal Harmonic Analysis Including Error Estimates in MATLAB using T_TIDE. *Computers and Geosciences*, 28, 929-937
- Pedreros, R., Howa, H.L., Michel, D., 1996. Application of grain size trend analysis for the determination of sediment transport pathways in intertidal areas. *Mar. Geol.*, 135, 35-49
- Philips, J.D., Van Dyke, C., 2016. Principles of geomorphic disturbance and recovery in response to storms. *Earth Surf. Process. Landforms*, 41, 971-979
- Philips, M.S., Harley, M.D., Turner, I.L., Splinter, K.D., Cox, R.J., 2017. Shoreline recovery on wave-dominated sandy coastlines: the role of sandbar morphodynamics and nearshore wave parameters. *Mar. Geol.*, 385, 146-159
- Pietro, L.S., O'Neal, M.A., Puleo, J.A., 2008. Developing terrestrial-LiDAR-based digital elevation models for monitoring beach nourishment performance. *J. Coast. Res.*, 24, 1555-1564
- Poizot, E., Mear, Y., Thomas, M., Garnaud, S., 2006. The application of geostatistics in defining the characteristic distance for grain size trend analysis. *Computers and Geosciences*, 32, 360-370
- Qi, H., Cai, F., Lei, G., Cao, H., Shi, F., 2010. The response of three main beach types to tropical storms in South China. *Mar. Geol.*, 275, 244–254
- Quartel, S., Ruessink, B.G., Kroon, A., 2007. Daily to seasonal cross-shore behaviour of quasi-persistent intertidal beach morphology. *Earth Surf. Process. Landforms*, 32, 1293-1307
- Reichmüth, B., Anthony, E.J., 2007. Tidal influence on the intertidal bar morphology of two contrasting macrotidal beaches. *Geomorphology*, 90, 101–114.

-
- Reyes, J.L., Martins, J.T., Benavente, J., Ferreira, Ó., Gracia, F.J., Alveirinho-Dias, J.M., López-Aguayo, F., 1999. Gulf of Cadiz beaches: a comparative response to storm events. *Boletín Instituto Español de Oceanografía*, 15, 221-228
- Ribberink, J.S., Al-Salem, A., 1992. Time-dependent sediment transport phenomena in oscillatory boundary-layer flow under sheet-flow conditions. *Delft Hydraulics, The Netherlands, Report H840.20 Part VI (Kustgenese/MaST)*
- Rocha, M.V.L., Coelho, C., Fortes, C.J.E.M., 2013. Numerical modeling of groins impact on nearshore hydrodynamics. *Ocean Engineering*, 74, 260-275
- Rogers, A.L., Ravens, T.M., 2008. Measurement of Longshore Sediment Transport Rates in the Surf Zone on Galveston Island, Texas. *J. Coast. Res.*, 2, 62-73
- Ruessink, B.G., 1998. The temporal and spatial variability of infragravity energy in a barred nearshore zone. *Cont. Shelf Res.*, 18, 585-605
- Ruggiero, P., Walstra, D.J.R., Gelfenbaum, G., van Ormondt, M., 2009. Seasonal-scale nearshore morphological evolution: Field observations and numerical modeling. *Coast Eng.*, 56, 1153-1172
- Sallenger, A.H., Richmond, B.M., 1984. High-frequency sediment level oscillations in the swash zone. In: Greenwood, B., Davis Jr. Jr., R.A. (Eds.). *Hydrodynamics and Sedimentation in Wave-dominated Coastal Environments. Mar. Geol.*, 60, 155-164
- Sarre, R.D., 1989. Aeolian sand drift from the intertidal zone on a temperate beach: potential and actual rates. *Earth Surf. Process. Landforms*, 14, 247-258
- Saville T., 1950. Model study of sand transport along an infinitely long straight beach. *Trans Amer. Geophys. Union*, 31, 555-565
- Schoonees, J.S., Theron, A.K., 1995. Accuracy and applicability of the SPM longshore transport formula. *Proceedings of the 24th ICCE, ASCE, New York*, 2595-2609
- Schoonees, J.S., Theron, A.K., 1996. Improvement of the most accurate longshore transport formula. *25th ICCE Orlando, USA*, 3652-3665
- Sedrati, M., Anthony, E.J., 2007. Storm-generated morphological change and longshore sand transport in the intertidal zone of a multi-barred macrotidal beach. *Mar. Geol.*, 244, 209-229
- Sénéchal, N., Abadie, S., Gallagher, E., MacMahan, J., Masselink, G., Michallet, H., Reniers, A., Ruessink, G., Russell, P., Sous, D., Turner, I., Arduin, F., Bonneton, P., Bujan, S., Capo, S., Certain, R., Pedreros, R., Garlan, T., 2011. The ECORS-Truc Vert'08 nearshore field experiment: presentation of a three-dimensional morphologic system in a macro-tidal environment during consecutive extreme storm conditions. *Ocean Dyn.*, 61, 2073-2098
- Sénéchal, N., Coco, G., Castelle, B., Marieu, V., 2015. Storm impact on the seasonal shoreline dynamics of a meso- to macrotidal open sandy beach (Biscarrosse, France). *Geomorphology*, 228, 448-461

-
- Sénéchal, N., Pavon, J., Asselot, R., Castelle, B., Taaouati, M., Ferreira, S., Bujan, S., 2016. Recovery assessment of two nearby sandy beaches with contrasting anthropogenic and sediment supply settings. *J. of Coastal Res.: Special Issue 75 - Proceedings of the 14th International Coastal Symposium, Sydney, 6-11 March 2016*, 462 – 466
- Shields, A., 1936. Anwendung der Ähnlichkeitsmechanik und der Turbulenz Forschung auf die Geschiebewegung. *Mitt. der Preuss. Versuchsamst. für Wasserbau und Schiffbau, Heft 26, Berlin, Deutschland*
- Short, A.D., 1990. Macro-Meso Tidal Beach Morphodynamics – An Overview. *J. Coast. Res.*, 7, 417-436
- Short, A.D., Trembanis, A.C., 2004. Decadal Scale Patterns in Beach Oscillation and Rotation Narrabeen Beach, Australia – Time series, PCA and Wavelet Analysis. *J. Coast. Res.* 20, 523-432
- Silva, A., Taborda, R., Rodrigues, A., Duarte, J., Cascalho, J., 2007. Longshore drift estimation using fluorescent tracers: New insights from an experiment at Comporta Beach, Portugal. *Mar. Geol.*, 240, 137-150
- Simm, J., 1996. Beach Management Manual. *CIRIA Report No. 153, London, England*
- Simmonds, D.J., O’Hare, T.J., Huntley, D.A., 1996. The Influence of Long Waves on Macrotidal Beach Morphology. *Proceedings of the 25th International Conference on Coastal Engineering, Orlando, FL, USA, 2-6 September 1996*, 3090-3103
- Simons, D.B., Richardson, E.V., Nordin, C.F., 1965. Bed Load Equation for Ripples and Dunes. *U.S. Geol. Survey Prof. Paper 462 H, Washington, USA*
- Sipka, V., Anthony, E.J., 1999. Morphology and hydrodynamics of a macrotidal ridge and runnel beach under modal low wave conditions. *Journal de Recherche Océanographique*, 24, 25-31
- Soulsby, R., 1997. Dynamics of marine sands. *Thomas Telford, UK*
- Stépanian, A., Vlaswinkel, B., Levoy, F., Larssonneur, C., 2001. Fluorescent tracer experiment on a macrotidal ridge and runnel beach: a case study at Omaha beach, North France. *Coastal Dynamics 2001, Lund, Sweden*, 1017-1027
- Stive, M.J.F., DeVriend, H.J., 1995. Modelling shoreface profile evolution. *Mar. Geol.*, 126, 235-248
- Suanez, S., Stéphan, P., 2006. Forçages météo-marins et dynamique morphosédimentaire saisonnière des cordons dunaires. Exemple de la baie de Saint-Michel-en-Grève (Côtes d’Armor, Bretagne). *Geomorphologie: Relief, Processus, Environnement*, 2, 91-110
- Sunamura, T., Horikawa, K., 1974. Two-dimensional beach transformation due to waves. *Proceedings 14th International Conference on Coastal Engineering, ASCE*, 920-938

-
- Swales, A., 2002. Geostatistical estimation of short-term changes in beach morphology and sand budget. *J. Coast. Res.*, 18, 338-351
- Taaouati, M., Nachite, D., 2011. Beach morphology and sediment budget variability based on high quality digital elevation models derived from field data sets. *Int. J. Geosci.*, 2, 111-119
- Terry, R.D., 1951. Suspended sediment study of surf at Huntington Beach, California. *Univ. S. Calif., unpublished report in Sedimentation*, 21 pp.
- Theuerkauf, E.J., Rodriguez, A.B., 2012. Impacts of Transect Location and Variations in Along-Beach Morphology on Measuring Volume Change. *J. Coast. Res.*, 28, 707-718
- Thorne, P.D., Vincent, C.E., Hardcastle, P.J., Rehman, S., Pearson, N., 1991. Measuring suspended sediment concentration using acoustic backscatter devices. *Mar. Geol.*, 98, 7-16
- Thorne, P.D., Davies, A.G., Bell, P.S., 2009. Observations and analysis of sediment diffusivity profiles over sandy rippled beds under waves. *J. Geophys. Res.*, 114, 1-16
- Thornton, E.B., 1968. A field investigation of sand transport in the surf zone. *Proc. Conf. Coastal Eng., 11th, Am. Soc. Civ. Eng.*, 1, 335-351
- Thornton, E.B., Humiston, R.T., Birkemeier, W., 1996. Bar/trough generation on a natural beach. *J. Geophys. Res.*, 101, 12097-12110
- Tonk, A., Masselink, G., 2005. Evaluation of Longshore Transport Equations with OBS Sensors, Streamer Traps and Fluorescent Tracer. *J. Coast. Res.*, 21, 915-931
- Turner, I.L., Russell, P.E., Butt, T., 2008. Measurements of wave-by-wave bed-levels in the swash zone. *Coast. Eng.*, 55, 1237-1242
- Van Gaalen, J.F., Kruse, S.E., Coco, G., Collins, L., Doering, T., 2011. Observations of beach cusp evolution at Melbourne Beach, Florida, USA. *Geomorphology*, 129, 131-140
- Van Heteren, S.A., van der Spek, A., van der Valk, B., 2011. Evidence and implications of middle- to late-Holocene shoreface steepening offshore the western Netherlands. *Proceedings Coastal Sediments 2011, Am. Soc. Civil Eng., New York*, 188-201
- Van Houwelingen, S., Masselink, G., Bullard, J., 2006. Characteristics and dynamics of multiple intertidal bars, north Lincolnshire, England. *Earth Surf. Process. Landforms*, 31, 428-443
- Van Maanen, B., de Ruiter, P.J., Ruessink, B.G., 2009. An evaluation of two along-shore transport equations with field measurements. *Coast. Eng.*, 56, 313-319
- Van Oyen, T., van Lancker, V., de Swart, H., 2013. De Noordzeebodem: een landschap vol pieken en dalen. *De Grote Rede*

-
- Van Rijn, L.C., 1993. Principles of sediment transport in rivers and estuaries and coastal seas. *Aqua Publications, Amsterdam, The Netherlands*
- Van Rijn, L. C., 2014. A simple general expression for longshore transport of sand, gravel and shingle. *Coast. Eng.*, 90, 23–39
- Verwaest, T., Delgado, R., Janssens, J., Reyns, J., 2011. Longshore sediment transport along the Belgian coast. *Proceedings of Coastal Sediments 2011*, 1528-1538
- Vijverberg, T., Winterwerp, J.C., Aarninkhof, S.G.J., Drost, H., 2011. Fine sediment dynamics in a shallow lake and implication for design of hydraulic works. *Ocean Dyn.*, 61, 187-202
- Vito and Afdeling Kust, 2009. Kustlijnkaarten – evolutie van het strandvolume en verschuiving van de hoog- en laagwaterlijn tot 2007.
- Vos, S.E., Lindenbergh, R.C., de Vries, S., 2017. Coastscan: Continuous monitoring of coastal change using terrestrial laser scanning. *Proceedings of the Coastal Dynamics 2017, Helsingør, Denmark, 12-16 June 2017*, 1518-1528
- Vos, S.E., Hobbelen, R.N.P., Spaans, L., de Vries, S., Lindenbergh, R.C., 2019. Crossshore sand patterns in the intertidal zone: a case study with permanent laser scanning at Kijkduin beach. *Proceedings of Coastal Sediments 2019, Tampa, USA, 27-31 May 2019*, 287-295
- Voulgaris, G., Mason, T., Collins, M.B., 1996. An energetics approach for suspended sand transport on macrotidal ridge and runnel beaches. *Proceedings of the 25th International Conference on Coastal Engineering, Orlando, FL, USA, 2-6 September 1996*, 3948-3961
- Voulgaris, G., Simmonds, D., Michel, D., Howa, H., Collins, M.B., Huntley, D., 1998. Measuring and modelling sediment transport on a macrotidal ridge and runnel beach: an intercomparison. *J. Coast. Res.*, 14, 315-330
- Vousdoukas, M.I., Kirupakaramoorthy, T., Oumeraci, H., de la Torre, M., Wübbold, F., Wagner, B., Schimmels, S., 2014. The role of combined laser scanning and video techniques in monitoring wave-by-wave swash zone processes. *Coast. Eng.*, 83, 150-165
- Waddell, E., 1976. Swash-groundwater-beach profile interactions. In: Davis, R.A., Ethington, R.L. (Eds.). *Beach and Nearshore Sedimentation. Society of Economic Paleontologists and Mineralogists, Oklahoma*, 115-125
- Wang, P., Ebersole, B.A., Smith, E.R., Johnson, B.D., 2002. Temporal and spatial variations of surf-zone currents and suspended sediment concentration. *Coast. Eng.*, 46, 175-211
- Watts, G.M., 1953. Development and field tests of a sampler for suspended sediment in wave action. *BEB Tech. Mem.*, 34-41

-
- Weiss, A., Clark, S.P., Rennie, C.D., Moore, S.A., Ahmari, H., 2015. Estimation of total suspended solids concentration from aDcp backscatter and hydraulic measurements. *Journal of Hydraulic Research*, 53, 670-677
- Westoby, M.J., Brasington, J., Glasser, N.F., Hambrey, M.J., Reynolds, J.M., 2012. "Structure-from-motion" photogrammetry: A low-cost, effective tool for geoscience applications. *Geomorphology*, 179, 300-314
- Woodroffe, C.D., 2007. The Natural Resilience of Coastal Systems: Primary Concepts. In: McFadden, L., Penning-Rowsell, E., Nicholls, R.J. (eds). *Managing Coastal vulnerability*. Elsevier, Amsterdam, pp. 45-60
- Wright, F.F., 1962. The development and application of a fluorescent marking technique for tracing sand movements on beaches. *Office of Naval Research, Geography Brand Technical Report, No. 2 NR 388-057*, 29 pp.
- Wright, L.D., Thom, B.G., 1977. Coastal depositional landforms: a morphodynamics approach. *Progress in Physical Geography*, 1, 412-459
- Wright, L.D., Nielsen, P., Short, A.D., Green, M.O., 1982. Morphodynamics of a macrotidal beach. *Mar. Geol.*, 50, 97-128
- Wright, L.D., Short, A.D., 1984. Morphodynamics variability of surf zones and beaches: a synthesis. *Mar. Geol.*, 56, 93-118
- Zhang, S., Jia, Y., Wang, Z., Wen, M., Fang, L., Zhang, Y., Liu, X., Shan, H., 2018. Wave flume experiments on the contribution of seabed fluidization to sediment resuspension. *Acta Oceanol. Sin.*, 37, 80-87



Appendix A: wave buoy and tide gauge measuring locations



Figure A1. Locations of the wave buoys from Meetnet Vlaamse Banken/Coastal Division. Directional waveriders in yellow, non-directional waveriders in red.

Table A1. Locations of the wave buoys from Meetnet Vlaamse Banken/Coastal Division. Coordinates are in WGS84.

	North	East
A2B	51°21'34.80"	03°07'11.40"
AKZ	51°25'05.40"	02°48'04.20"
BVH	51°23'30.60"	03°12'01.50"
KWI	51°21'00.00"	02°42'21.00"
OST	51°14'48.60"	02°55'39.60"
RAV	51°13.17.70"	02°42'30.00"
TRG	51°08'15.04"	02°34'58.97"
WHI	51°22'52.72"	02°26'20.82"



Figure A2. Locations of the water level measurements from Meetnet Vlaamse Banken/Coastal Division.

Table A2. Locations of the water level measurements from Meetnet Vlaamse Banken/Coastal Division. Coordinates are in WGS84.

	North	East
OST	51°14'01''	02°55'25''
NPT	51°09'02''	02°43'41''

Appendix B: nearshore flow velocity

The hydrodynamic conditions measured at -8 m TAW during the first nearshore measuring campaign are presented in Figure B1 and Figure B2. The research period is divided in two, based on the timing of the monthly profiles which is indicated by t_0 , t_1 and t_2 . Water level variations were very similar for the two periods, with variations of 5.5 m during spring and 3 m during neap tide. The wave conditions, on the other hand, were different for the two periods. The mean significant wave height and period were both 5 % larger for period 2. During period 1 the maximum wave height was 0.98 m, whereas for period 2 it was 1.74 m. The dominant wave direction was from the north during period 1 and from the north and west during period 2. The flow velocity as measured by the Aquadopp was converted to along- and cross-shore flow velocities. Positive along-shore velocities mean that the currents were directed to the northeast, while for negative velocities they were directed to the southwest. For the cross-shore velocity positive velocities indicate shoreward currents, negative velocities indicate seaward currents. Peaks in along-shore flow velocity were 0.7 m/s, whereas peaks in cross-shore flow velocity were only 0.2 m/s. Flow velocities were 1.3 times higher during flood than during ebb.

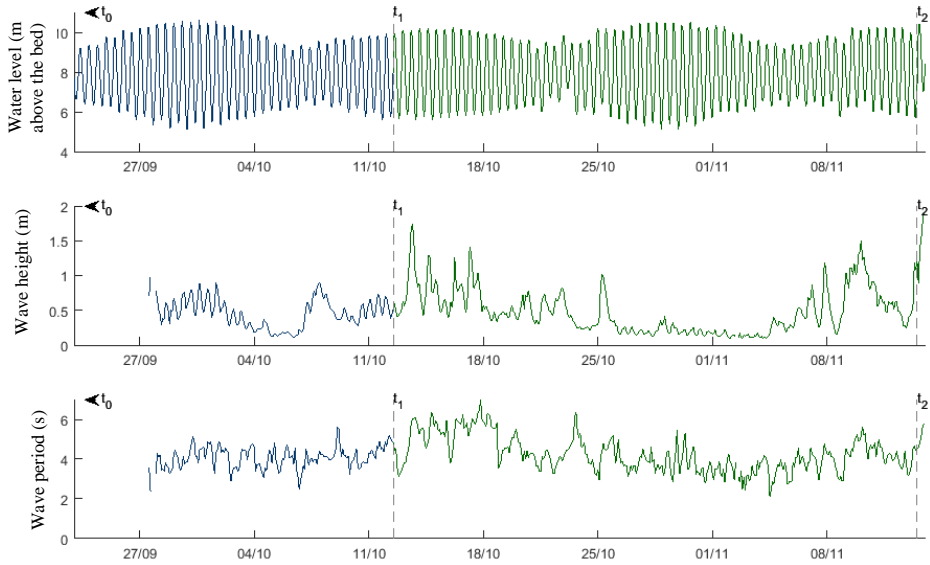


Figure B1. Time series of water level, significant wave height and significant wave period with the topographic surveys indicated by dashed lines at t_0 , t_1 and t_2 .

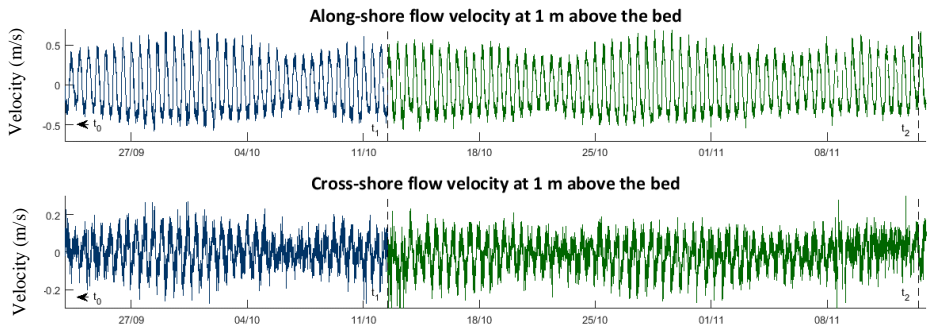


Figure B2. Total, along- and cross-shore flow velocity (m/s). The bed level is 8.2 m below TAW. The topographic surveys are indicated with dashed lines

Appendix C: OBS calibration

OBS are used to measure turbidity which is a measure for SSC. OBS send an infra-red light beam and detect the light that is scattered by the sediment particles. The response of OBS depends strongly on the size, composition and shape of the suspended particles. Therefore the sensors should be calibrated using sediment samples from the study site. The OBS were calibrated with the “bucket method” using sediment samples from the beach of Mariakerke (Figure C1). This sediment was slowly added to a bucket of water. The sediment was kept in suspension with a magnetic stirrer. The OBS signal was determined and a water sample was taken each time sediment was added. The water samples were filtered to obtain SSC values. The maximum SSC that was reached during calibration was 700 mg/l.



Figure C1. The bucket with the water being stirred by the magnetic stirrer (not pictured, on the bottom of the bucket) and an OBS.

In Figure C2 the three calibration curves of the OBS are presented. The corresponding calibration formulas are:

$$\begin{aligned}SSC_{10} &= turbidity \cdot 0.1841 + 71.766 && R^2 \text{ of } 0.51 \\SSC_{30} &= turbidity \cdot 0.2338 + 5.1059 && R^2 \text{ of } 0.71 \\SSC_{50} &= turbidity \cdot 0.2264 + 43.477 && R^2 \text{ of } 0.59\end{aligned}$$

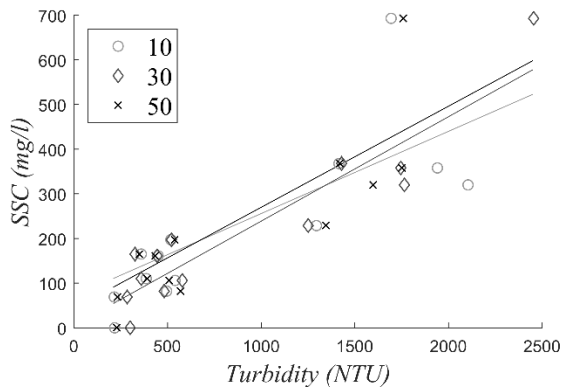


Figure C2. Calibration curves for the three OBS used in this study

Appendix D: background of TLS

Laser scanning emerged as a surveying technique in the 1990's using the LiDAR technique. A laser is used to emit a focused pulse to a spot on the beach and the two way travel time of the pulse is easily converted in a range distance with an accuracy of millimeters. 3D coordinates of this spot on the beach are obtained in combination with the known position and orientation of the laser system. In the beginning LiDAR technology was mainly implemented in airborne platforms. After the airborne success, LiDAR technology also got implemented on vehicles, referred to as mobile laser scanning, and on static platforms, referred to as terrestrial laser scanning.

A terrestrial laser scanner integrates a LIDAR sensor with a rotating head and mirror, resulting in a near 360x360° coverage of the 3D environment of the scanner. The range of such scanners is anywhere between 1 m and ~5 km. Typically a LIDAR system internally extracts one range from the return pulse, by selecting *e.g.* the time of maximal energy, or the time half of the significant return energy is received.

Often TLS is used from different station positions and the different point clouds, obtained from each standpoint, are combined to form a common point cloud. Alternatively, the scanner is kept stationary and the same scene is scanned repeatedly to detect changes. If this repeated scanning is automatized we obtain what we call a permanent TLS. It is permanent in two ways: spatially, in the sense that it always scanning from the same standpoint. And temporarily, in the sense that such system can be employed in a near continuous way, that is, once the surroundings of the scanner is scanned once, it automatically starts over again.

- Summarized from Vos *et al.* (2017)

Appendix E: human interference

Human activities on the study sites include (but are not limited to) reshaping of the dry beach with bulldozers (Mariakerke), horse and carriage racing (Groenendijk), tourism, and shrimp fishing with horses and trawls (nets dragged over the seafloor). All photographs are taken at the study sites during intertidal measuring campaigns.



Figure E1. Examples of human interference: tourism, reshaping of the beach, and shrimp fishing.





Research output

Peer-reviewed journal publications

Brand, E., Montreuil, A-L., Dan, S., Chen, M., 2018. Macro-tidal beach morphology in relation to nearshore wave conditions and suspended sediment concentrations at Mariakerke, Belgium. *Regional Studies in Marine Science*, 24, 97-106

Brand, E., De Sloover, L., De Wulf, A., Montreuil, A-L., Vos, S., Chen, M., 2019. Cross-shore suspended sediment transport in relation to topographic changes in the intertidal zone of a macro-tidal beach (Mariakerke, Belgium). *Journal of Marine Science and Engineering*, 7, 1-16

Brand, E., Montreuil, A-L., Houthuys, R., Chen, M., 2019. Relating waves, tide, and sediment supply to changes in intertidal beach topography on macro-tidal, sandy beaches. *Marine Geology - under review*

Brand, E., Chen, M., Montreuil, A-L., 2019. Optimizing measurements of sediment transport in the intertidal zone. *Earth-Science Reviews - under review*

Montreuil, A-L., Chen, M., Brand, E., Strypsteen, G., Rauwoens, P., Vandenbulcke, A., De Wulf, A., Dan, S., Verwaest, T., 2017. Dynamics of Surface Moisture Content on a Macrotidal Beach. *Journal of Coastal Research*, 85, 206-210

Conference proceedings

Brand, E., Chen, M., Montreuil, A-L., Dan, S., 2017. Intertidal beach recovery in relation to nearshore hydrodynamics, Mariakerke, Belgium. *Proceedings of HydroSenSoft 2017, 28 February – 3 March 2017, Madrid, Spain*, 1-7

Brand, E., Chen, M., Montreuil, A-L., Dan, S., 2017. Spatio-temporal variability in intertidal beach morphology on a seasonal scale, Mariakerke, Belgium. *Proceedings of Coastal Dynamics 2017, 12-16 June 2017, Helsingør, Denmark*, 1049-1058

Brand, E., Montreuil, A-L., Chen, M., 2019. The effect of turbulence and particle size on suspended sediment concentration measurements in the intertidal zone. *Coastal Sediments 2019, May 2019*, 2435-2442

Montreuil, A-L., Chen, M., Brand, E., Dan, S., 2017. Monitoring Aeolian Activity During a Storm Events Using a Video System. *Proceedings of Coastal Dynamics 2017, 12-16 June 2017, Helsingør, Denmark*, 461-470

Conference abstracts

Brand, E., Chen, M., Montreuil, A-L., Vandenbulcke, A., De Wulf, A., Dan, S., Verwaest, T., 2018. Measuring suspended sediment transport in the intertidal zone of a macro-tidal beach (Mariakerke, Belgium) [abstract]. *Book of Abstracts NCK days 2018, 21-23 March, Haarlem*

Brand, E., Montreuil, A-L., Dan, S., Chen, M., 2017. Morphological changes on a monthly scale, Mariakerke, Belgium [abstract]. *Book of Abstracts NCK days 2017, 15-17 March, Den Helder*





Acknowledgements

First, I would like to thank my promotor prof. dr. Margaret Chen for your guidance, support, and supervision during all stages of my research. My special gratitude also goes to dr. Anne-Lise Montreuil for your co-supervision of my research, your valuable advise, and constant support throughout my PhD.

This PhD research was part of the CREST project, which was funded by the Strategic Basic Research (SBO) program of the Instituut voor Innovatie door Wetenschap en Technologie (IWT). I would like to thank all the collaborators from this project for our inspirational meetings. I would especially like to express gratitude to my colleagues from activity 3: dr. Sebastian Dan for the collaboration on the Mariakerke measurements; prof. dr. Alain de Wulf, Lars de Sloover, Annelies Vandenbulcke, and Jeffrey Verbeurgt for all the effort you put into the beach topography measurements and in making them as accurate as possible; dr. Rik Houthuys for our valuable discussions; prof. dr. Pieter Rauwoens and Glenn Strypsteen for our collaboration on the measuring campaigns; and prof. dr. Jaak Monbaliu, Tina Mertens, and Toon Verwaest for your guidance and for leading our activity.

My deep gratitude goes to the director of Flanders Hydraulics Research (FHR), prof. dr. Frank Mostaert, for having research facilities at my disposal.

I would also like to thank the head of the department at the VUB, prof. dr. Ann van Griensven, the secretary, Hilde, and the other professors, colleagues, and PhD students for your support of this thesis work.

For assistance with the field campaigns I wish to thank FHR and Vlaams Instituut voor Zeeonderzoek (VLIZ) for the use of their equipment. For the design of the measuring set-up and the deployment of the frame and the equipment I would specifically like to thank Hans Vereecken, Styn Claeys, Leonid Verzhbitskiy, and Yves van de Water from FHR. I would also like to thank the people working in the sediment laboratory at FHR, especially Ellen

Bastiaensen, for the analysis of the many sediment samples. Furthermore, I would like to thank dr. Sander Vos from TU Delft for the deployment of the permanent terrestrial laser scanner. The monthly topographic profiles and the wave buoy, tide gauge, and wind station measurements are courtesy of Coastal Division, Department of Mobility and Public Works, Flanders, and the Agency for Maritime and Coastal Services, Coastal Division, respectively.

Last, but not least, I would like to thank my parents, brother and sister, other family, friends, especially Eline and Hein, and above all Jochem for all their support.



